QA: QA

MDL-WIS-PA-000005 REV 00 AD 01

March 2008

Total System Performance Assessment Model/Analysis for the License Application Addendum 01

Volume II

Prepared for:
U.S. Department of Energy
Office of Civilian Radioactive Waste Management
Office of Repository Development
1551 Hillshire Drive
Las Vegas, Nevada 89134-6321

Prepared by:
Sandia National Laboratories
OCRWM Lead Laboratory for Repository Systems
1180 Town Center Drive
Las Vegas, Nevada 89144

Under Contract Number
DE-AC04-94AL85000

DISCLAIMER

This report was prepared as an account of work sponsored by an agency of the United States Government. Neither the United States Government nor any agency thereof, nor any of their employees, nor any of their contractors, subcontractors or their employees, makes any warranty, express or implied, or assumes any legal liability or responsibility for the accuracy, completeness, or any third party's use or the results of such use of any information, apparatus, product, or process disclosed, or represents that its use would not infringe privately owned rights. Reference herein to any specific commercial product, process, or service by trade name, trademark, manufacturer, or otherwise, does not necessarily constitute or imply its endorsement, recommendation, or favoring by the United States Government or any agency thereof or its contractors or subcontractors. The views and opinions of authors expressed herein do not necessarily state or reflect those of the United States Government or any agency thereof.

CONTENTS

Page

CONTENTS (Continued)

Page

FIGURES

Page

FIGURES (Continued)

Page

FIGURES (Continued)

Page

FIGURES (Continued)

Page

FIGURES (Continued)

Page

FIGURES (Continued)

Page

FIGURES (Continued)

Page

FIGURES (Continued)

Page

FIGURES (Continued)

Page

FIGURES (Continued)

Page

FIGURES (Continued)

Page

FIGURES (Continued)

Page

FIGURES (Continued)

Page

FIGURES (Continued)

Page

TABLES

INTENTIONALLY LEFT BLANK

7[a]. MODEL VALIDATION AND CONFIDENCE BUILDING

One distinguishing characteristic of validating and building confidence in the Total System Performance Assessment for the License Application (TSPA-LA) Model is the iterative nature of the process. The results presented in this addendum were generated with an updated version of the TSPA-LA Model, v5.005, and address issues that were identified during detailed post-development analysis, checking, and review of the TSPA-LA Model v5.000 results described in the parent document. The issues were primarily related to inaccuracies in model implementation and identification of unintended conservatisms as documented in Appendix P of the parent document. Changes were made to the TSPA-LA Model to address the issues presented in Appendix P of the parent document and to address unintended conservatisms in the TSPA-LA Model, as indicated in Appendix P[a] of this addendum. Appendix P[a] of this addendum includes updated tables that summarize the issues that have been addressed in the TSPA-LA Model v5.005.

Appendix P of the parent document describes the identified issues and errors, and assesses their anticipated impacts. The overall impacts on mean annual dose were projected to be "negligible" or "small" with one issue assessed as "significant" in a specified timeframe. These projected impacts were based on the understanding of the TSPA-LA Model v5.000 results during post-development analysis and review activities. As described below and listed in Tables P-6[a] and P-7[a], the projected impacts were confirmed in the TSPA-LA Model v5.005 results, indicating that the v5.000 results were well understood. The validation portion of the model documentation in the parent document was judged adequate for the intended purpose of TSPA-LA Model performance analyses in evaluating the postclosure performance of the repository and its compliance with U.S. Nuclear Regulatory Commission Proposed Rule 10 CFR 63.113 [DIRS 180319] and the performance measures defined in proposed 10 CFR 63.303 [DIRS 178394] for the individual protection standard after permanent closure in proposed 10 CFR 63.311a(1) and (2) [DIRS 178394], the individual protection standard for human intrusion in 10 CFR 63.321(a)(1) and (2) [DIRS 178394], and the separate standards for protection of groundwater in 10 CFR 63.331 [DIRS 180319], Table 1. The next iteration of the evaluation is the subject of this addendum. Confidence has been enhanced because the process has proceeded to identify, describe, and fix issues and errors during development of a thorough understanding of the results. However, it is still necessary to re-assess the adequacy of the validation portion of the model documentation of the parent document and update activities if necessary. Thus, in preparing this addendum, each validation activity for TSPA-LA Model v5.000 was reviewed to determine which activities were affected by changes made between TSPA-LA Model v5.000 and v5.005. Where validation activities could potentially be affected by model changes, these validation activities were repeated using v5.005 to verify that model changes did not adversely affect the overall validation of the TSPA-LA Model. Additional verification and validation results beyond those presented in the parent document are also provided to further enhance confidence in the TSPA-LA Model. The following validation activities were conducted for TSPA-LA Model v5.005 and are documented in this addendum:

- Computer code and input re-verification (Section 7.2[a]) including:
  - Verification testing for the Human Intrusion Submodel inadvertently omitted from the parent document (Section 7.2.4.1.12[a])

  - Summary of an assessment of the range of validity for all TSPA-LA Model submodels inadvertently omitted from the parent document (Section 7.2.6[a])

- Demonstration of Model Stability (Section 7.3[a])
  - Comparison between TSPA-LA Model v5.000 and v5.005 expected dose results (Section 7.3.1[a])
  - Reevaluation of the statistical stability of TSPA-LA Model v5.005 results (Section 7.3.1[a])
  - Confirmation of numerical accuracy of expected dose results for the Seismic Fault Displacement Modeling Case (Section 7.3.2.7[a])
  - Reevaluation of the temporal stability testing for the Human Intrusion Modeling Case as the result of a change to the timestep size for this modeling case (Section 7.3.3.6[a])
  - Evaluation of the temporal stability of the Nominal Modeling Case (Section 7.3.3.7[a])
- Surrogate Waste Form Validation (Section 7.5[a])
  - Reevaluation of the adequacy of using commercial spent nuclear fuel (CSNF) as a surrogate for naval spent nuclear fuel (NSNF) using TSPA-LA Model v5.005 (Section 7.5.3[a])
- Reevaluation of the corroboration of the TSPA-LA Model results documented in the parent document with auxiliary analyses (Section 7.7[a]), including:
  - Updated analyses of single realizations for the Early Failure Scenario Class, the Igneous Intrusion Modeling Case, and the Seismic Ground Motion (GM) Modeling Case for 1,000,000 years, including additional analyses of outlier realizations (Section 7.7.1[a])
  - Additional analyses of single realizations including: (1) the Nominal Scenario Class (Section 7.7.1.5[a]), (2) a Seismic GM Modeling Case for 10,000 years (Section 7.7.1.7[a]), and (3) the Human Intrusion Scenario (Section 7.7.1.6[a])
  - Updated evaluation with a Simplified TSPA Analysis (Section 7.7.2[a])
  - Updated evaluation with the Electric Power Research Institute (EPRI) Analysis (Section 7.7.3[a])
  - Reevaluation of a comparison of results from the Performance Margin Analysis (PMA) (Section 7.7.4[a]).

These additional verification and validation activities are presented to further enhance confidence in the TSPA-LA Model. Table 7.1-1[a] includes the verification and validation analyses presented in this addendum as well as those documented in the parent document. The analyses presented in this addendum confirm that TSPA-LA Model v5.005 is within the range of validation previously documented in the parent document.

7.1[a] MODEL VALIDATION STRATEGY

Table 7.1-1 of the parent document has been revised to include the verification and validation analyses presented in this addendum. Table 7.1-1[a] includes cross-references for the model validation analyses documented in Section 7 of the parent document and Section 7[a] of this addendum.

INTENTIONALLY LEFT BLANK

Table 7.1-1[a]. TSPA-LA Model v5.005 Validation Analyses

Activity Category/Subcategory	Purpose	Activity Description	Document Section
During–Development Validation Activities (Technical Work Plan Validation (SNL 2008 [DIRS 184920], Section 2.3.5.1))			
Computer Code and Input Verification			
Model Testing and Verification	Testing of software that is the basis for the TSPA-LA Model.	Verify GoldSim software, version 9.60.100 (STN: 10344-9.60-01 [DIRS 181903]) and 9.60.300 (STN: 10344-9.60-03 [DIRS 184387]).	7.2.1 and 7.2.1[a]
	Checking to determine whether the correct input parameters are used.	Verify input parameters.	7.2.3 and 7.2.3[a]
	Test cases to determine whether the model is working correctly, saving appropriate results, interfacing with DLLs, feeding the correct information among model components, and not exceeding the applicable range of model components.	Includes verification of DLLs, submodels, model components, and coupling among submodels and model components; and comparison with other models (e.g., stand-alone models from analysis model reports). In addition, the verification of coupling among submodels and model components includes subsystem analyses of annual release across model interfaces, drift-wall condensation, and localized corrosion initiation.	7.2.2, 7.2.4, 7.2.4[a], 7.2.5, 7.2.6[a]; Tables 7.2-1 and 7.2-2
Model Stability Testing			
Statistical Stability of Mean Annual Dose	Determine confidence interval around total mean annual dose and mean annual dose for each modeling case using three replicates.	TSPA-LA Model v5.000: Generate total mean annual dose and mean annual dose for each modeling case using three replicates with different random seeds. Determine a confidence interval around the estimate of the overall mean with a t-test. TSPA-LA Model v5.005: Determine stability by comparison with results from TSPA-LA Model v5.000. Determine a confidence interval around the estimate of the overall mean with a bootstrap procedure.	7.3.1, 7.3.1[a]
Numerical Accuracy of Expected Annual Dose Calculation – Igneous Scenario Class	Demonstrate accuracy of calculation of expected annual dose for the modeling cases of the Igneous Scenario Class.	For the Igneous Intrusion Modeling Case, demonstrate accuracy of the quadrature integration technique by increasing the discretization used in the integral. Increase the number of specified event times from 10 to 50. Calculate expected annual dose for five epistemic realizations for both 10,000 and 1,000,000 years. For the Volcanic Eruption Modeling Case for 10,000 years, demonstrate accuracy of the combined Monte Carlo and quadrature integration techniques by increasing the sample size used in the Monte Carlo integration and the discretization used in the quadrature integration. Calculate expected annual dose for 10,000 years for five epistemic realizations, increasing the aleatory LHS sample size from 40 to 120, and the number of specified event times from 10 to 20. Conclusions for 10,000 years apply to the 1,000,000 year calculations.	7.3.2

Table 7.1-1[a]. TSPA-LA Model v5.005 Validation Analyses (Continued)

Activity Category/Subcategory	Purpose	Activity Description	Document Section
Numerical Accuracy of Expected Annual Dose Calculation – Seismic Scenario Class	Demonstrate accuracy of calculation of expected annual dose for the modeling cases of the Seismic Scenario Class.	For the Seismic GM Modeling Case for 1,000,000 years, demonstrate the accuracy of the Monte Carlo integration technique by means of increased sample size. Repeat Replicate 1 (300 epistemic realizations) with a different aleatory seed to generate a second set of 9,000 dose histories (30 independent aleatory samples for each epistemic realization). Pool the two sets of 9,000 dose histories and generate expected annual dose based on the pooled set of 60 independent aleatory samples per epistemic realization, and compare to expected annual dose for the base case of 30 independent aleatory samples per epistemic realization. For the Seismic GM Modeling Case for 10,000 years, demonstrate accuracy of the quadrature integration technique by increasing the discretization used in each integral. Increase the number of specified event times from 6 to 12 and the number of specified damage levels from 5 to 8. Calculate expected annual dose for 5 epistemic realizations. For the Seismic FD Modeling Case, demonstrate accuracy of the quadrature integration technique by increasing the discretization used in each integral. Increase the number of specified event times from 6 to 12 and the number of specified damaged areas from 3 to 6. Calculate expected annual dose for 5 epistemic realizations for both 10,000 and 1,000,000 years.	7.3.2 and 7.3.2[a]
Justification of Simplifications for the Seismic GM Modeling Case for 10,000 Years	For the Seismic GM Modeling Case for 10,000 years, demonstrate that simplifications of the Seismic Consequences Abstraction used in the calculation of expected annual dose are reasonable.	Estimate the effect on mean annual dose of drip shield plate rupture and of framework failure. Estimate the effect on mean annual dose of accounting for rockfall effects on temperature and seepage entering the drift. Estimate the contribution to mean annual dose from WP rupture and puncture. Estimate the contribution to mean annual dose from damage to CSNF WPs.	7.3.2
Temporal Stability	Demonstrate stability of expected annual dose for temporal discretization in GoldSim.	Comparison of expected annual dose histories for five epistemic vectors for the following modeling cases: Waste Package EF; Seismic GM (10,000 years); Igneous Intrusion (10,000 and 1,000,000 years); and Drip Shield EF (10,000 years). Compare expected annual dose histories for different temporal discretizations. Assess the temporal stability for the Nominal Modeling Case (1,000,000 years). Assess the temporal stability for the Human Intrusion Modeling Case.	7.3.3 and 7.3.3[a]; Table 7.3.3-2[a]

Table 7.1-1[a]. TSPA-LA Model v5.005 Validation Analyses (Continued)

Activity Category/Subcategory	Purpose	Activity Description	Document Section
Spatial Discretization	Evaluate the impact due to the spatial discretizations inherited by the TSPA-LA Model from the supporting natural and engineered-barrier process models.	Evaluate the appropriateness of use of the inherited spatial discretization schemes of the process model abstractions that feed the TSPA-LA Model. These abstractions include the process models: Mountain-Scale UZ Flow, EBS TH Environment, UZ Transport, and SZ Flow and Transport abstractions.	7.3.4.1
	Evaluate the impact due to the spatial discretizations created within the TSPA-LA Model.	Describe the spatial discretization of the repository on the basis of percolation subregions and the binning of the percolation subregions by quantiles (0.0 to 0.05, 0.05 to 0.3, 0.3 to 0.7, 0.7 to 0.95, and 0.95 to 1.0).	7.3.4.2
		Demonstrate the appropriateness and validity of using the representative TH histories as inputs to the EBS Thermal-Hydrologic Environments Submodel of the TSPA-LA Model, as opposed to using the comprehensive data set available from the MSTHM.	7.3.4.3
Stability of UZ Transport Modeling for the Igneous Intrusion Modeling Case	Evaluate the stability of results in reference to the maximum number of particles allowed per species for the Igneous Intrusion Modeling Case for 10,000 years.	Analyze the differences in UZ releases of ^{99}Tc, ^{233}U, ^{234}U, ^{237}Np, and ^{239}Pu, and in cumulative dose for three cases (500,000; 750,000; and 900,000 particles).	7.3.5
Stability of UZ Transport Modeling for the Seismic GM Modeling Case	Evaluate the stability of results in reference to the maximum number of particles allowed per species for the Seismic GM Modeling Case for 10,000 years.	Analyze the differences in UZ releases of ^{99}Tc, ^{233}U, ^{234}U, ^{237}Np, and ^{239}Pu and in cumulative dose for three cases (500,000; 750,000; and 900,000 particles.).	7.3.5
Stability of UZ Transport Modeling for the Drip Shield EF Modeling Case	Evaluate the stability of results in reference to the maximum number of particles allowed per species for the Drip Shield EF Modeling Case for 1,000,000 years.	Analyze the differences in UZ releases of ^{99}Tc, ^{233}U, ^{234}U, ^{237}Np, and ^{239}Pu, and in cumulative dose for three cases (500,000; 750,000; and 900,000 particles).	7.3.5
Uncertainty Characterization Reviews			
Ranking of Scenario Classes	Prioritize scenario classes of higher significance to dose.	Develop a risk-based ranking of TSPA-LA scenario classes and modeling cases in order to focus the uncertainty characterization reviews of the most important component model abstractions.	7.4.2
Key Uncertain Parameters	Identify the key uncertain parameters that are important to dose.	Select the key uncertain parameters that are important to dose in the Seismic, Igneous, and Nominal Modeling Cases for characterization review based on both importance rankings from past TSPA scoping studies and recommendations provided by model abstraction developers and experienced TSPA analysts.	7.4.3

Table 7.1-1[a]. TSPA-LA Model v5.005 Validation Analyses (Continued)

Activity Category/Subcategory	Purpose	Activity Description	Document Section
Uncertainty-Characterization Review Findings and their Implementation	Review uncertainty characterization and address findings.	Perform uncertainty characterization of the selected key parameters impacting dose for the Seismic, Igneous, and Nominal Modeling Cases and implement corrective actions for observed deficiencies.	7.4.4
Surrogate Waste Form Validation			
Spent Fuel Categories	Comparison of naval surrogate fuel to naval fuel (Category 1).	Perform probabilistic runs to compare the naval surrogate (Zircaloy-clad commercial fuel) with naval fuel for Nominal, Igneous Intrusion, and Volcanic Eruption Modeling Cases.	7.5.3 and 7.5.3[a]
	Comparison of the DOE surrogate fuel to each DOE spent fuel category (Category 2 through Category 11).	Perform probabilistic run using Drip Shield EF Modeling Case to compare the DOE surrogate with plutonium/uranium alloy spent fuel (Category 2), plutonium/uranium-carbide spent fuel (Category 3), mixed-oxide spent fuel (Category 4), uranium/thorium-carbide spent fuel (Category 5), uranium/thorium-oxide spent fuel (Category 6), uranium-metal spent fuel (Category 7), uranium-oxide spent fuel (Category 8), aluminum-based spent fuel (Category 9), miscellaneous spent fuel (Category 10) for two inventories, and uranium-zirconium hydride spent fuel (Category 11).	7.5.4
Selected Sensitivity Analyses	Justification of the DOE surrogate dissolution model.	Perform probabilistic comparison of fuel degradation models for Category 2 through Category 11 and air alteration rates for Category 5 and Category 7.	7.5.5
	Justification of the DOE surrogate dissolution model.	Perform comparison of uranium-metal dissolution model, uranium-metal dissolution model with air alteration, and instantaneous dissolution (Category 7). Perform similar comparison for the uranium/thorium-carbide dissolution model (Category 5).	7.5.5
	Effects of fuel surface area and free inventory and uncertainty of radionuclide inventory.	Perform probabilistic comparison of uranium-metal nominal surface area with bounding surface area and free inventory and comparison of nominal inventory with the bounding inventory (Category 7).	7.5.5
	Uncertainty in number of WPs.	Perform probabilistic comparison of aluminum-based spent fuel for nominal and bounding number of WPs (Category 9).	7.5.5
	Comparison of radionuclides that contribute to annual dose from surrogate DOE spent fuel, HLW, uranium-metal spent fuel (Category 7), uranium/thorium-carbide spent fuel (Category 5), and uranium/thorium-oxide spent fuel (Category 6).	Analyze plots of key radionuclides that contribute to total annual dose for the DOE surrogate spent fuel only, HLW only, Category 7 only, Category 5 only, and Category 6 only.	7.5.6

Table 7.1-1[a]. TSPA-LA Model v5.005 Validation Analyses (Continued)

Activity Category/Subcategory	Purpose	Activity Description	Document Section
	Justification of the DOE surrogate fuel.	Compare of the weighted sum of Category 2 through Category 11 spent fuel with a single WP of the DOE surrogate spent fuel.	7.5.5
Post–Development Validation Activities (Technical Work Plan Validation (SNL 2008 [DIRS 184920], Section 2.3.5.2))			
Corroboration of Direct Input Abstraction Results with Validated Process Models			
Corroboration of Abstraction Results with Underlying Process Models	Evaluate consistency of the abstraction results with the underlying validated key natural system environment models.	Perform quantitative and qualitative evaluation of how well the direct input abstraction results corroborate with the underlying validated key natural system environment models. Provide the evidence that builds confidence in the direct inputs.	7.6.4.1
	Evaluate consistency of the abstraction results with the underlying validated key engineered barrier system models.	Perform quantitative and qualitative evaluation of how well direct input abstraction results corroborate the underlying validated key EBS models. Provide the evidence that builds confidence in the direct inputs.	7.6.4.2
	Evaluate consistency of the abstraction results with the underlying validated key drip shield, WP, and waste form degradation and mobilization models.	Perform quantitative and qualitative evaluation of how well the direct input abstraction results corroborate the underlying validated key drip shield, WP, and waste form degradation and mobilization models. Provide the evidence that builds confidence in the direct inputs.	7.6.4.3
	Evaluate consistency of the abstraction results with the underlying validated key disruptive events models.	Perform quantitative and qualitative evaluation of how well the direct input abstraction results corroborate the underlying validated key seismic and igneous disruptive events models. Provide the evidence that builds confidence in the direct inputs.	7.6.4.4
	Evaluate consistency of the abstraction results with the underlying validated biosphere model.	Provide the evidences that build confidence in the direct inputs from the biosphere model to the TSPA-LA Model.	7.6.4.5
Corroboration of Results with Auxiliary Analyses			
Analysis of Single Realizations	Evaluate a realization that contributes significantly to mean annual dose for the Early Failure Modeling Cases.	Select a realization each from the Waste Package EF Modeling Case and Drip Shield EF Modeling Case and analyze it to examine how the transport of key radionuclides is affected by coupling various components of the EBS, UZ, and SZ domains following the WP failure under varying physical-chemical-thermal-mechanical conditions. Also select an outlier realization and examine it to understand what leads to the extreme dose.	7.7.1 and 7.7.1[a]

Table 7.1-1[a]. TSPA-LA Model v5.005 Validation Analyses (Continued)

Activity Category/Subcategory	Purpose	Activity Description	Document Section
	Evaluate a realization that contributes significantly to mean annual dose for the Igneous Intrusion Modeling Case.	Select a realization from the Igneous Intrusion Modeling Case and analyze it to examine how the transport of key radionuclides is affected by coupling various components of the EBS, UZ, and SZ domains following the waste package failure under varying physical-chemical-thermal-mechanical conditions. Also select an outlier realization and examine it to understand what leads to the extreme dose.	7.7.1 and 7.7.1[a]
	Evaluate a realization that contributes significantly to mean annual dose for the Seismic GM Modeling Case.	Select a realization from the Seismic GM Modeling Case and analyze it to examine how the transport of key radionuclides is affected by coupling various components of the EBS, UZ, and SZ domains following the WP failure under varying physical-chemical-thermal-mechanical conditions. Both the 1,000,000-year and 10,000-year modeling cases were examined.	7.7.1 and 7.7.1[a]
	Evaluate a realization that contributes significantly to mean annual dose for the Nominal Modeling Case.	Select a realization from the Nominal Modeling Case and analyze it to examine how the transport of key radionuclides is affected by coupling various components of the EBS, UZ, and SZ domains. Also evaluate statistical outlier for this modeling case. Also select an outlier realization and examine it to understand what leads to the extreme dose.	7.7.1[a]
	Evaluate a realization that contributes significantly to mean annual dose for the Human Intrusion Modeling Case.	Select a realization from the Human Intrusion Modeling Case and analyze it to examine how the transport of key radionuclides is affected by coupling various components of the EBS, UZ borehole, and SZ domains following the human intrusion event. Also select an outlier realization and examine it to understand what leads to the extreme dose.	7.7.1[a]
Comparison with Other Simple Models	Compare the TSPA-LA Model component results with a simplified analysis.	Perform a Simplified TSPA Analysis and compare the results with those of the TSPA-LA Model.	7.7.2 and 7.7.2[a]
	Compare with the Energy and Power Research Institute (EPRI) TSPA Analysis.	Develop a comparison of the approach and results of the TSPA independently conducted by EPRI using its code IMARC for the postclosure performance of the Yucca Mountain repository.	7.7.3 and 7.7.3[a]

Table 7.1-1[a]. TSPA-LA Model v5.005 Validation Analyses (Continued)

Activity Category/Subcategory	Purpose	Activity Description	Document Section
Performance Margin Analyses	Provide objective evidence for assessing performance margin and degree of conservatism or non conservatism in the TSPA-LA Model.	Conduct several auxiliary analyses (see Section 7.7.4 of the parent document for a list) utilizing revisions to selected component models in the TSPA-LA Model, including conceptual or uncertainty alternatives, to assess the performance margin in the TSPA-LA Model and to evaluate whether the TSPA-LA Model dose is underestimated. The analyses include both individual component revisions as well as a combined analysis that incorporates all of the selected component revisions.	7.7.4 and 7.7.4[a]
Corroboration of Results with Natural Analogues			
Cerro Negro	Validation of ASHPLUME for the Volcanic Eruption Modeling Case.	Comparison Cerro Negro ash-fall measurements with the results from ASHPLUME.	7.8.1
Peña Blanca, Nopal I Uranium Deposit	Validation of the UZ and SZ Transport Model.	Evaluation of geochemical data collected from rock and water samples with respect to distance from the Nopal I ore deposit.	7.8.2
Independent Technical Reviews Performed in Preparation of the TSPA-LA Model			
TSPA-VA Peer Review	Evaluate the TSPA-VA methodology and prediction of the future behavior of the total system.	Performed peer review of the TSPA-VA and the supporting process models. The review was conducted by an independent group of external experts from 1997 to 1999.	7.9.1
TSPA-SR Peer Review	Evaluation of the TSPA-SR for methodology and ability to meet the needs for SR and future LA compliance.	Performed peer review of the TSPA-SR and selected supporting documents to evaluate the approach used in the performance assessment, and how well the TSPA-SR and the future TSPA-LA Model needs were addressed. The review was conducted by an international panel of experts managed by the OECD/NEA in 2002.	7.9.2
Draft TSPA-LA Technical Review	Evaluate the earlier draft iterations of the TSPA-LA Model as they were being drafted as to the degree of validation of the model for its intended purpose.	Perform technical review on the evaluation of the degree to which the draft TSPA-LA Model was valid for its intended purpose for the 10,000-year compliance period for which the model was prepared. The review was conducted by a team of experts during 2004, 2005, and early part of 2006.	7.9.3

INTENTIONALLY LEFT BLANK

7.2[a] COMPUTER CODE AND INPUT VERIFICATION

7.2.1[a] Selection and Verification of the Integrated System Software: GoldSim

A revised version of the GoldSim software (GoldSim V9.60.300, STN: 10344-9.60-03 [DIRS 184387]) was used in all updated TSPA-LA Model results reported in this addendum. Information about GoldSim is discussed in Section 7.2.1 of the parent document.

The revised version of GoldSim was qualified in accordance with IM-PRO-004, *Qualification of Software*. The updated software was obtained from Software Configuration Management in accordance with IM-PRO-003, *Software Management*, and was installed in accordance with installation test instructions listed in *User Information Document for: GoldSim Version 9.60* (DOE 2007 [DIRS 181108], Section 3.1). GoldSim was used to develop the analyses for the TSPA-LA Model within the limitations and the range of verification guidance presented in Appendix G of the *User's Guide, GoldSim Probabilistic Simulation Environment, Version 9.60* (GoldSim Technology Group 2007 [DIRS 181727]). Additional information regarding the GoldSim software is discussed in Section 3.8 of the parent document, Section 3.8[a] of this addendum, and in the documents listed in Table 3-8[a].

7.2.2[a] Verification of Dynamically Linked Libraries as Single Modules and in an Integrated System

No change.

7.2.3[a] Verification of Inputs in Total System Performance Assessment Input Database

Parameters used in the analyses presented in this addendum are documented in the TSPA Input Database described in Section 4.7 of the parent document, with additional detail provided in Section 7.2.3 of the parent document. Each TSPA-LA Model simulation described in this addendum accesses the TSPA Input Database in order to obtain values for each model's parameters from sources listed in Table 4-1 of the parent document and Table 4-1[a] of this addendum. Parameter values are maintained as originally entered, without transformation or post-processing, and are manually entered into the database (this is described in more detail in Section 7.2.3 of the parent document). Figure 4-3 of the parent document shows the structural framework of the TSPA Input Database, which is described in Section 4.7 of the parent document.

The value of every parameter is checked and verified before using it for a performance-assessment analysis. Any discovered errors are documented in the TSPA-LA Model Log; corrected values are entered into the database and, if determined to be necessary by an impact analysis (e.g., Appendix P of the parent document), the impacted calculations are performed again. The parameter verification is documented on the Parameter Verification Form (Section 4.7 of the parent document). Only users with access to the TSPA-LA Model's controlled-access input database can verify parameter values. The verification process includes recording the checker's name, along with the date and time, in order to identify the last user who changed any parameter categories. Strict control of access and documentation increases confidence in the security, integrity, and traceability of information entered into, or downloaded from, the TSPA Input Database. In this same way, the TSPA Input Database was verified with

the new information (listed in Table 4-1[a]) that supports the analyses documented in this addendum.

7.2.4[a] Verification of Single Model Components

The TSPA-LA Model is composed primarily of submodels derived from abstraction models that are documented in analysis and/or model reports. Verification and validation activities used to improve confidence in numerical models implemented in the TSPA-LA Model are described in Section 7.2.4 of the parent document. As discussed in Section 7.2.4 of the parent document, the approach to verification is to compare TSPA-LA Model file results with results of stand-alone implementations reported in analysis and/or model reports or validation test reports, where applicable. Additional verification activities that were not included in the parent document are presented in Section 7.2.4.1.12[a] of this addendum. These additional verification activities were conducted only for the Human Intrusion Modeling Case. Verification tests of input and submodels specific to the Human Intrusion Modeling Case included verifying inputs in the TSPA database, verifying the submodels (such as the borehole pipe model), and verifying proper coupling among submodels.

7.2.4.1[a] Verification Results

The results of the submodel implementation verification activities are presented in Sections 7.2.4.1.1 through 7.2.4.1.11 of the parent document. These apply to TSPA-LA Model v5.005 without change. One additional verification of the Human Intrusion Submodel is provided in Section 7.2.4.1.12[a] of this addendum. This verification activity consists of verifying Human Intrusion Submodel inputs in the TSPA-LA Model database, verifying selected Human Intrusion Submodels (such as the borehole pipe model), and verifying proper coupling among Human Intrusion Submodels. The results of the verification of the Human Intrusion Submodel (output DTN: MO0801TSPAMVAC.000 [DIRS 185080]) are discussed in Section 7.2.4.1.12[a].

7.2.4.1.1[a] Drift Seepage

No change.

7.2.4.1.2[a] Drift Wall Condensation Submodel Verification

No change.

7.2.4.1.3[a] Engineered Barrier System Chemical Environment

No change.

7.2.4.1.4[a] Waste Package and Drip Shield Degradation

No change.

7.2.4.1.5[a] Waste Form Degradation and Mobilization

No change.

7.2.4.1.6[a] Engineered Barrier System Transport

No change.

7.2.4.1.7[a] Unsaturated Zone Transport

No change.

7.2.4.1.8[a] Saturated Zone Flow and Transport

No change.

7.2.4.1.9[a] Biosphere

No change.

7.2.4.1.10[a] Igneous Scenario Class Modeling Cases

No change.

7.2.4.1.11[a] Seismic Scenario Class Modeling Cases

No change.

7.2.4.1.12[a] Human Intrusion Scenario

Verification of the Human Intrusion Scenario focuses on an alternate implementation of the UZ Transport Submodel where the radionuclide transport from the engineered barrier system (EBS) to the saturated zone (SZ) is confined to a borehole penetrating the waste package (WP) and extending through the unsaturated zone (UZ) to the SZ. A simplified deterministic analysis was performed in order to verify the implementation of the Human Intrusion Submodel. The verification test utilized one Latin hypercube sample (LHS) vector for the epistemic and aleatory parameter values. Beginning at 200,000 years into the simulation, the source term for the realization was redefined as a single release into the EBS of one gram of the non-sorbing radionuclide ^{129}I and one gram of the sorbing radionuclide ^{237}Np. The rest of the radionuclide inventory was set to zero for the simulation. This allowed a comparison of the simple mass release from the EBS to the mass leaving the borehole at the water-table. A specific percolation rate of 25 mm/yr was assigned for the simulation and was used to check that both the EBS and the borehole-pipe element were using the same rate (as specified in the model implementation, Section 6.7.3.2 of the parent document) and to approximate the time needed for the cumulative mass release from the borehole to reach 0.5 grams for a simulation without considering matrix diffusion. Two simulations were performed: the first allowed for matrix diffusion into the surrounding rock matrix and the second did not consider matrix diffusion. The selected realization is number 8,309 (out of 9,000 total realizations) and represents epistemic vector 277 and aleatory vector 29 (output DTN: MO0710ADTSPAWO.000 [DIRS 183752]). The aleatory vector 29 is defined as a CSNF WP release from a WP located in percolation subregion 4.

The source term was implemented by adding the radionuclide mass for ^{129}I and ^{237}Np to the CSNF interface cell representing the WP outer corrosion barrier (OCB) during the 250-year

timestep beginning 200,000 years into the simulation. To ensure that most of the mass would reach the borehole rapidly, no diffusion was allowed from the interface cell back to the upstream cell representing the corrosion products domain. The selected percolation rate was implemented by changing the input value for the percolation rate for the borehole to 25 mm/yr for any CNSF WP release from a WP located in percolation subregion 4. As part of this verification, simulation results were examined to make sure that the CSNF EBS seepage feed (model parameter *Seepage_Flux_Feed_EBS*) was set to 0.00081 m^3/year, the product of the borehole area (0.0324 m^2), and the percolation rate of 25 mm/yr. The outflow rate from the borehole pipe element was also checked and was given to be 2.56674 x 10^{-11} m^3/s (0.00081 m^3/year).

For both simulations, 99.99 percent of the ^{129}I and 99.98 percent of the ^{237}Np are released from the EBS into the borehole in the first timestep. Also, ^{233}U produced by decay of ^{237}Np is released from the EBS. The results for the borehole release to the SZ from the two simulations are presented on Figure 7.2-17[a]. For the simulation with matrix diffusion considered, it can be seen on Figure 7.2-17[a] that the total release of ^{129}I from the borehole is very close to the applied EBS mass release of one gram (0.9999 grams). Because of decay, the total release of ^{237}Np is only 0.9785 g. When the product of the mass release of ^{233}U, its daughter product from the borehole and the ratio of the atomic weights of ^{237}Np and ^{233}U, is added to the ^{237}Np release the total release increases to 0.9970 g. Note that a very small amount (3.539 x 10^{-7} g) of ^{229}Th, ^{233}U's daughter product, is also produced. For ^{129}I, there is a short delay of the mass release associated with the diffusion of mass between the fracture and rock matrix. This delay is approximately 1,250 years as defined by the 0.5 gram breakthrough level in the cumulative results. For ^{237}Np, the delay is approximately 64,000 years. Note that the matrix retardation for ^{237}Np in this simulation is 47.8, which is close to 51.2, the ratio of the breakthrough time of ^{237}Np to that of ^{129}I, which has a retardation coefficient of 1.0.

As shown on Figure 7.2-17[a], for the simulation without matrix diffusion, most of the ^{129}I and ^{237}Np mass leaving the EBS has exited the borehole within one timestep (250 years). Based on the volumetric rate of water entering the borehole (0.00081 m^3/year), the fracture area of 0.0004211 m^2 within the borehole cross-section and the fracture saturation of 0.0253, over the 190 m borehole length (Section 6.7.3.2 of the parent document) the advective transport velocity in the fracture, is approximately 76 m/year, which translates into an advective transport time of 2.5 years. A comparison of the time between the mass application and the time of the 0.5 gram breakthrough level in the cumulative mass release curve, with a transport time of 2.5 years, is not possible because of the coarseness of the simulation timesteps. By the end of the timestep starting at 200,000 years, 99.04 percent of ^{129}I and 99.03 percent of ^{237}Np have exited the borehole. This release pattern is consistent with a very short transport time through the borehole when matrix diffusion is not considered.

The analysis presented above verifies that the UZ Transport Submodel for the Human Intrusion Scenario is implemented correctly. This verification test for the submodel specific to the Human Intrusion Modeling Case, combined with the verification of the TSPA-LA Model's submodels documented in the parent document, are used to assert that the Human Intrusion Scenario is verified.

7.2.5[a] Verification of Coupling among Submodels and Model Components

No change.

7.2.6[a] Verification of Range of Applicability of Submodels and Model Components

A discussion of the verification of the range of applicability of submodels and model components is provided in Section 7.2.6 of the parent document. An assessment of the range of validity for all TSPA-LA Model submodels (output DTN: MO0709TSPALAMO.000 [DIRS 182981]) was conducted over the specified range of validity. The summary results of this assessment were inadvertently left out of Section 7.2.6 of the parent report. The summary results of this verification assessment are documented below. The records that document the implementation and checking of the TSPA-LA Model are located in the relevant records package.

During the development of the TSPA-LA Model, fatal error encounters and flag setting conditions signaling an out-of-range condition did occur. In many cases, when an out-of-range condition occurred, the provided abstractions were revised to preclude the occurrence of the out-of-range condition. The abstractions were revised to: (1) constrain the calculated values by removing undue uncertainty that could broaden the calculated results, (2) expand the range of validity of the abstraction, or (3) provide additional guidance on how to handle out-of-range conditions. However, an assessment of the range of validity for all TSPA-LA Model submodels (output DTN: MO0709TSPALAMO.000 [DIRS 182981]) revealed that for the 1,000,000-year performance runs, three submodels of the Waste Form Degradation and Mobilization Model Component were applied below the lower temperature limit in the specified range of validity. For the 10,000-year simulations, the temperatures remain within the range of validity.

In the 1,000,000-year performance runs, WPs return to ambient temperatures in the modeled duration. The ambient temperature from the EBS TH Environment Submodel (Section 6.3.2) can be as low as 17°C. The lower temperature limit for the In-Package Chemistry Abstraction (SNL 2007 [DIRS 180506], Section 1[a]) and the Dissolved Concentration Limits Abstraction (SNL 2007 [DIRS 177418], Section 6.3.3.3) is 25°C. The lower temperature limit for the HLW Glass Waste Form Degradation Abstraction is 20°C (BSC 2004 [DIRS 169988], Section 1.2). As discussed below, the application of these three submodels below the stated range of applicability is not expected to have a significant affect on the EBS release calculations; therefore, the TSPA-LA Model applies the provided abstractions below the lower temperature limits without further modifications.

The lower temperature limit for the range of applicability of the In-Package Chemistry Abstraction is 25°C. The pH and ionic strength abstractions were developed for conditions at 25°C, but there is no explicit temperature dependence in the abstractions for pH and ionic strength within the waste form domain. Through the use of sensitivity studies and conservative modeling choices, the effects of temperature were determined to be negligible and the range of applicability was extended up to temperatures of 100°C (SNL 2007 [DIRS 180506], Section 6.6[a] and 8.1[a]). Because of the pH buffering capacity in the waste form cells results in a high degree of confidence in the minimum and maximum pH at 25°C (SNL 2007 [DIRS 180506], Section 6.10.8.1[a]) and because sensitivity studies reveal that temperature has a

negligible effect on ionic strength (SNL 2007 [DIRS 180506], Section 6.6.6 and 6.6[a]), the application of pH and ionic strength abstractions developed at 25°C to temperatures as low as 17°C is not anticipated to produce results that are outside the range of uncertainty captured in the abstractions for pH and ionic strength.

The lower temperature limit for the range of applicability of the Dissolved Concentration Limits Abstraction is 25°C. Because actinides in carbonate systems, such as those that will prevail in the EBS, have retrograde solubility, abstractions for the solubility of actinides were developed for conditions at 25°C and include additional uncertainty to expand the temperatures range of applicability up to 100°C, but there is no explicit temperature dependence in the abstractions for actinide solubility in the EBS (SNL 2007 [DIRS 177418], Section 6.3.3.3). The TSPA-LA Model applies the Dissolved Concentration Limits Abstraction at temperatures below 25°C. Because actinides have retrograde solubility, it is possible that dissolved concentration limits below 25°C could be higher than those implemented in the TSPA-LA Model. But because the Dissolved Concentration Limits Abstraction includes additional uncertainty to account for differences in temperature conditions (SNL 2007 [DIRS 177418], Section 6.3.3), it is anticipated that dissolved concentration limits at lower temperatures would be within the range of uncertainty captured in the Dissolved Concentration Limits Abstraction. Radium solubility is higher at higher temperatures and the abstraction developed at 100°C is conservatively applied to all temperatures below 100°C.

The lower temperature limit for the range of applicability of the HLW Glass Waste Form Degradation Abstraction is 20°C. The HLW Glass Waste Form Degradation Abstraction has explicit temperature dependence in the rate expression and below 20°C, the TSPA-LA Model applies the applicable temperature in the rate expression. The lower temperature limit of the HLW Glass Waste Form Degradation Abstraction was determined by the ranges considered in the experimental results used to validate the rate model (BSC 2004 [DIRS 169988], Section 7.3), which showed that the Arrhenius relationship for glass degradation rate is maintained between 20°C and 90°C. This relationship is not anticipated to change between 17°C and 20°C. Therefore, applying the rate model at 17°C to high-level radioactive waste (HLW) glass that is still intact within the waste form domain when the WP temperatures drop below 20°C, is not expected to have any effect on mass transport calculations.

7.3[a] MODEL STABILITY

7.3.1[a] Statistical Stability

As outlined in Section 7.3 of the parent document, the calculated total mean annual dose is an expected value over epistemic and aleatory uncertainties of estimates of annual dose (Equation 7.3-1 of the parent document). The expectation of annual dose over aleatory uncertainty is evaluated first, the result of which is called (for brevity) ‘expected annual dose’. The accuracy of the integral over aleatory uncertainty is discussed in Section 7.3.2 of the parent document. The integral of expected annual dose over epistemic uncertainty is referred to as the mean annual dose and is evaluated numerically by using a Monte Carlo technique. The mean annual dose is statistically stable if the sample size employed in the Monte Carlo technique produces an adequate estimate of the mean annual dose.

Section 7.3.1 of the parent document presents analyses that demonstrate the statistical stability of the total mean annual dose (summed over all modeling cases) and the mean annual dose for each modeling case for TSPA-LA Model v5.000. This section compares uncertainty and sensitivity analyses generated by TSPA-LA Model v5.000 and TSPA-LA Model v5.005 and concludes that the results from TSPA-LA Model v5.005 are also statistically stable. Additionally, this section describes the bootstrap sampling procedure (Davison and Kuonen 2002 [DIRS 184463]) used in this addendum to compute confidence intervals for the total mean annual dose for TSPA-LA Model v5.005. Confidence intervals are presented for both 20,000 years (Figure 7.3.1-47[a]) and 1,000,000 years (Figure 7.3.1-48[a]).

7.3.1.1[a] Replicated Sampling Procedure (Procedure for Demonstrating Stability)

No change.

7.3.1.2[a] Stability Analysis Results for Modeling Cases

Human Intrusion Modeling Case—Because of the error involving the timesteps used in the Human Intrusion Modeling Case (Appendix P, Table P-6, Item 6 of the parent document), coarseness of the temporal stability analysis for TSPA-LA Model v5.000 (Section 7.3.1.2), and absence of sensitivity analysis results for the Human Intrusion Modeling Case in the parent document, the statistical stability of the Human Intrusion Modeling Case is demonstrated in this addendum by repeating the replicated sampling procedure. Figure 7.3.1-14a[a] shows the mean annual dose for each of the three replicates of the Human Intrusion Modeling Case, along with the median and the 5th and 95th percentiles of the distribution of the expected annual dose. Figure 7.3.1-14b[a] displays the confidence interval for this modeling case. The high degree of similarity among replicates and the very narrow confidence interval indicates that the mean annual dose for this modeling case is estimated accurately, and the sample size of 300 is adequate.

7.3.1.3[a] Stability Analysis Results for Total Mean Annual Dose

No change.

7.3.1.4[a] Conclusion

No change.

7.3.1.5[a] Statistical Stability of Model Results

As discussed in Section 7.3.1 of the parent document, a replicated sampling procedure provides an effective approach to estimating the potential sampling error in quantities derived from Latin hypercube sampling (Iman 1982 [DIRS 146012]). With this procedure, the LHS is repeatedly generated with different random seeds. Each LHS is used to produce an estimate of the mean annual dose. The ensemble of estimates of the mean annual dose is used to compute an overall mean and standard error. Confidence intervals for the mean annual dose are estimated by means of the *t*-distribution. Appendix J, Section J4.10, of the parent document provides details on the replicated sampling procedure and the application of the *t*-distribution. The analysis presented in the parent document concludes that the LHS size of 300 is sufficient to produce a statistically stable estimate of the total mean annual dose and of the mean annual dose for each modeling

case. The confidence intervals provide a quantitative assessment of the accuracy of the estimates of total mean annual dose and mean annual dose for each modeling case.

Section 4[a] identifies additional direct inputs used in generating the TSPA-LA Model results presented in this addendum. Appendix P[a] lists the changes and corrections made to the TSPA-LA Model in updating from v5.000 to v5.005. Model changes summarized in Appendix P[a] are relatively minor in that the features, events, and processes (FEPs) that determine radionuclide releases from the repository remain constant in the TSPA-LA Model (also see Appendix P of the parent document). Moreover, the LHSs used to generate results from the two models are nearly identical. Table 7.3.1-1[a] summarizes the differences in the sampled parameters in the two LHSs. Both LHSs are of the same size (300) and, with three exceptions, the pairing of sampled values is the same in each LHS. The technique chosen to correct the distributions for FHH_Isotherm_k_CP_a and FHH_Isotherm_s_CP_a resulted in new orderings of the sampled values for these parameters, and the removal of an unintended correlation between WRIP_beta_rand_a and PCE_Delta_pCO2_a (Table K3-2) resulted in a new ordering for the sampled values for WRIP_beta_rand_a. As a consequence, the two LHSs differ in the pairing of the sampled values for these three parameters with the sampled values of the other parameters. Because the changes are relatively minor and both model versions use nearly identical LHSs, the replicated sampling procedure is not repeated with TSPA-LA Model v5.005, except for the Human Intrusion Modeling Case (Section 7.3.1.2[a]). Instead, results from TSPA-LA Model v5.000 are compared to results from TSPA-LA Model v5.005 to demonstrate the statistical stability of results from TSPA-LA Model v5.005.

7.3.1.5.1[a] Expected Annual Dose for Nominal Modeling Case

Figure 7.3.1-17[a] shows the distribution of expected annual dose for 1,000,000 years and statistics for this distribution for the Nominal Modeling Case for (a) TSPA-LA Model v5.000 and (b) TSPA-LA Model v5.005. The general trends and the range of uncertainty in expected annual dose are similar for both models. Because of the correction of the error in computing the weld volume (Appendix P, Section P6, of the parent document), weld flaws are roughly three times more likely to occur in the results from TSPA-LA Model v5.005 than in the results from TSPA-LA Model v5.000. Consequently, weld failures occur earlier in the TSPA-LA Model v5.005 results, as is evident in the few realizations showing expected dose prior to 100,000 years. Despite the earlier occurrence of WP failures in the results from TSPA-LA Model v5.005, Figure 7.3.1-18[a] shows that the statistics for the distribution of expected annual dose are similar for both models, and the scatterplots in Figure 7.3.1-19[a] illustrate (at the selected times) that the expected annual dose is the same for most epistemic sample elements. Expected annual dose increases in TSPA-LA Model v5.005 results after 600,000 years for a few sample elements are due to the corrections to models for waste form and iron oxyhydroxide colloids (Appendix P, Section P18, and Table P-6, Items 5 and 12 of the parent document). Comparison of Figure K4.5-2a of the parent document and Figure K4.5-2a[a] demonstrates that the uncertain inputs that predominately determine uncertainty in expected annual dose are almost identical for both model versions. Because (1) model changes are relatively minor, (2) both models use nearly identical LHSs of the same size, (3) model results show close agreement in both the magnitude and range of uncertainty of expected annual dose, (4) the uncertain inputs that predominately determine uncertainty in expected annual dose are identical for both versions, and (5) TSPA-LA Model v5.000 produces a statistically stable estimate of mean annual dose

(demonstrated in Section 7.3.1.2 of the parent document), it is reasonable to conclude that the sample size used in TSPA-LA Model v5.005 produces a statistically stable estimate of mean annual dose for the Nominal Modeling Case.

7.3.1.5.2[a] Expected Annual Dose for Drip Shield Early Failure Modeling Case

Figure 7.3.1-20[a] and Figure 7.3.1-21[a] show statistics for the distribution of expected annual dose for 20,000 years and 1,000,000 years, respectively, for the Drip Shield Early Failure (EF) Modeling Case. The corresponding distributions for expected annual dose from TSPA-LA Model v5.000 and TSPA-LA Model v5.005 are shown on Figure 8.2-3 of the parent document and Figure 8.2-3[a], respectively. The general trends and the range of uncertainty in expected annual dose are similar for both models. The small but general reduction in expected annual dose for TSPA-LA Model v5.005 results for 20,000 years (Figures 7.3.1-20[a] and 7.3.1-22[a]) is due to the change in the calculation of the seepage fraction (Appendix P, Section P2). Figure 7.3.1-22[a] and Figure 7.3.1-23[a] show that, for most sample elements, the expected annual dose is similar in both model versions. The increase in expected annual dose in TSPA-LA Model v5.005 results for a few sample elements is due to the corrections to models for waste form and iron oxyhydroxide colloids (Appendix P, Section P18, and Table P-6, Items 5 and 12 of the parent document). In particular, the outlying value of expected annual dose at 1,000 years is due to a contribution to expected annual dose from ^{241}Am sorbed to iron oxyhydroxide colloids, which transports relatively rapidly through the natural barriers. For most sample elements, ^{241}Am contributes negligibly to expected annual dose in both model versions. The decrease in expected annual dose in TSPA-LA Model v5.005 results for a few sample elements in Figure 7.3.1-23[a] is due to the change in longitudinal dispersivity, which reduces the contribution to expected annual dose of ^{226}Ra (Appendix P, Section P15 of the parent document). Despite these differences, Figure 7.3.1-22[a] and Figure 7.3.1-23[a] demonstrate that the distribution of expected annual dose is similar for both model versions.

The comparison of Figure K5.7.1-2a of the parent document and Figure K5.7.1-2a[a] demonstrates that the uncertain inputs that predominately determine uncertainty in expected annual dose before 10,000 years are almost identical for both model versions; the comparison of Figure K5.7.1-4a and Figure K5.7.1-4a[a] shows the same conclusion after 10,000 years. Moreover, Section 7.7.1.2 and Section 7.7.1.2[a] demonstrate that the processes affecting radionuclide releases are essentially unchanged from TSPA-LA Model v5.000. It is reasonable to conclude that the sample size used in TSPA-LA Model v5.005 produces a statistically stable estimate of mean annual dose for the Drip Shield EF Modeling Case because (1) model changes are relatively minor, (2) both models use nearly identical LHSs of the same size, (3) model results show close agreement in both the magnitude and range of uncertainty of expected annual dose, (4) the uncertain inputs that predominately determine uncertainty in expected annual dose are identical for both versions, and (5) TSPA-LA Model v5.000 produces a statistically stable estimate of mean annual dose (demonstrated in Section 7.3.1.2 of the parent document).

7.3.1.5.3[a] Expected Annual Dose for Waste Package Early Failure Modeling Case

Figure 7.3.1-24[a] and Figure 7.3.1-25[a] show statistics for the distribution of expected annual dose for 20,000 years and 1,000,000 years, respectively, for the Waste Package EF Modeling Case. The corresponding distributions for expected annual dose from TSPA-LA Model v5.000

and TSPA-LA Model v5.005 are shown on Figure 8.2-5 of the parent document and Figure 8.2-5[a], respectively. The general trends and the range of uncertainty in expected annual dose are similar for both models. Expected annual dose between about 10,000 years and 14,000 years is generally smaller in TSPA-LA Model v5.005 results as shown in Figure 7.3.1-24[a] due to corrections in the calculations for the seepage fraction (Appendix P, Section P2). This item is addressed by TSPA-LA Model v5.005 in Section 6.3.3[a]. Figure 7.3.1-26[a] and Figure 7.3.1-27[a] show that the expected annual dose is the same for most epistemic sample elements. The decrease in expected annual dose (Figure 7.3.1-27[a]) in TSPA-LA Model v5.005 results for a few sample elements is due to the change in longitudinal dispersivity, which reduces the contribution to expected annual dose of ^{226}Ra (Appendix P, Section P15 of the parent document). The comparison of Figure K5.7.2-2a of the parent document and Figure K5.7.2-2a[a] demonstrates that the uncertain inputs that predominately determine uncertainty in expected annual dose before 10,000 years are identical for both model versions; the comparison of Figure K5.7.2-4a of the parent document and Figure K5.7.2-4a[a] shows the same conclusion after 10,000 years. Moreover, Section 7.7.1.1 of the parent document and Section 7.7.1.1[a] demonstrate that the processes affecting radionuclide releases are essentially unchanged from TSPA-LA Model v5.000. Because of these similarities, and because TSPA-LA Model v5.000 produces a statistically stable estimate of mean annual dose for the Waste Package EF Modeling Case (as demonstrated in Section 7.3.1.2 of the parent document), it is reasonable to conclude that the sample size used in TSPA-LA Model v5.005 produces a statistically stable estimate of mean annual dose for the Waste Package EF Modeling Case.

7.3.1.5.4[a] Expected Annual Dose for Igneous Intrusion Modeling Case

Figure 7.3.1-28[a] and Figure 7.3.1-29[a] show statistics for the distribution of expected annual dose for 20,000 years and 1,000,000 years, respectively, for the Igneous Intrusion Modeling Case. The corresponding distributions for expected annual dose from TSPA-LA Model v5.000 and TSPA-LA Model v5.005 are shown on Figure 8.2-7 of the parent document and Figure 8.2-7[a], respectively. The general trends and the range of uncertainty in expected annual dose are similar for both models, although the expected annual dose is generally reduced in magnitude after 10,000 years in the results from TSPA-LA Model v5.005. This reduction is a consequence of the corrected distribution for the longitudinal dispersivity (LDISP in Table K3-2), as described in Appendix P, Section P15 of the parent document. Figure 7.3.1-30[a] and Figure 7.3.1-31[a] show that, for most epistemic sample elements, the expected annual dose is the same for both models. However, prior to 3,000 years, for a few epistemic sample elements the expected annual dose is much higher in the results from TSPA-LA Model v5.005, due to the corrections to models for iron oxyhydroxide colloids (Appendix P, Section P18, and Table P-6, Items 5 and 12 of the parent document). In particular, the outlying values of expected annual dose at 1,000 years are due to contributions to the expected annual dose from ^{241}Am sorbed to iron oxyhydroxide colloids, which transport relatively rapidly through the natural barriers. For most sample elements, ^{241}Am contributes negligibly to expected annual dose in either model version. At 100,000 years, the outlying values of expected annual dose in TSPA-LA Model v5.005 results are due to contributions to expected annual dose from ^{239}Pu sorbed to iron oxyhydroxide colloids, which were not observed in the results from TSPA-LA Model v5.000 due to the errors affecting iron oxyhydroxide colloids. Additionally, after 100,000 years, the expected annual dose for most epistemic sample elements is somewhat less in the results from TSPA-LA Model v5.005; for a few sample

elements, the expected annual dose is much lower than in the results from TSPA-LA Model v5.000. The reduction in expected annual dose is attributable to the reduction in the contribution of ^{226}Ra (compare Figure 8.2-8b of the parent document and Figure 8.2-8b[a]), which in turn results from the corrected distribution for the longitudinal dispersivity (Appendix P, Section P15 of the parent document).

The comparison of Figure K6.7.1-2a of the parent document and Figure K6.7.1-2a[a] demonstrates that the uncertain inputs that predominately determine uncertainty in expected annual dose before 10,000 years are the same for both model versions; the comparison of Figure K6.7.2-2a of the parent document and Figure K6.7.2-2a[a] shows the same conclusion after 10,000 years. Moreover, Section 7.7.1.3 of the parent document and Section 7.7.1.3[a] demonstrate that the processes affecting radionuclide releases are essentially unchanged from TSPA-LA Model v5.000. Because of these similarities, and because TSPA-LA Model v5.000 produces a statistically stable estimate of mean annual dose for the Igneous Intrusion Modeling Case (as demonstrated in Section 7.3.1.2 of the parent document), it is reasonable to conclude that the sample size used in TSPA-LA Model v5.005 produces a statistically stable estimate of mean annual dose for the Igneous Intrusion Modeling Case.

7.3.1.5.5[a] Expected Annual Dose for Volcanic Eruption Modeling Case

No changes to the TSPA-LA Model affected the evaluation of the Volcanic Eruption Modeling Case. Therefore, the results for this modeling case are not different from those reported in the parent document.

7.3.1.5.6[a] Expected Annual Dose for Seismic Ground Motion Modeling Case

Figure 7.3.1-32[a] shows statistics for the distribution of expected annual dose for 20,000 years for the Seismic GM Modeling Case. The corresponding distributions for expected annual dose from TSPA-LA Model v5.000 and TSPA-LA Model v5.005 are shown in Figure 8.2-11a of the parent document and Figure 8.2-11a[a], respectively. The general trends and the range of uncertainty in expected annual dose are similar for both models. Figure 7.3.1-33[a] shows that expected annual dose is essentially unchanged for all epistemic sample elements. The high degree of similarity in the 20,000-year results from both model versions can be attributed to the simplifications to the seismic damage abstractions for this modeling case (Section 7.3.2.6 of the parent document) and to the dominant contribution of ^{99}Tc to expected annual dose for this modeling case (Figure 8.2-12a of the parent document and Figure 8.2-12a[a]). The changes to the seismic damage models summarized in Appendix P[a] do not affect the 20,000-year results because of the simplifications to the seismic damage abstractions (Section 7.3.2.6 of the parent document), and few of the errors detailed in Appendix P have any effect on the mobilization or transport of ^{99}Tc. The comparison of Figure K7.7.1-2a of the parent document and Figure K7.7.1-2a[a] shows that the uncertain model inputs that are important contributors to the uncertainty in expected annual dose for the Seismic GM Modeling Case before 10,000 years are the same for both model versions. Because of these similarities, and because TSPA-LA Model v5.000 produces a statistically stable estimate of mean annual dose for the Seismic GM Modeling Case (as demonstrated in Section 7.3.1.2 of the parent document), it is reasonable to conclude that the sample size used in TSPA-LA Model v5.005 produces a statistically stable estimate of mean annual dose for the Seismic GM Modeling Case for 20,000 years.

Figure 7.3.1-34[a] shows the distribution of expected annual dose for 1,000,000 years and statistics for this distribution for the Seismic GM Modeling Case for (a) TSPA-LA Model v5.000 and (b) TSPA-LA Model v5.005. Due primarily to improving upon the conservative treatment of synergisms between seismic events and nominal corrosion processes (Appendix P, Section P3 of the parent document), in many sample elements fewer CSNF WPs experience seismic damage in the results from TSPA-LA Model v5.005 (shown by a comparison of Figure 8.1-5b of the parent document and Figure 8.1-5b[a]), which in turn results in the reduction in magnitude of expected annual dose before about 300,000 years. Because seismic damage occurs to fewer CSNF WPs, these WPs remain intact until compromised by nominal corrosion processes, which are relatively unchanged (see discussion of Nominal Modeling Case results in Section 7.3.1.5.1[a]). Thus, after 300,000 years, the general trends in expected dose are more representative of the expected dose due to nominal corrosion processes (compare Figure 7.3.1-34b[a] to Figure 7.3.1-17[a]). Statistics for the distribution of expected annual dose for the Seismic GM Modeling Case for 1,000,000 years are shown on Figure 7.3.1-35[a]; Figure 7.3.1-36[a] shows comparisons of expected annual dose for each sample element at selected times. These figures illustrate the general reduction in expected annual dose due to improving the treatment of synergisms between seismic damage and nominal corrosion processes. However, for a few sample elements, expected annual dose is higher at 600,000 years (Figure 7.3.1-36c[a]) and 1,000,000 years (Figure 7.3.1-36d[a]) in the results from TSPA-LA Model v5.005. For these sample elements, increases in expected annual dose are observed at these times because WPs are less likely to be breached by earlier seismic events, which in turn means that more of the waste inventory is contained in the EBS until later times, when WPs are breached due to general corrosion. In addition, the corrections to the calculation of stability of iron oxyhydroxide colloid can lead to larger plutonium releases for those sample elements in which general corrosion failures occur prior to 1,000,000 years.

Despite the differences evident in expected annual dose, Figure 7.3.1-35[a] shows that the range of uncertainty in expected annual dose is similar for both model versions. The comparison of Figure K7.7.2-2a of the parent document and Figure K7.7.2-2a[a] shows that the uncertain model inputs that are important contributors to the uncertainty in expected annual dose for the Seismic GM Modeling Case for 1,000,000 years are generally the same for both model versions. Section 7.7.1.4 of the parent document and Section 7.7.1.4[a] demonstrate that, once WP failure has occurred, the subsequent processes affecting radionuclide releases are essentially unchanged from TSPA-LA Model v5.000. Because of these similarities, and because TSPA-LA Model v5.000 produces a statistically stable estimate of mean annual dose for the Seismic GM Modeling Case (as demonstrated in Section 7.3.1.2 of the parent document), it is reasonable to conclude that the sample size used in TSPA-LA Model v5.005 produces a statistically stable estimate of mean annual dose for the Seismic GM Modeling Case for 1,000,000 years.

7.3.1.5.7[a] Expected Annual Dose for Seismic Fault Displacement Modeling Case

Figure 7.3.1-37[a] and Figure 7.3.1-38[a] show statistics for the distribution of expected annual dose for 20,000 years and 1,000,000 years, respectively, for the Seismic Fault Displacement (FD) Modeling Case. The corresponding distributions for expected annual dose from TSPA-LA Model v5.000 and TSPA-LA Model v5.005 are shown on Figure 8.2-13 of the parent document and Figure 8.2-13[a], respectively. The general trends and the range of uncertainty in expected annual dose are similar for both models. Figure 7.3.1-39[a] and Figure 7.3.1-40[a] show that, for

most epistemic sample elements, the expected annual dose is the same for both models. However, prior to 3,000 years, for a few epistemic sample elements the expected annual dose is much higher in the results from TSPA-LA Model v5.005, due to the corrections to models for iron oxyhydroxide colloids (Appendix P, Section P18, and Table P-6, Items 5 and 12 of the parent document). Additionally, after 100,000 years, the expected annual dose for a few sample elements is much lower than in the results from TSPA-LA Model v5.000 due to the corrected distribution for the longitudinal dispersivity (Appendix P, Section P15 of the parent document). The comparison of Figure K7.8.1-2a of the parent document and Figure K7.8.1-2a[a] demonstrates that the uncertain inputs that predominately determine uncertainty in expected annual dose before 10,000 years are similar for both model versions; the comparison of Figure K7.8.2-2a of the parent document and Figure K7.8.2-2a[a] shows the same conclusion after 10,000 years. Moreover, because the processes that determine radionuclide releases following a fault displacement are similar to those investigated for the early failure modeling cases (i.e., advection and diffusion), and these processes are essentially the same in the Early Failure Modeling Cases for both model versions (as demonstrated by Sections 7.7.1.1 and 7.7.1.2 of the parent document and 7.7.1.1[a], and 7.7.1.2[a]), it is reasonable to conclude that the processes affecting radionuclide releases in the Seismic FD Modeling Case are essentially unchanged from TSPA-LA Model v5.000. Because of the similarities in model results, and because TSPA-LA Model v5.000 produces a statistically stable estimate of mean annual dose for the Seismic FD Modeling Case (as demonstrated in Section 7.3.1.2 of the parent document), it is reasonable to conclude that the sample size used in TSPA-LA Model v5.005 produces a statistically stable estimate of mean annual dose for the Seismic FD Modeling Case.

7.3.1.5.8[a] Total Mean Annual Dose for 20,000 Years

Figure 7.3.1-41[a] shows the distribution of total expected annual dose for 10,000 years and statistics for this distribution for (a) TSPA-LA Model v5.000 and (b) TSPA-LA Model v5.005. The general trends and the range of uncertainty in total expected annual dose are the same for both models. Figure 7.3.1-42[a] shows that the statistics for the distribution of total expected annual dose are similar for both models, and the scatterplots in Figure 7.3.1-43[a] illustrate (at the selected times) that the total expected annual dose is the same for most epistemic sample elements. The similarity in total expected annual dose from both model versions is due primarily to the similarity in expected annual dose from the Seismic GM Modeling Case (Section 7.3.1.5.6[a]) because this case is the dominant contributor to the total expected annual dose in both model versions (compare Figure 8.1-3 of the parent document to Figure 8.1-3[a]). The comparison of Figure K8.1-2a of the parent document and Figure K8.1-2a[a] demonstrates that the uncertain inputs that predominately determine uncertainty in total expected annual dose are the same for both versions. The comparison of Figure 8.1-3a of the parent document and Figure 8.1-3a[a] shows that the contribution of each modeling case to total mean annual dose is unchanged. Finally, Section 7.7.1[a] demonstrates that processes affecting radionuclide releases in each modeling case are essentially unchanged from TSPA-LA Model v5.000. In summary, it is reasonable to conclude that the sample size used in TSPA-LA Model v5.005 produces a statistically stable estimate of total mean annual dose for 20,000 years because (1) model changes are relatively minor, (2) both models use nearly identical LHSs of the same size, (3) model results show close agreement in both the magnitude and range of uncertainty of total expected annual dose, (4) the uncertain inputs that predominately determine uncertainty in total expected annual dose are identical for both versions, (5) the contribution of each modeling case

to total mean annual dose is unchanged, (6) important processes affecting radionuclide releases are unchanged, and (7) TSPA-LA Model v5.000 produces a statistically stable estimate of total mean annual dose (demonstrated in Section 7.3.1 of the parent document).

7.3.1.5.9[a] Total Mean Annual Dose for 1,000,000 Years

Figure 7.3.1-44[a] shows the distribution of total expected annual dose for 1,000,000 years and statistics for this distribution for (a) TSPA-LA Model v5.000 and (b) TSPA-LA Model v5.005. Figure 7.3.1-44[a] shows some differences in the general trend in total expected annual dose between the two sets of model results. The comparison of Figure 8.1-3b of the parent document and Figure 8.1-3b[a] shows that the differences in the trends in dose history result from changes that affect the Seismic GM Modeling Case. Specifically, as discussed in Section 7.3.1.5.6[a], improving upon the conservative treatment of synergisms between seismic events and nominal corrosion processes (Appendix P, Section P3, of the parent document) results in changes in total mean annual dose between about 100,000 years and 600,000 years. The range of uncertainty in total expected annual dose is compared for the two sets of model results in Figure 7.3.1-45[a]. Before 600,000 years, the reduction in the magnitude of the mean, median, 5th and 95th percentiles for total expected annual dose is due to the reduction in CSNF WP damage in the Seismic GM Modeling Case in the TSPA-LA Model v5.005. After 600,000 years, the reduction in magnitude of the mean of total expected annual dose is due to the corrected distribution for the longitudinal dispersivity (documented in Section 6.3.10[a] of this addendum), which results in a general reduction in the expected annual dose for the Igneous Intrusion Modeling Case (Section 7.3.1.5.4[a]). However, the range of uncertainty in total expected annual dose is generally the same for the two sets of model results.

Figure 7.3.1-46[a] illustrates (at the selected times) that the total expected annual dose is similar for many epistemic sample elements. Figure 7.3.1-46b[a] shows the reduction in the total expected annual dose at 200,000 years, which was noted in the comparison in the uncertainty in the total expected annual dose discussed above. The comparison of Figure K8.2-2a and Figure K8.2-2a[a] demonstrates that the uncertain inputs that predominately determine uncertainty in total expected annual dose after 10,000 years are the same for both versions. Finally, Section 7.7.1[a] demonstrates that processes affecting radionuclide releases in each modeling case are essentially unchanged from TSPA-LA Model v5.000.

In summary, although there are significant differences in the total expected annual dose between approximately 100,000 to 300,000 years, the important processes affecting radionuclide releases remain unchanged, and (1) model changes to the TSPA-LA Model v5.005 are relatively minor, (2) both models use nearly identical LHSs of the same size, (3) the uncertain inputs that predominately determine uncertainty in total expected annual dose are the same for both versions, (4) model results are similar in both the magnitude and range of uncertainty of total expected annual dose over the majority of the simulation, and (5) the relative contributions of each modeling case to total mean annual dose is unchanged. Since the TSPA-LA Model v5.000 produces a statistically stable estimate of total mean annual dose (demonstrated in Section 7.3.1 of the parent document), it is reasonable to conclude that the sample size used in TSPA-LA Model v5.005 produces a statistically stable estimate of total mean annual dose for 1,000,000 years.

7.3.1.6[a] Procedure for Computing Confidence Intervals

To provide a quantitative assessment of the accuracy of the estimate of total mean annual dose for TSPA-LA Model v5.005, a bootstrap sampling procedure is used to generate confidence intervals. Bootstrap simulation is a numerical procedure for estimating confidence intervals for statistics of interest. Given a sample of size *n*, the general approach in bootstrap simulation is to: (1) assume that the sample is an adequate approximation of the underlying distribution; (2) perform *r* replications of the set of values by randomly selecting, with replacement, *n* values from the sample; and (3) calculate *r* values for the statistic of interest. Davison and Kuonen (2002 [DIRS 184463]) provide an outline of the bootstrap procedure. The underlying assumption that the sample is an adequate approximation of the underlying distribution is justified because (1) the assumption has already been justified for TSPA-LA Model v5.000, as demonstrated by the stability analysis presented in Section 7.3.1 of the parent document; (2) TSPA-LA Model v5.005 produces results with uncertainty ranges similar to those observed for the TSPA-LA Model v5.000 results; and (3) uncertain inputs that dominate uncertainty in total expected annual dose are generally the same for TSPA-LA Model v5.000 and TSPA-LA Model v5.005.

Figure 7.3.1-47[a] displays the confidence interval for total mean annual dose for a simulation of 20,000 years, computed by using the bootstrap technique for both versions of the TSPA-LA Model. The upper and lower confidence bounds displayed on Figure 7.3.1-47[a] are the 97.5 percentile and 2.5 percentile, respectively, for the sampling distribution of total mean annual dose. Figure 7.3.1-47[a] shows that, with a probability 0.975, the true mean is estimated to lie more than an order of magnitude below the individual protection standard of 15 mrem for 10,000 years after permanent closure as specified in 10 CFR 63.311(a)(1) [DIRS 178394]. The narrowness of the confidence interval (less than ±0.2 mrem/yr) over the 20,000-year simulation and the relatively large separation between the confidence interval and the regulatory limit relative to the width of the confidence interval indicates that total mean annual dose for this modeling case is estimated with sufficient accuracy. The corresponding confidence interval for TSPA-LA Model v5.000 (Replicate 1) is shown for comparison.

Figure 7.3.1-48[a] shows the confidence interval for total mean annual dose for 1,000,000 years. Again, the upper and lower confidence bounds displayed on Figure 7.3.1-48[a] are the 97.5 percentile and 2.5 percentile, respectively, for the sampling distribution of total mean annual dose. Similar to the 20,000-year simulation, the narrowness of the confidence interval (less than ±0.5 mrem/yr) over the 1,000,000-year simulation and the separation between the confidence interval and the regulatory standard of 350 mrem specified in U.S. Nuclear Regulatory Commission Proposed Rule 10 CFR 63.311(a)(2) [DIRS 178394]) indicates that total mean annual dose for this modeling case is estimated with sufficient accuracy.

7.3.1.7[a] Conclusion

In Section 7.3.1 of the parent document, statistical stability of the total mean annual dose was evaluated by means of a replicated sampling procedure. The comparison of three estimates of total mean annual dose and the associated distributions of uncertainty in expected annual dose showed that the three independent LHS replicates produced statistically similar values of the total mean annual dose, as well as similar distributions of uncertainty in expected annual dose. The analysis concluded that the results of TSPA-LA Model v5.000 are statistically stable.

Statistical stability of the total mean annual dose presented in this addendum was evaluated by means of comparisons between TSPA-LA Model v5.000 and TSPA-LA Model v5.005 and results from these models, for all except the Human Intrusion Modeling Case. The relatively few changes between the models, and the similarities evident in the results of the models, support the conclusion that because the results of TSPA-LA Model v5.000 are demonstrated to be statistically stable, the results of TSPA-LA Model v5.005 are also statistically stable. Confidence intervals are computed for TSPA-LA Model v5.005 using a bootstrap procedure. The replicated sampling procedure was repeated for the Human Intrusion Modeling Case to demonstrate statistical stability.

Table 7.3.1-1[a]. Uncertainty Distribution Changes for TSPA-LA Model v5.005

Parameter Listing (Table K3-2)	TSPA-LA Model Description	TSPA-LA Model v5.000	TSPA-LA Model v5.005
LDISP	Section 6.3.10.2, Section 6.3.10.2[a], Table 6.3.10-2	Normal: (Log_{10}-transformed) Mean: 2.0 m Standard Deviation: 0.75 m	Truncated Normal: (Log_{10}-transformed) Mean: 2.0 m Standard Deviation: 0.75 m Maximum 2 Standard Deviation
FHH_Isotherm_k_CP_a	Table 6.3.8-4[a], Table P-6, 7	Uniform (1.048 to 1.370)	Uniform (1.030 to 1.326)
FHH_Isotherm_s_CP_a	Table 6.3.8-4[a], Table P-6, 7	Uniform (1.525 to 1.852)	Uniform (1.493 to 1.799)
KdU_Zeo_a	Section 6.3.9.2, Section 6.3.9.3, Table 6.3.9-2, Table P-6, 11	Piecewise Uniform (0 to 20 mL/g)	Piecewise Uniform (0 to 30 mL/g)
KdSe_Vit_a	Section 6.3.9.2, Section 6.3.9.3, Table 6.3.9-2, Table P-6, 10	Truncated log normal (1 to 25 mL/g)	Truncated lognormal (0 to 25 mL/g)
Kd_Np_Rev_U_Col_a	Section 6.3.7.6.2, Section 6.3.7.6.3, Table 6.3.7-64, Table 6.3.7-64[a], Table P-6, 8	Log Uniform (1 to 500 mL/g)	Log Uniform (10 to 500 mL/g)

INTENTIONALLY LEFT BLANK

7.3.2[a] Numerical Accuracy of Expected Annual Dose

No change.

7.3.2.1[a] Nominal Modeling Case

No change.

7.3.2.2[a] Waste Package Early Failure Modeling Case

No change.

7.3.2.3[a] Drip Shield Early Failure Modeling Case

No change.

7.3.2.4[a] Igneous Intrusion Modeling Case

No change.

7.3.2.5[a] Volcanic Eruption Modeling Case

No change.

7.3.2.6[a] Seismic Ground Motion Modeling Case

No change.

7.3.2.6.1[a] Seismic Ground Motion Modeling Case for 10,000 Years

No change.

7.3.2.6.1.1[a] Accuracy of Expected Annual Dose Calculations

No change.

7.3.2.6.1.2[a] Additivity in Annual Dose from Multiple Seismic Events

This section has been edited for clarity and replaces the corresponding section in the parent document.

As noted in Section 6.1.2.4.4 of the parent document, Equation 6.1.2-22 is based on the assumption that the annual dose from two or more events causing cumulative damage to WPs is reasonably approximated by the sum of the annual doses from the events modeled independently. Figure 7.3.2-12 of the parent document illustrates the change in annual dose at 10,000 years due to changes in damage fraction, after an event at 100 years, for epistemic realization 1. The change in annual dose is proportional to changes in damage fraction up to the damage fraction of about 10^{-5}. Beyond the damage fraction of 10^{-5}, annual dose does not increase proportionally with increasing damage fraction. Thus, when two or more seismic events cause cumulative damage fraction exceeding 10^{-5}, the additivity assumption results in an overestimate of the annual dose resulting from seismic events. The dose resulting from a single event causing

damage fraction exceeding 10^{-5} is not overestimated since this quantity is computed by interpolation between the level curves shown on Figure 7.3.2-9 of the parent document.

To estimate the degree of conservatism incurred by this additivity assumption, expected annual dose from one seismic event was calculated by evaluating the first integral term in Equation 6.1.2-22:

$$\bar{D}_{SG}\left(\tau\left|1,\mathbf{e}_i\right.\right) \quad \int_0^{\tau}\left(\lambda_1\left(\mathbf{e}_i\right)e^{-\lambda_1(\mathbf{e}_i)t}\left(\int_{A_{\min}}^{A_{\max}} D_{SG}\left(\tau\left|\left[1,t,A\right],\mathbf{e}_i\right.\right)d_{A1}\left(A\left|\mathbf{e}_i\right.\right)dA\right)\right)dt \qquad \text{(Eq. 7.3.2-1[a])}$$

The integral displayed in Equation 7.3.2-1[a] computes the expected annual dose from the first seismic event that damages co-disposed (CDSP) WPs. The second integral in Equation 6.1.2-22 computes the additional expected annual dose from the second and subsequent seismic events. Figure 7.3.2-13 of the parent document shows the expected annual dose from the first damaging seismic event; Figure 7.3.2-14 of the parent document shows the expected annual dose from all damaging seismic events for all 300 epistemic realizations. The comparison of the expected annual dose from the first damaging event to the expected annual dose from all damaging events shows that the second and subsequent damaging events add somewhat to the magnitude of the expected annual dose but do not change the magnitude or range of uncertainty to any great extent. Consequently, the additivity assumption, while conservative, does not result in a significant overestimate of the expected annual dose.

7.3.2.6.1.3[a] Simplifications to the Seismic Consequences Abstraction

No change.

7.3.2.6.2[a] Seismic Ground Motion Modeling Case for 1,000,000 Years

No change.

7.3.2.7[a] Seismic Fault Displacement Modeling Case

The analysis presented in the parent document showed the expected annual dose for the Seismic Fault Displacement Modeling Case is estimated with sufficient accuracy. However, the analysis showed the calculation's accuracy could be improved by further discretization of the aleatory variables. In particular, Figure 7.3.2-26 (of the parent document) compares the expected annual dose for five epistemic realizations for a base case of aleatory discretization and an expanded case; the expected annual dose generally increased by approximately 30 percent in the expanded case. To determine whether further refinement in aleatory discretization would lead to additional increases in expected annual dose, a second expanded case was formed and expected annual dose was evaluated. In this second expansion case the number of times of fault displacement events was increased from 6 to 23 and the number of damage areas was again increased from 3 to 5. The results did not show further increase in expected annual dose (output DTN: MO0801TSPAADSA.000 [DIRS 185078], file *LA_v5.000_SF_010800_10k_Dose_Compare_Rev01.JNB*), confirming the assessment that expected annual dose is computed with sufficient numerical accuracy.

7.3.2.8[a] Human Intrusion Modeling Case

No change.

7.3.3[a] Temporal Stability

This material supplements the corresponding section in the parent document.

Another issue related to the stability of the TSPA-LA Model results is temporal discretization of the model. In order to calculate transport of radionuclides, the TSPA-LA Model numerically solves partial differential equations in various submodels (e.g., FEHM for UZ transport) and model abstractions (e.g., SZ 3-D transport). The numerical solution involves computations with discrete timesteps which is referred to as temporal discretization. Temporal discretization may affect the accuracy of the solution of the differential equations and, thereby, affect the results of the TSPA-LA Model. Several different TSPA-LA Model runs were documented in Section 7.3.3 of the parent document that evaluated the potential for variability in model output due to timestep size. These analyses demonstrated that the output of the TSPA-LA Model is not significantly affected by refining the temporal discretization and concluded that the temporal discretization used in the TSPA-LA Model is adequate. Included in Section 7.3.3.6[a] of this addendum is an update to the temporal stability for the Human Intrusion Modeling Case necessitated by the correction of an error documented in Appendix P, Table P-6, Item 6, of the parent document. In addition, a temporal stability assessment of the Nominal Modeling Case has been added as Section 7.3.3.7[a] of this addendum.

7.3.3.1[a] Selection of Modeling Cases

No change.

7.3.3.2[a] Methodology

No change.

7.3.3.3[a] Waste Package Early Failure Modeling Case

No change.

7.3.3.4[a] Igneous Intrusion Modeling Case

No change.

7.3.3.5[a] Seismic Ground Motion Modeling Case

No change.

7.3.3.6[a] Human Intrusion Modeling Case

In the Human Intrusion Modeling Case, a single stylized intrusion occurs at 200,000 years. Annual dose is computed by the GoldSim component of the TSPA-LA Model for each combination of a sampled intrusion location (characterized by WP type, percolation rate and entry point into the SZ) and epistemic realization. For each epistemic realization, the ensemble

of dose histories is averaged to compute expected dose, as described by Equation 6.1.2-26 in Section 6.1.2.5 of the parent document. At the time of the intrusion, percolation begins to flow through the waste and transport the radionuclides down the borehole to the SZ. Thus, the dose following an intrusion has a large initial value that decreases rapidly as radionuclide inventory is depleted or decays.

To complete a comprehensive analysis of temporal stability for the TSPA-LA Model, an additional analysis is presented in this addendum for the Human Intrusion Scenario, which includes the correction of a timestep error documented in Appendix P, Table P-6, Item 6, of the parent document. In the parent document, temporal stability for the Human Intrusion Modeling Case was judged to be adequate, despite the presence of the timestep error and the coarseness of the temporal resolution of expected dose (see Figures 7.3.3-10 and 7.3.3-11 of the parent report). Because of the correction of the timestep error and the coarseness evident in the parent document, the base timestep scheme for the Human Intrusion Modeling Case was revised to that shown in Table 7.3.3-2[a], and temporal stability was re-assessed for TSPA-LA Model v5.005. Figure 7.3.3-10[a] compares the base-case timestep results with the alternative timestep scheme for the 1,000,000 Year simulation period. Figure 7.3.3-11[a] focuses on the dose immediately after the intrusion (out to 220,000 years only) and shows that the base-case timestep size in TSPA-LA Model v5.005 provides results that are nearly identical to the alternate timestep scheme. The similarity in expected annual dose for the two timestep schemes confirms that the Human Intrusion Modeling Case is stable with respect to temporal discretization.

7.3.3.7[a] Nominal Modeling Case

The Nominal Modeling Case estimates the annual dose resulting from WP failures from nominal corrosion processes (i.e., general corrosion, microbial influenced corrosion, stress corrosion cracking [SCC]), as well as the effects of general corrosion of DS materials (Section 6.3.5 of the parent document). The number and type of WP failures at each point in time is estimated by the use of several software packages, as described in Section 6.3.5.1.3 of the parent document; the radionuclide transport and dose resulting from this sequence of failures is estimated by the GoldSim component of the TSPA-LA Model, as described in Section 6.1.2.4.1 of the parent document.

The time of failure of a WP depends on the temperature-dependent general corrosion rates applied to the WP, which change over time as temperature changes. Thus, the temporal discretization, which defines when the value of the general corrosion rate will be updated, is influential to the annual dose resulting from nominal corrosion processes.

In the base case, the coarse timestep discretization beyond 200,000 years used to calculate general corrosion was taken from the thermal hydrology histories. The temperature and relative humidity data did not fluctuate significantly once ambient conditions within the repository were reestablished and a coarse timestep discretization was selected to represent the data. The general corrosion calculations used the same timestep discretization. In the temporal stability study, the timestep discretization used by the general corrosion calculations was refined by updating the timestep scheme in the thermal hydrology history files. The number of data points was increased from 68 in the base case to 279 in the temporal stability run. The timesteps for the base case are found in the files with an .ou extension within output DTN: MO0710ADTSPAWO.000

([DIRS 183752], Input_File_Set_064.zip) and the timesteps for the alternative time scheme are in the files with an .ou extension within output DTN: MO0801TSPAWPDS.000 ([DIRS 185077], Replacement_Input_File_Set_25.zip). The GoldSim timestep schedule was not altered for this analysis. The new timestep discretization was selected so that the maximum timestep size used in the general corrosion calculations was 10,000 years. The timestep schedule maintained the timestep scheme previously used for the first 750 years. From 200 years up until 1000 years, the timestep size was 50 years. From 1,000 years to 10,000 years the timestep size was 100 years, compared to a maximum 2,000 year timestep over this time period in the base case. From 10,000 years to 20,000 years the timestep size was 500 years, compared to a maximum 5,000 year timestep over this time period in the base case. From 20,000 years to 50,000 years the timestep size was 1000 years, compared to a maximum 10,000 year timestep over this time period in the base case. From 50,000 years to 75,000 years the timestep size was 2500 years, compared to a maximum 20,000 year timestep over this time period in the base case. From 75,000 years to 100,000 years the timestep size was 5000 years, compared to a maximum 30,000 year timestep over this time period in the base case. Beyond 100,000 years the timestep size was 10,000 years until the last time point at 999,950 years, compared to a maximum 300,000 year timestep over this time period in the base case.

Figure 7.3.3-12[a] compares the base-case timestep results with the alternative timestep scheme for the 1,000,000 year simulation period. The few realizations with expected annual dose before 200,000 years appear similar for either timestep scheme. However, in the base case, the coarse timesteps used after 200,000 years result in observable jumps in expected annual dose at 200,000; 300,000; 500,000 and 700,000 years. At these timesteps, the number of WP failures (from SCC) calculated by the WP degradation code WAPDEG V4.07 (STN: 10000-4.07-01 [DIRS 181064]) increases sharply. The stress corrosion crack growth rate is given by a power law function of stress intensity factor and repassivation slope n (Equation 6.3.5-14 of the parent document). The stress intensity factor is evaluated at the beginning of each WAPDEG timestep and is a function of the crack depth that drives the crack propagation. The large timesteps taken past 100,000 years combined with the sensitivity of the crack growth rate to the stress intensity factor, which is raised to the power 4n, where n has a mean value of 1.165 (SNL 2007 [DIRS 181953], Table 8-15), can cause dramatic changes in the crack growth rate at each timestep. As a result, the crack growth rate can change from a small value for the timestep in which the crack initiates to a much larger value at the beginning of the next timestep, resulting in almost immediate penetration of many cracks and WP failures. Use of shorter timesteps in the alternative scheme improves the calculation of the crack growth rate, which removes the jumps in the number of WP failures by SCC, which in turn is reflected in the expected annual dose curves for the alternative scheme. The increase in expected annual dose from using the increased number of timesteps in the alternative time scheme is due to an increase in the number of WP failures calculated by the WAPDEG code. Between the two cases, the number of WP failures were approximately the same midway between each large timestep used in the base case (output DTN: MO0801TSPAWPDS.000 [DIRS 185077], file: LA_v5.005_NC_000300_006_Dose_ Assessment.doc), but the base case underestimated the number of WP failures in the second half of the WAPDEG timestep. The WAPDEG code applies an average penetration depth over an entire timestep to determine the general corrosion and stress corrosion consequences for each timestep. Applied as an average, the calculated results for a large timestep are overestimated in the beginning of the timestep and underestimated at the end of the timestep. Thus, because the TSPA-LA Model ends at the end of a WAPDEG timestep, the number of failures is underestimated at the end of the realization.

Figure 7.3.3-13[a] compares statistics on expected annual dose for the base-case and the alternative timestep scheme. The comparison shows that both the magnitude of expected annual dose and the range of uncertainty in expected annual dose are similar for both timestep schemes. This similarity in statistics for expected annual dose for the two timestep schemes indicates that the Nominal Modeling Case is sufficiently stable with respect to temporal discretization and that any underestimation in dose due to the large WAPDEG timesteps taken in the base case is not significant.

The timestep scheme for the base case model was selected for computational efficiency. In the base case calculations, the WAPDEG calculations accounted for about 40 to 50 percent of the simulation time. In the sensitivity study, the WAPDEG calculation time increased by a factor of four, doubling the run time. Because the TSPA-LA Model results were judged to be sufficiently stable with respect to temporal discretization and because improving the smoothness of the expected annual dose curves would involve significant additional calculation time, the base case timestep scheme was used in the TSPA-LA Model for the Nominal Modeling Case.

Table 7.3.3-2[a]. Revised Timestep Schemes used in Temporal Stability Analysis

Modeling Case	Base-Case Timestep Scheme (v5.000)	Base-Case Timestep Scheme (v5.005)	First Alternate Timestep Scheme
Human Intrusion (intrusion occurs at 200,000 yr)	250 yr from 0 to 10k yr 500 yr from 10k to 100k yr 1,000 yr from 100k to 120k yr 2,000 yr from 120k to 160k yr 4,000 yr from 160k to 1M yr	250 yr from 0 to 10k yr 500 yr from 10k to 100k yr 1,000 yr from 100k to 120k yr 2,000 yr from 120k to 158k yr 4,000 yr from 158k to 198k yr 250 yr from 198k to 204k yr 1,000 yr from 204k to 212k yr 4,000 yr from 212k to 1M yr	250 yr from 0 to 10k yr 500 yr from 10k to 100k yr 1,000 yr from 100k to 120k yr 2,000 yr from 120k to 158k yr 4,000 yr from 158k to 198k yr 40 yr from 198k to 204k yr 400 yr from 204k to 212k yr 4,000 yr from 212k to 1M yr

Source: Output DTNs: MO0709TSPAREGS.000 [DIRS 182976], File: V5.000_HI_009000_002.gsm (for Base Case v5.000); MO0710ADTSPAWO.000 [DIRS 183752], File: v5.005_HI_009000_000.gsm, (for Base Case v5.005); and MO0801TSPAADSA.000 [DIRS 185078], File: v5.005_HI_009000_001.gsm, (for Alternate).

INTENTIONALLY LEFT BLANK

7.3.4[a] Analyses of Spatial Discretization

No change.

7.3.5[a] Stability of FEHM Particle Tracking Model

No change.

7.4[a] UNCERTAINTY AND VARIABILITY CHARACTERIZATION REVIEWS

No change.

7.5[a] SURROGATE WASTE FORM VALIDATION

This material supplements the corresponding material in the parent document.

The purpose of the analyses documented in Section 7.5 of the parent document is to show that the surrogate representation of naval spent fuel (Category 1 DOE spent nuclear fuel [DSNF]) and the DSNF surrogate, the average of DSNF Categories 2 through 11, are appropriate. The averaging of Categories 2 through 11 is related to the spatial averaging that is analyzed in Section 7.3.4 of the parent document.

The updated analyses presented in this addendum were conducted to confirm that Zircaloy-clad CSNF adequately represents Category 1 DSNF in TSPA-LA Model v5.005. Category 1 DSNF, naval spent fuel in the TSPA-LA Model, is represented as Zircaloy-clad CSNF. Section 7.5.3[a] discusses the analyses using TSPA-LA Model v5.005 where the naval source term replaced the CSNF source term for the Drip Shield EF and Igneous Intrusion Modeling Cases.

7.5.1[a] Methodology

No change.

7.5.2[a] Spent Fuel Categories and Representation in Model

No change.

7.5.3[a] Naval Spent Fuel, Category 1

Analyses were performed to confirm the adequacy of the use of CSNF as a surrogate for NSNF. These analyses are outlined in Table 7.5-5 of the parent document. The analyses were conducted for simulations of 10,000 years, and a qualitative argument for the extension of the results beyond 10,000 years is also presented. For this addendum, TSPA-LA Model v5.005 was exercised explicitly using NSNF inventories in place of the CSNF inventory. The dose results from these cases were compared to demonstrate that CSNF inventory bounds the NSNF inventory.

7.5.3.1[a] Comparison of the Naval Spent Nuclear Fuel and Commercial Spent Nuclear Fuel Inventories for 10,000 Years and 1,000,000 Years

No change.

7.5.3.2[a] Disposition of Commercial Spent Nuclear Fuel as a Surrogate for Naval Spent Nuclear Fuel for the Early Failure Modeling Cases

NSNF was analyzed using inventories, or source terms, supplied by the Navy for radionuclides that are available for release from naval spent fuel. The source terms are based on a hypothetically failed WP of naval spent fuel for the Drip Shield EF and Igneous Intrusion Modeling Cases. These source terms were provided by the Naval Nuclear Propulsion Program (McKenzie 2007 [DIRS 182657]). The analyses of naval spent fuel are special cases developed to compare CSNF and naval spent fuel for the Drip Shield EF and Igneous Intrusion Modeling Cases. For these analyses, the NSNF source term (radionuclides available for release within a failed WP) was modeled in a failed CSNF WP, and the radionuclides were then subject to all of the transport processes that are applied to dissolved CSNF (e.g., solubility, sorption, and chemistry along the transport pathway from dissolved CSNF to the reasonably maximally exposed individual [RMEI]) in the TSPA-LA Model.

In the modeled repository, there are 8,213 WPs of CSNF, 417 of which represent naval spent fuel (SNL 2007 [DIRS 180472], Table 6-2[a]). The TSPA-LA Model does not explicitly include naval spent fuel but bounds its behavior with 417 CSNF WPs that represent naval spent fuel. The special case analyses in this section were conducted to demonstrate that the annual dose from naval spent fuel is bounded by the annual dose from CSNF.

For the validation of CSNF as a surrogate for naval spent fuel for the non-disruptive event cases, the Drip Shield EF Modeling Case was chosen over the Waste Package EF Modeling Case because of the following considerations. First, the transport of radionuclides within the EBS for the Drip Shield EF Modeling Case is advection dominated with some diffusion. The transport of radionuclides within the EBS for the Waste Package EF Modeling Case is diffusion dominated since the drip shield (DS) stays intact. The Waste Package EF Modeling Case would produce lower radionuclide doses compared to the Drip Shield EF Modeling Case and, therefore, can be considered a subset of the Drip Shield EF Modeling Case for the NSNF analysis. In addition, in the TSPA-LA Model, the Waste Package EF Modeling Case applies not only a temperature threshold to transport, but a relative humidity threshold to transport radionuclides from the waste form to the WP OCB. Since the naval source term is a release from a failed WP, it is implemented in the TSPA-LA Model by applying the release to the WP transport cell and, therefore, bypasses the relative humidity threshold for transport from the waste form transport cell. The result of using the Waste Package EF Modeling Case for the analysis would be an early release of radionuclides to the accessible environment for the naval source term, which would be inconsistent with a later release of radionuclides for the CSNF source term. The delay in release from the waste form to the WP OCB due to the relative humidity threshold for transport is not implemented in the Drip Shield EF Modeling Case. Therefore, for the Drip Shield EF Modeling Case, the timing of the release of radionuclides to the accessible environment from a failed WP with a CSNF source term is more consistent with the timing of the release from a failed WP where the naval source term has been substituted for the CSNF source term in the WP transport cell.

For the Drip Shield EF Modeling Case, a single DS failure was forced to occur at the first timestep of the simulation. Two simulations using TSPA-LA Model v5.005 were run: one for a single CSNF WP and one for a single WP where the naval source term replaced the CSNF source term. The simulations were run for 10,000 years and used a unified sampling of epistemic and aleatory uncertainty over 300 model realizations. The results, in terms of a mean annual dose over the unified sampling of epistemic and aleatory uncertainty, are shown on Figure 7.5-4[a]. As noted in the results documented in the parent document, the results of this analysis show that over a 10,000-year period, the dose associated with the naval source term is less than that of the CSNF source term. At 10,000 years, the mean annual dose from a failed WP with a naval source term is over two orders of magnitude lower than the mean annual dose for a failed CSNF WP, confirming the appropriateness of the use of a CSNF WP as a surrogate for a naval WP.

7.5.3.3[a] Disposition of Commercial Spent Nuclear Fuel as a Surrogate for Naval Spent Nuclear Fuel for the Igneous Intrusion Modeling Case

A similar analysis conducted for the Igneous Intrusion Modeling Case is used to confirm the appropriateness of the use of CSNF as a surrogate for NSNF. For both the CSNF and naval source term stylized analysis, the time of the igneous intrusion was forced to occur at a specified timestep, and a single WP was failed. Using TSPA-LA Model v5.005, simulations were run for 10,000 years and used a unified sampling of epistemic and aleatory uncertainty over 300 model realizations. The results, in terms of a mean annual dose over the unified sampling of epistemic and aleatory uncertainty, are shown on Figure 7.5-5[a]. As was the case for the Drip Shield EF Modeling Case, the results for the Igneous Intrusion Modeling Case show that for a 10,000-year period, the dose associated with the naval source term is less than that of the CSNF source term, again justifying the use of a CSNF WP as a surrogate for a naval WP.

7.5.3.4[a] Disposition of Commercial Spent Nuclear Fuel as a Surrogate for Naval Spent Nuclear Fuel for the Volcanic Eruption Modeling Case

No change.

7.5.3.5[a] Disposition of Commercial Spent Nuclear Fuel as a Surrogate for Naval Spent Nuclear Fuel for the Human Intrusion Modeling Case

No change.

7.5.3.6[a] Disposition of Commercial Spent Nuclear Fuel as a Surrogate for Naval Spent Nuclear Fuel for the Nominal Modeling Case

Note, minor reference change from the parent document.

The use of CSNF as a surrogate for NSNF for the first 10,000 years of the Nominal Modeling Case is justified because there are no WP failures during this time period, and because the naval WP is more robust than the commercial WP. The 1,000,000 year Nominal Modeling Case is a stylized case (see Section 8.2.1 of the parent document) where the WP fails by SCC and general corrosion sometime after the first 10,000 years. These effects are accounted for in the 1,000,000 year Seismic GM Modeling Case. The use of CSNF as a surrogate for NSNF for the 1,000,000 year Nominal Modeling Case is justified because of the NSNF is adequately represented by

CSNF in the early failure cases, and again because the naval WP is more robust than the commercial WP.

7.5.3.7[a] Disposition of Commercial Spent Nuclear Fuel as a Surrogate for Naval Spent Nuclear Fuel for the Seismic Modeling Cases.

No change.

7.5.4[a] U.S. Department of Energy Spent Fuel, Categories 2 through 11

No change.

7.5.5[a] Selected Sensitivity Analyses

No change.

7.5.6[a] Summary of Results for U.S. Department of Energy Spent Fuel

The additional analyses presented in this section of the addendum confirm that comparing naval spent fuel with Zircaloy-clad CSNF demonstrates that CSNF bounds the results of naval spent fuel for both non-disruptive (Drip Shield EF) and disruptive event (Igneous Intrusion) modeling cases. Additional analyses performed by the Naval Nuclear Propulsion Project as documented in Section 7.5.3.7 of the parent document confirm the use of CSNF as a surrogate for naval spent fuel for the seismic scenarios (Gisch 2004 [DIRS 171782]). Representing naval spent fuel by CSNF as its surrogate in the TSPA-LA Model adequately bounds the behavior of naval spent fuel (Section 7.5.3[a]).

No additional analyses were conducted for the remaining categories of DSNF.

7.6[a] CORROBORATION OF ABSTRACTION MODEL RESULTS WITH VALIDATED PROCESS MODELS

No change.

7.7[a] CORROBORATION OF RESULTS WITH AUXILIARY ANALYSES

The auxiliary analyses are an important aspect of determining whether the TSPA-LA Model is yielding reasonable results (e.g., that the model is producing the results that would be expected). To supplement the results presented in Section 7.7 of the parent document, the following auxiliary analyses were performed using TSPA-LA Model v5.005 and documented in this addendum: (1) single realization analysis of various modeling cases, including additional analyses for outlier realizations; (2) comparison of the results of the TSPA-LA Model with a Simplified TSPA Analysis (Section 7.7.2[a]); (3) comparison of the results of the TSPA-LA Model with the TSPA independently developed by EPRI (Section 7.7.3[a]); and (4) PMA (Section 7.7.4[a]). A summary of the additional auxiliary analyses included in this addendum is provided below.

7.7.1[a] Analyses of Single Realizations

Analyses of single realizations provide insight into the coupling of various submodel processes within the TSPA-LA Model. The analyses presented in Section 7.7.1 of the parent document and Section 7.7.1[a] of this addendum include an in-depth explanation about how the transport of key radionuclides is affected by coupling various components of the EBS, UZ, and SZ domains following WP failure under a variety of physical, chemical, thermal, and mechanical conditions. The insight gained provides assurance that the various submodel processes are working as expected and, in turn, helps provide confidence in the TSPA-LA Model.

The single realization analyses presented in this addendum evaluate seven modeling cases that are used to cover the range of WP failure mechanisms considered in the TSPA-LA Model and highlight various processes affecting and controlling radionuclide releases under a variety of conditions. The seven modeling cases are: (1) Waste Package EF Modeling Case (Section 7.7.1.1[a]), (2) Drip Shield EF Modeling Case (Section 7.7.1.2[a]), (3) Igneous Intrusion Modeling Case (Section 7.7.1.3[a]), (4) Seismic GM Modeling Case (Section 7.7.1.4[a]), (5) Nominal Modeling Case (Section 7.7.1.5[a]), (6) Human Intrusion Modeling Case (Section 7.7.1.6[a]), and (7) Seismic GM Modeling Case for the 10,000-year duration (Section 7.7.1.7[a]). The durations for all modeling cases, except where noted, was 1,000,000-years.

The methodology for calculating expected annual dose (i.e., the expectation of annual dose over aleatory uncertainty) for the various modeling cases is described in Section 6.1.2 of the parent document, which discusses how to differentiate epistemic uncertainty from aleatory uncertainty in the TSPA-LA Model. Although the treatment of aleatory uncertainty varies with each modeling case, the general methodology for selecting a realization for detailed analysis is similar for all seven modeling cases described in this section. First, an epistemic uncertainty vector is chosen from the set of epistemic uncertainty vectors. The two primary criteria for selecting a particular epistemic uncertainty vector are that (1) the *functional form* (shape) of the expected annual dose (for the chosen epistemic vector) is similar to that of the mean annual dose (computed by taking expectation over all epistemic uncertainty vectors) and (2) the *magnitude* of the expected annual dose for the chosen epistemic vector is similar or higher than the mean annual dose over the time period of interest. These criteria are intended to help select epistemic uncertainty vectors that highlight processes of most interest for each modeling case. Since the expected annual dose for an epistemic vector is calculated by taking the expectation over aleatory uncertainty, each expected annual dose is further broken down in order to select the realization(s) representing individual aleatory uncertainty vectors. An aleatory vector is chosen by comparing its dose contribution to other aleatory vectors in the set and that which best describes the behavior of the expected annual dose for the epistemic vector over the time period of interest. For the Igneous Intrusion, Human Intrusion, Nominal, and the two Seismic GM Modeling Cases, one GoldSim realization, representing a unique combination of epistemic and aleatory uncertainties, is chosen for detailed analyses. For the Waste Package EF and Drip Shield EF Modeling Cases, two GoldSim realizations, representing two aleatory uncertainty vectors (corresponding to CSNF and CDSP WP locations) for a given epistemic uncertainty vector, are selected to adequately describe the expected annual dose for the chosen epistemic uncertainty vector. More details about how a specific single realization was selected for analysis are presented in each subsection.

In addition to the detailed explanation of results from the chosen realization (representing a typical epistemic and aleatory vector), an outlier realization is analyzed for selected modeling cases. The realization is chosen in such a way that the expected dose is one of the highest for the period of interest. The motivation for analyzing an outlier realization is to understand the combination of parameters or submodels that lead to the large expected dose, because the mean annual dose is influenced more by an outlier realization than by any other realization.

The analysis for the outlier realization is limited to highlighting the primary reasons for its high dose and contrasting them to the results presented for the typical realization. The outlier realization analysis for a given modeling case is presented at the end of the section where the detailed single realization analysis for the same modeling case is described. The outlier realization analysis is conducted for all modeling cases except for the two Seismic GM Modeling Cases because the epistemic vector chosen for the detailed analysis in the two Seismic GM Modeling Cases also has large expected dose.

All single realization analyses discussed below are carried out by running the single realizations using GoldSim software (GoldSim v9.60.300, STN: 10344 9.60-03 [DIRS 184387]). However, the results of the expected annual doses are based on calculations performed by using EXDOC_LA software (EXDOC_LA V2.0, STN: 11193-2.0-00 [DIRS 182102]) with proper weighting of scenario-specific probabilities and expectations over aleatory and epistemic uncertainties.

7.7.1.1[a] Waste Package Early Failure Modeling Case

This section presents analyses of two realizations selected from the 6,000 realization base-case run performed for calculating expected annual dose from the Waste Package EF Modeling Case (GoldSim filename: LA_v5.005_EW_006000_000.gsm; output DTN: MO0710ADTSPAWO.000 [DIRS 183752]). The distribution of expected annual dose, along with the mean and various quantiles, is shown on a linear time scale (Figure 7.7.1-1a[a]) and on a log-time scale (Figure 7.7.1-1b[a]), the latter to more clearly illustrate the variation in dose at early times. The 300 displayed expected annual dose histories correspond to 300 epistemic uncertainty vectors. Each expected annual dose history is calculated as a weighted average of twenty aleatory uncertainty vectors (Equation 6.1.2-13 of the parent document). The twenty aleatory uncertainties are derived by considering the five spatial percolation subregions, two environments (seeping and non-seeping environments) for each percolation subregion, and two WP types for each environment (Section 6.1.2.4 of the parent document). Early failure of one WP is modeled for each of the aleatory vectors. Epistemic vector 281 is chosen for detailed analysis since it has an expected annual dose curve similar to the mean (Figure 7.7.1-1[a]). The twenty aleatory uncertainty vectors corresponding to epistemic vector 281 are GoldSim realization numbers 5601 through 5620 (Figure 7.7.1-2[a]).

The mean annual dose from this modeling case has several peaks (Figure 7.7.1-1b[a]). The first broad peak between 1,000 and 10,000 years is due to contributions from CDSP WPs, predominantly, as the relative humidity in the CDSP WPs in the various percolation subregions exceeds 95 percent and diffusive transport begins (Section 5.1.4 of the parent document). A second set of dose peaks between 10,000 and 30,000 years reflects dose contributions from CSNF WPs when the relative humidity inside CSNF WPs in the various percolation subregions

rises above 95 percent. The last broad dose peak occurs after the DSs fail (between approximately 250,000 and 300,000 years) and water flux through the WPs starts.

The radionuclides that contribute most to the mean annual dose are shown on Figure 7.7.1-3[a]. ^{99}Tc and ^{129}I are the top dose contributors at the peak of the mean annual dose, which occurs around 12,500 years. Beyond about 30,000 years, ^{239}Pu and ^{242}Pu are the major dose contributors. In the sections that follow, the transport characteristics of ^{99}Tc are discussed as an example of all highly soluble, weakly, or negligibly sorbing radionuclides. ^{239}Pu and ^{242}Pu provide examples of sparingly soluble, strongly sorbing radionuclides.

In order to investigate peaks in the mean annual dose curve, it was necessary to inspect two GoldSim realizations (representing two aleatory uncertainty vectors for the same epistemic uncertainty vector). One realization corresponds to an early CSNF WP failure, whereas the second corresponds to an early CDSP WP failure. Each affects expected annual dose at different times. Realization 5608 is chosen to represent the early failure of a CSNF WP, while realization 5618 is chosen to represent the early failure of a CDSP WP. These two realizations were chosen because both exhibit early failure of CSNF and CDSP WPs within percolation Subregion 3, which represents about 40 percent of the total repository area. Also, both represent a seeping environment, where releases are typically greater than from a non-seeping environment. The annual doses from these two realizations are highlighted on Figure 7.7.1-2[a], along with 18 other realizations representing aleatory uncertainty vectors for epistemic vector 281. These two realizations are examined more closely in the sections that follow.

Early Failure CSNF Package—Realization 5608

Figure 7.7.1-4[a] shows the annual dose attributable to 21 radionuclides for realization 5608 (GoldSim filename: LA_v5.005_EW_006000_002.gsm; output DTN: MO0801TSPAMVAC.000 [DIRS 185080]). Two radionuclides, ^{99}Tc and ^{129}I, dominate the first sharp peak in dose at 12,000 years. There is a broad peak due to ^{239}Pu between 20,000 and 100,000 years and a much broader peak after the DS fails at 292,000 years, due primarily to ^{242}Pu and ^{237}Np. At no time do radionuclides irreversibly attached to colloids contribute significantly to dose.

The peak dose (12,000 years) is due to the almost pulse-like releases of ^{99}Tc and ^{129}I from CSNF packages; these two radionuclides are transported essentially without retardation through the EBS, UZ, and SZ. In the Waste Package EF Modeling Case, the CSNF matrix is modeled to degrade instantaneously when the WP is breached and the temperature is above 100°C (Section 6.3.7.4.1.3 of the parent document). However, releases of radionuclides cannot occur until there is a continuous film of water within the WP to support diffusive transport, which is modeled to occur once the relative humidity rises above the threshold of 95 percent in the absence of flow. In realization 5608, the relative humidity exceeds 95 percent at 11,500 years, causing releases by diffusive transport to start. All of the highly soluble radionuclides (such as technetium and iodine) that are part of the CSNF inventory dissolve into the available water volume, establishing a large concentration gradient between the waste form domain and invert. This gradient drives diffusion and rapidly depletes the mass in the waste form domain. Figure 7.7.1-5[a] shows the technetium release rate from the waste form, invert (EBS), UZ, and SZ for realization 5608. The initial pulse-like release from the waste form is attenuated only slightly by transport through the WP corrosion products domain and the invert domain. As

indicated on Figure 7.7.1-5a[a], these two curves virtually coincide. The release rate is somewhat attenuated in the UZ and SZ due to hydrodynamic dispersion, which is caused by fracture-matrix interactions in the volcanic rock units and transport through alluvium. Figure 7.7.1-5b[a] shows the SZ breakthrough curves for technetium, reversibly attached plutonium, and irreversibly attached plutonium. The median SZ travel times for technetium for epistemic vector 281 range from 30 to 60 years over the four SZ regions. The small but sharp increase in the SZ release rate around 164,000 years (Figure 7.7.1-5a[a]) is due to a small step change in the SZ breakthrough curve from Source Region 2 reflecting coarse time discretization, rather than a physical process, which when convolved with the UZ release leads to such behavior.

In contrast to technetium, plutonium has a propensity to sorb strongly to most surfaces and also form a sparingly soluble solid, which results in entirely different geochemical behavior from that of the more soluble and weakly sorbing radionuclides like ^{99}Tc. Unlike technetium, which exhibits a large pulse-like release, the release of plutonium from the waste form rises to a value below that of technetium and remains relatively constant for a long time (Figure 7.7.1-6a[a]). This plutonium release characteristic reflects the fact that dissolved plutonium concentrations are solubility limited, whereas technetium concentrations are limited by the waste form degradation rates and transport rates. As a result, a considerable mass of plutonium released from the degraded waste form reprecipitates within the waste form domain. Figure 7.7.1-7a[a] shows dissolved plutonium concentrations within the CSNF waste form domain. All isotopes contribute to their dissolved elemental concentrations in proportion to their mass in the waste form cell; therefore, ^{239}Pu dominates plutonium concentrations at early times and ^{242}Pu dominates at later times (after most ^{239}Pu has decayed). The mass of plutonium modeled as having precipitated in the waste form domain remains there as a solid (PuO_2) throughout the one-million-year simulation in realization 5608. The decrease in plutonium solubility observed around 292,000 years (Figure 7.7.1-7a[a]) is due to a change in the in-package chemistry from initiation of flow (about 0.14 m^3/yr) through the WP following the failure of the DS. This initiation of flow causes the in-package chemistry to be calculated based on the evaluation of both the vapor influx and liquid influx (Section 6.3.7.2.1 of the parent document), which results in the change in pH and ionic strength (Figure 7.7.1-7b[a]) and thereby the plutonium solubility. Note that CSNF colloids remain unstable throughout the simulation even though pH and ionic strength change (Figure 6.3.7-11b of the parent document), so the concentration of plutonium irreversibly associated with CSNF colloids remains minimal as seen on Figure 7.7.1-6b[a].

Besides solubility, sorption onto WP corrosion products controls the plutonium concentration and releases from the WP. The effect of sorption on the plutonium concentration within the WP corrosion products can be seen on Figure 7.7.1-6b[a], where there is an initial spike in the concentration which then decreases due to sorption. The spike results from the initial calculation of small K_d on corrosion products as minimum initial values for the radionuclide concentrations are used by the surface-complexation based competitive sorption model to calculate the sorption coefficients. Once the radionuclide concentrations rise above the minimum values, the K_ds adjust to higher values in the next timestep (Figure 7.7.1-8[a]). The low initial K_d allows a pulse of radionuclides, most notably ^{239}Pu and ^{243}Am, to be released through the WP corrosion products and sorbed onto the invert before significant K_ds are calculated in the corrosion products. This is a model limitation due to the explicit-in-time solution method for the competitive sorption calculations. However, the current implementation is adequate because it

causes only a minor over-prediction of the ^{239}Pu release to the invert in a single timestep. Because of decay of ^{243}Am to ^{239}Pu, the dissolved concentration of ^{239}Pu in the WP corrosion products is calculated to exceed that in the waste form domain. In the subsequent timesteps, the establishment of higher K_ds causes the WP corrosion products domain ^{239}Pu concentration to drop below that of the waste form domain and then below that of the invert. As a result, there is backward diffusion from the invert into the WP corrosion products (represented by a negative release rate on Figure 7.7.1-6a[a]). Advective transport through the invert depletes the mass and eventually drops the concentration in the invert below that in the WP corrosion products and positive release from the WP to the invert is reinstated. The diffusion gradient between the invert and the UZ remains positive, however, resulting in continuous down-gradient releases (Figure 7.7.1-6a[a]). The release rates decrease in the UZ and further in the SZ, due to dispersion, sorption, and radioactive decay during transport. The SZ breakthrough curves for reversibly attached plutonium and irreversibly attached plutonium show median travel times of 16,000 to 39,000 years and 11,000 to 12,000 years, respectively (Figure 7.7.1-5b[a]). The small concentration of ^{239}Pu irreversibly attached to CSNF colloids in the waste form domain (Figure 7.7.1-6b[a]) shows that colloidal transport of ^{239}Pu is not important in this realization.

The release rate of ^{242}Pu (Figure 7.7.1-9a[a]) correlates well with its dissolved concentrations (Figure 7.7.1-9b[a]). The share of ^{242}Pu relative to the elemental solubility increases with time as mentioned earlier, so its concentration and release rate also increases. Release from the WP corrosion product domain is significantly reduced due to sorption onto the WP corrosion products. Unlike ^{239}Pu where the concentration in the WP corrosion products domain exceeded that in the waste form domain in the initial timestep due to ingrowth from decay of ^{243}Am (at 11,500 years), ^{242}Pu is not the daughter of a significant short-lived parent, and the concentration in the WP corrosion products domain remains below that of the waste form domain. At 292,000 years, the DS breaches so water flux through the WP starts and causes a sharp increase in the release rate from the WP.

Early Failure Co-Disposed Package—Realization 5618

Figure 7.7.1-10[a] shows the contributions to annual dose by the major radionuclides for realization 5618 (GoldSim filename: LA_v5.005_EW_006000_003.gsm; output DTN: MO0801TSPAMVAC.000 [DIRS 185080]). Three radionuclides, ^{14}C, ^{99}Tc, and ^{129}I, dominate the first peak, which starts around 1,000 years when the relative humidity of the CDSP WP rises above 95 percent. Although the CDSP WP is failed at the start of the simulation, only the DSNF is assumed to degrade instantaneously; whereas, the CDSP HLW glass degrades according to its temperature- and pH-dependent degradation rate (BSC 2004 [DIRS 169988], Section 8.1). Relative contributions from degradation of DSNF and HLW glass to combined waste form release for selected radionuclides is shown on Figure 7.7.1-11[a]. Radionuclides released from degraded DSNF are evident at the end of the first timestep (250-year duration), with a gradual rise in the cumulative release as the HLW glass degrades. The line for ^{14}C is flat because there is no ^{14}C inventory in the HLW glass. The slow degradation of HLW glass leads to a gradual release of ^{99}Tc from the HLW waste form domain (Figure 7.7.1-12[a]) compared to that from the CSNF waste form (Figure 7.7.1-5[a]). The lower inventory of ^{99}Tc within DSNF compared to that within CSNF (on a per-package basis; Table 6.3.7-5 of the parent document) results in a lower initial release rate. Once again a small but observable lowering and delay of the release rate peak occurs in the UZ and SZ (Figure 7.7.1-12[a]).

Figure 7.7.1-13a[a] shows the release rates of ^{239}Pu from the different domains. Figure 7.7.1-13b[a] shows the concentration of ^{239}Pu in each successive domain of the EBS transport model: HLW glass, DSNF, WP corrosion products, and invert. Each domain has a distinct chemistry and solubility control on plutonium concentration. Most plutonium is precipitated in both the HLW glass domain and the DSNF domain at the outset of the simulation but is depleted first in the DSNF domain by about 4,000 years. After that time, the concentration of plutonium in the DSNF domain is controlled by transport from the upstream HLW cell. Kinetic sorption and desorption processes, that are modeled in the WP corrosion products domain, control the concentration of plutonium and maintain it at the solubility limit. As diffusive release continues to the invert, the plutonium mass is depleted from the corrosion products domain and by 75,000 years, the dissolved concentrations cannot be maintained at the solubility limits leading to its gradual decline. This reduction in corrosion product domain concentration increases the concentration gradient between the HLW and WP corrosion products domains and increases the release rate from the waste form domain (Figure 7.7.1-13a[a]). Plutonium within the HLW glass waste-form domain is depleted after 176,000 years (Figure 7.7.1-14a[a]), and total plutonium release rate from the waste form domain drops to zero (Figure 7.7.1-13a[a]). In addition to the dissolved concentrations, Figure 7.7.1-13b[a] also shows the concentrations of ^{239}Pu irreversibly attached to glass waste form colloids. The ionic strength in the waste form domain (Figure 7.7.1-14b[a]) remains above the threshold for stable glass waste form colloid (Figure 6.3.7-11a of the parent document) until about 45,000 years, at which time stable colloids form. However, the concentration of ^{239}Pu irreversibly attached to waste form colloids remains orders of magnitude below the dissolved ^{239}Pu concentration. The net result is that the colloidal release of ^{239}Pu is not significant in realization 5618.

The release rate characteristics of ^{242}Pu from the various domains for the CDSP packages (Figure 7.7.1-15a[a]) are similar to those of ^{239}Pu (Figure 7.7.1-13a[a]), except that, due to its longer half-life (375,000 years), ^{242}Pu does not decay as quickly and later-time releases are significant. Just like ^{239}Pu, ^{242}Pu becomes depleted in the DSNF domain at 4,000 years, but the concentration in the WP corrosion products domain remains steady due to sorption and desorption. Early in the simulation, the concentration of ^{242}Pu in the HLW waste form domain is low since the elemental concentration is dominated by the more abundant isotopes, ^{239}Pu and ^{240}Pu (Figure 7.7.1-14a[a]). As ^{239}Pu and ^{240}Pu decay, the concentration of ^{242}Pu increases, maintaining the dissolved concentration of total plutonium at the solubility limit (of about 0.0085 mg/L between 100,000 years and 280,000 years). At around 176,000 years the plutonium becomes depleted within the HLW waste form domain and the ^{239}Pu and ^{242}Pu concentrations drop (Figures 7.7.1-14a[a] and 7.7.1-15b[a]). As a result, the diffusion gradient from the WP corrosion products domain to the upstream waste form domain reverses, leading to increasing down-gradient release (represented by a positive release rate) and depletion of the mass in the waste form domain. Once the mass of plutonium has been depleted, the dissolved concentration of plutonium in the waste form domain decreases and plutonium once again diffuses from the WP corrosion products domain to the waste form domain (represented by a negative release rate on Figure 7.7.1-15b[a]). Initially, release of ^{242}Pu irreversibly attached to glass waste form colloids is low; however, after the DS fails, ^{242}Pu release increases due to advective release from the WP. This is the only significant release of colloidal radionuclides for this modeling case, with the release rate of irreversibly attached plutonium nearly equal to that of dissolved plutonium.

Waste Package Early Failure Modeling Case: Outlier

For the purpose of analyzing an outlier realization, epistemic vector 247 was chosen as shown on Figure 7.7.1-16[a]. Figure 7.7.1-17[a] shows the 20 aleatory realizations that are associated with epistemic vector 247 and correspond to GoldSim realizations 4921 through 4940. Two realizations (realization 4930 and 4940) are highlighted as they represent the highest unweighted dose for an early failed CSNF WP and a CDSP WP, respectively. The major radionuclide dose contributors for realizations 4930 and 4940 are shown on Figure 7.7.1-18[a]. The annual dose contributions from various aleatory vectors for the outlier epistemic vector 247 (Figure 7.7.1-17[a]) show the same general features as those shown for epistemic vector 281 discussed previously (Figure 7.7.1-2[a]): broad peaks between 1,000 and 10,000 years due to the contribution of ^{99}Tc from early failed CDSP WP; a series of peaks between 10,000 and 30,000 years representing contribution of ^{99}Tc from early failed CSNF packages located in various percolation subregions, where relative humidity increases above 95 percent threshold level at different times ; and peaks due to ^{239}Pu and ^{242}Pu that occur after ^{99}Tc peaks. Despite these similarities, the dose magnitudes are quite different among the two epistemic vectors: the magnitude of ^{99}Tc dose is an order of magnitude higher for epistemic vector 247 and up to two orders of magnitude higher for ^{242}Pu dose. Although all uncertain parameters are sampled separately among the two epistemic vectors, a comparison analysis reveals that these differences stem primarily from the sampled value of the probability of WP early failure with some contribution from differences in the solubility of plutonium in the WP and the SZ breakthrough curve for plutonium.

The probability of early failure of a WP (the pW_i term of Equation 6.1.2-13 of the parent document, equivalent to GoldSim parameter UNC_WP_EF_conv_from_ln) is the weighting term used by EXDOC when computing the expected dose for an epistemic vector. This term is about an order of magnitude higher for epistemic vector 247 (sampled value of 4.6×10^{-3} representing 99.98 percentile of the distribution) compared to that of epistemic vector 281 (sampled value of 3.3×10^{-4} representing 94.77 percentile of the distribution) and is responsible mostly for the outlier behavior of epistemic vector 247. The unweighted annual doses from 20 GoldSim realizations for these two vectors are quite similar as shown on Figures 7.7.1-2[a] and 7.7.1-17[a], underlining the importance of the weighting factor in determining the expected dose.

Figure 7.7.1-19[a] shows the SZ breakthrough curves for epistemic vector 247. The median travel time for dissolved and reversibly sorbed plutonium (denoted as aqueous) ranges from 49,000 to 110,000 years, which is significantly longer than for epistemic vector 281 with median travel times of 16,000 to 39,000 (Figure 7.7.1-5b[a]). This explains the delay in the ^{239}Pu peak in epistemic vector 247 compared to that in epistemic vector 281.

The mean plutonium solubilities within each EBS transport domain depends on the domain chemistry, but the sampled parameters Pu_Eps_1_low_a and Pu_Eps_1_high_a add uncertainty to the mean value thereby influencing the plutonium solubility throughout the EBS for both the CSNF and CDSP WPs. These parameters are above the 97th percentile for epistemic vector 247, but near the 50th percentile for epistemic vector 281, which causes an order of magnitude increase in the solubilities for epistemic vector 247. This is reflected in the higher concentrations within the waste form and WP seen on Figure 7.7.1-20a[a] compared to Figure 7.7.1-6b[a] and at early times on Figure 7.7.1-20b[a] versus 7.7.1-9b[a]. With the higher plutonium concentrations,

release is greater for epistemic vector 247. Unlike epistemic vector 281, ^{242}Pu becomes depleted within the WP.

7.7.1.2[a] Drip Shield Early Failure Modeling Case

This section presents an analysis of two out of the 3,000 realizations selected from the realization base-case run performed for calculating the expected annual dose from the Drip Shield EF Modeling Case (GoldSim filename: LA_v5.005_ED_003000_000.gsm; output DTN: MO0710ADTSPAWO.000 [DIRS 183752]). The 3,000 realizations in GoldSim represent 300 epistemic uncertainty vectors where each epistemic vector is used for 10 aleatory uncertainty vectors.

In the stylized Drip Shield EF Modeling Case, a single CSNF or CDSP WP is modeled in a seeping environment under a DS that is assumed to be completely failed (breached) at the start of the simulation. Furthermore, the WP is assumed to fail completely from localized corrosion at the onset of drift seepage when the in-drift temperatures are still hot.

The expected annual dose from all 300 epistemic vectors, along with the statistics on the distribution of expected annual dose, is shown on Figure 7.7.1-21[a]. Figure 7.7.1-22[a] shows the major radionuclides that contribute to the mean annual dose. There is an early peak due to ^{99}Tc and ^{129}I, whereas ^{239}Pu , ^{242}Pu, and ^{237}Np are the top contributors later on. Epistemic vector 228 was chosen for further analysis because it has a shape similar to the mean annual dose curve and has a higher dose than the mean annual dose curve for the simulated duration (Figure 7.7.1-21[a]).

The expected annual dose from epistemic vector 228 is calculated as a weighted average of annual dose for ten aleatory vectors (Equation 6.1.2-14 of the parent document). The ten aleatory vectors that correspond to epistemic vector 228 are GoldSim realizations 2271 to 2280, and their unweighted annual dose histories are shown on Figure 7.7.1-23[a]. The ten aleatory vectors represent only the dripping environments in five percolation subregions for both CSNF and CDSP WP types. As outlined in Equation 6.1.2-14 of the parent document, the dose from each realization is then multiplied by the probability of early DS failure, the fraction of waste type, the seepage fraction, and the percolation bin fraction, the latter being equal to the number of WPs in the percolation subregion divided by the total number of WPs in the repository. These weighted doses are then summed to derive the expected annual dose for epistemic vector 228, shown on Figure 7.7.1-21[a]. GoldSim realizations 2273 and 2278 are highlighted on Figure 7.7.1-23[a] to show the relative difference in unweighted dose behavior between a CSNF WP type (realization 2273) and CDSP WP type (realization 2278) located in the same percolation subregion (percolation subregion 3). Both realizations are considered for further analysis in this section (GoldSim filenames: LA_v5.005_ED_003000_002.gsm and LA_v5.005_ED_003000_003.gsm; output DTN: MO0801TSPAMVAC.000 [DIRS 185080]). The major radionuclides contributing to dose for realization 2278 are shown on Figure 7.7.1-24[a], and they are similar to the major dose contributors for the mean annual dose (Figure 7.7.1-22[a]). The early part of the dose curve is dominated by ^{99}Tc, the middle part is dominated by ^{239}Pu, and the latest part is dominated by ^{242}Pu (after ^{239}Pu has decayed). ^{79}Se is also important early on since no solubility-controlling solid for selenium is included in the TSPA-LA Model and it is retarded only moderately during transport (^{79}Se shows spiky behavior

later on due to the particle tracking algorithm used in the UZ transport model to track mass (Section 6.3.9 of the parent document)). The major radionuclides contributing to dose for realization 2273 are similar to the ones shown for realization 2278 and thus are not shown separately.

During the first 5,000 years, annual dose is dominated by the unretarded or weakly retarded species that have no solubility constraints, such as ^{99}Tc, ^{79}Se, and ^{14}C. After 5,000 years, and until about 250,000 years, ^{239}Pu dominates dose (Figure 7.7.1-24a[a]). As shown on Figure 7.7.1-24b[a], the dose from ^{239}Pu is a combination of dissolved plutonium and plutonium that is irreversibly sorbed onto colloids. The dose from ^{239}Pu irreversibly associated with the slow traveling fraction of colloids is comparable to the dose from dissolved ^{239}Pu. At later times (after about 300,000 years), ^{242}Pu is the dominant contributor to dose, as was demonstrated for the Waste Package EF Modeling Case discussed previously (Section 7.7.1.1[a]). Here again, the dose from ^{242}Pu is a combination of dissolved and irreversibly sorbed colloidal plutonium (Figure 7.7.1-24b[a]). Unlike the Waste Package EF Modeling Case, releases from the WP in this Drip Shield EF Modeling Case are mainly advective with low ionic strengths, so that colloidal transport becomes important early on.

The transport behaviors described above and depicted on Figure 7.7.1-24[a] are expected because ^{99}Tc, ^{79}Se, and ^{14}C are transported as solutes with little or no retardation in the engineered barrier and natural systems. Despite their similar transport properties and travel times to the biosphere, these three radionuclides exhibit variations in terms of dose due to differences in the initial inventory, decay rates, and biosphere dose conversion factors (BDCFs) for each of the radionuclides. In contrast to ^{99}Tc, ^{79}Se, and ^{14}C, the transport of ^{239}Pu is strongly affected by retardation in the EBS, UZ, and SZ. This retardation is caused by reversible sorption onto WP corrosion products and invert material (crushed tuff) in the EBS and on the rock matrix in the UZ and SZ. Almost all the ^{239}Pu that is associated irreversibly with colloids (embedded in HLW glass waste form colloids) is transported faster than dissolved ^{239}Pu due to a lesser degree of fracture matrix interaction in the UZ and SZ, so that colloidal ^{239}Pu contributes more significantly to dose earlier than dissolved ^{239}Pu.

Releases from Engineered Barrier System—The release of ^{99}Tc out of the EBS occurs around 500 years for the CDSP WP and around 750 years for the CSNF WP, even though the WP fails early at the start of the simulation (Figure 7.7.1-25[a]). This delay is due to the effects of temperature since no transport (diffusive or advective) is allowed as long as temperatures remain above the boiling point of water (100°C). Figure 7.7.1-25[a] shows that the temperature within a CDSP WP does not fall below 100°C until approximately 400 years after closure and, for CSNF WPs, the temperature does not fall below 100°C until after approximately 600 years. [Note that the radionuclide transport related calculations start as soon as the WP temperatures drop below 100°C but the release rate information is not available as an output until the end of the user specified timestep. For the first 10,000 years of simulation in this modeling case, the selected timestep size is 250 years.]

A number of processes in both the WP and invert influence the release of radionuclides from the EBS. Figure 7.7.1-25[a] shows the mass flux of ^{99}Tc out of the EBS into the UZ from both CSNF and CDSP WPs (from realizations 2273 and 2278, respectively). The ^{99}Tc release curve for the CDSP WP starts around 500 years and initially decreases as drift-wall condensation flux

changes from Stage 2 to Stage 3 (discussed next). Technetium is released instantaneously from the CSNF WPs, dropping off rapidly on this log-log plot.

Figure 7.7.1-26[a] shows water flow rate into WPs as a function of time for CDSP and CSNF WPs. The initially high flow rate for the CDSP WP occurs during Stage 2 drift-wall condensation; that is, for those times between when the temperature at the first location in a drift drops below boiling and when the temperature at the last location drops below boiling (Section 6.3.3.2 of the parent document). Flow into the CDSP WP becomes equal to the seepage rate after 500 years, when Stage 2 ends. The CSNF package shows low initial seepage because there is no Stage 2 drift-wall condensation for the hotter CSNF WP.

Figure 7.7.1-26[a] also shows how seepage into each WP increases with each change in climate state because of corresponding increases in the percolation rate. Changes in climate occur around 600 years; 2,000 years; and 10,000 years; and each change in a climate state is marked by an instantaneous change in seepage rates through the EBS (Figure 7.7.1-26[a]). The small increase in seepage rates at about 2,000 years is in response to a change in climate state from monsoonal to glacial-transition. A considerably larger increase in seepage rate occurs around 10,000 years in response to the change in climate from glacial-transition to the post-10,000 year climate state with its higher percolation and higher seepage rate.

The fractions of each waste form that have degraded for CDSP and CSNF packages are shown on Figure 7.7.1-27[a]. The CSNF waste form is completely degraded when the WP fails at the start of the simulation because the temperature exceeds 100°C, and CSNF degradation is modeled as being instantaneous above this temperature. Although not shown on Figure 7.7.1-27[a], the same is true for DSNF, which is assumed to degrade instantaneously upon WP breach at all temperatures. On the other hand, HLW glass in the CDSP package (Figure 7.7.1-27[a]) degrades according to the modeled degradation rate, which declines gradually as WP temperature decreases until all of the HLW glass has degraded by about 10,000 years (in this realization).

Unsaturated Zone—After their releases from the EBS, radionuclides enter the UZ and are partitioned among the UZ fractures and matrix. Most radionuclide mass released from the EBS is partitioned into the UZ fractures because the DS is failed and the WP is in the seeping environment of the given percolation subregion, so that most of the transport is by advection. Figure 7.7.1-28[a] shows the fraction of mass released to the UZ fractures for selected radionuclides from a CDSP WP located in seeping environment of percolation subregion 3. The ^{239}Pu mass in dissolved state and reversibly associated with colloids (denoted as aqueous) is differentiated from the mass irreversibly associated with slow traveling colloids, which is not in equilibrium with the mass in solution. Figure 7.7.1-28[a] shows that, at a minimum, 80 percent of the mass flux enters the UZ fractures but more commonly (at later times, especially beyond 10,000 years) greater than 95 percent of the mass flux is partitioned into the UZ fractures. The spikes down to zero (near the end of the simulation) are due to numerical approximations in the partitioning algorithm when essentially all of the ^{239}Pu has decayed and the actual release is approximately zero. Because of fast transport times in the UZ fractures, there is little delay in the first arrival of radionuclide mass at the SZ, as shown on Figure 7.7.1-29[a]. Almost all of the ^{99}Tc mass released from the EBS is also released out of the UZ in a short time and the cumulative release curves virtually overlay each other. However, only about 62 percent of the

^{242}Pu mass released from the EBS is released out of the UZ by 1,000,000 years. This reduction in the mass of ^{242}Pu released from UZ is attributed to the diffusive interaction between UZ fracture and matrix continuum with sorption in the matrix that leads to reduced mass transport through the UZ, particularly for the repository release nodes located in the southern part of the UZ transport domain (SNL 2008 [DIRS 184748], Figure D.2-5[b]).

Saturated Zone—Transport of ^{99}Tc through the SZ is relatively fast because it does not sorb to the SZ volcanic and alluvium units and almost all of the mass released out of the UZ is released from the SZ without any appreciable delay (Figure 7.7.1-29[a]). Transport of ^{242}Pu in the SZ shows a small delay over the simulated time period despite the potential to be retarded considerably from sorption onto the volcanic and alluvium units. This is because, in this realization, one of the fastest SZ breakthrough curves is sampled (out of a set of 200 breakthrough curves) for transport of plutonium with a median travel time of less than 10,000 years (SNL 2008 [DIRS 183750], Figure 6-9[a]). Almost all of the ^{242}Pu mass released out of the UZ is released from the SZ by the end of the simulated time period.

Drip Shield Early Failure Modeling Case: Outlier

For the purpose of analyzing an outlier realization, epistemic vector 244 was chosen as shown on Figure 7.7.1-30[a] because it has the highest annual dose from about 5,000 years to beyond 100,000 years for this Drip Shield EF Modeling Case. As discussed previously, each of the 300 curves shown on Figure 7.7.1-30[a] is a combination of ten aleatory vectors representing seeping environments in five percolation subregions for both CSNF and CDSP WP types. The unweighted annual dose from each of the ten aleatory vectors is multiplied by the corresponding probability of early DS failure, the WP type, the seepage fraction, and the percolation bin fraction, and then summed over aleatory vectors to derive the expected annual dose for the curve shown (Equation 6.1.2-14 of the parent document). Figure 7.7.1-31[a] shows the unweighted annual dose for the ten aleatory vectors corresponding to GoldSim realizations 2431 to 2440 for epistemic vector 244. Realization 2433 for the CSNF WP type is chosen for further analysis as it has a higher annual dose compared to a CDSP WP (e.g., realization 2438).

The major radionuclide dose contributors for realization 2433 are shown on Figure 7.7.1-32[a]. For the most part, the main contributors are similar to those in realizations 2273 and 2278 previously discussed. The major dose contributing radionuclide is ^{99}Tc before 1,000 years as it is not solubility limited and transports unretarded through the EBS, UZ, and SZ. The dose from ^{99}Tc decreases quickly as its inventory is depleted following waste form degradation. ^{237}Np is the major contributor at 2,000 years and also beyond 200,000 years. The peak around 5,000 years is due to the slow traveling fraction of colloids with irreversibly sorbed ^{243}Am and ^{239}Pu. From 6,000 years to 200,000 years, a combination of dissolved and reversibly sorbed ^{239}Pu mass on colloids (denoted as aqueous) and irreversibly sorbed ^{239}Pu mass on colloids dominate the dose.

Although all uncertain parameters are sampled separately for each epistemic vector, a comparison analysis reveals that for epistemic vector 244, the high dose for radionuclides of interest stem primarily from the sampling of iron oxyhydroxide colloid concentration and the solubility uncertainties. The concentration of iron oxyhydroxide colloids from corrosion of stainless steel inside the WP is determined by the epistemic uncertain parameter,

Conc_Col_FeOx_SS_Sampled_a. This parameter has a sampled value of about 5.1 mg/L in realization 2433, which is at the 92nd percentile. For comparison, the value of this parameter in realization 2273 described earlier is about 0.076 mg/L, which is at the 45th percentile.

The solubility limits of both neptunium and plutonium are high in realization 2433. Equation 6.3.7-13a of the parent document shows the importance of ε_1 (the term accounting for thermodynamic uncertainty) in determining the solubility for neptunium and plutonium. Both neptunium and plutonium have high sampled values of ε_1 in realization 2433. As discussed in Section 6.3.7, neptunium solubility is controlled by NpO_2 when stainless steel is present in the WP and by Np_2O_5 after the stainless steel is gone. The sampled value of ε_1 for NpO_2 is at the 90th percentile and the sampled value of ε_1 for Np_2O_5 is at the 99.7th percentile. Np_2O_5 has a higher base solubility than NpO_2 so there is a jump in dose when the solubility controlling phase changes just after 200,000 years (Figure 7.7.1-32[a]). Plutonium also has an extremely high value of ε_1 as it is sampled at the 99th percentile in realization 2433. These high values of ε_1 for neptunium and plutonium mean high solubility limits in the WP.

Seepage fraction (that is used to determine fraction of WPs in a seeping environment) and seepage rate are both important parameters in the Drip Shield EF Modeling Case. Figure 7.7.1-33[a] presents the seepage fraction statistics of the Drip Shield EF Modeling Case run for 6,000 realizations along with the seepage fraction for realization 2433. The seepage fraction for realization 2433 is only slightly below the mean and median seepage fraction indicating that seepage fraction is not the reason for the high doses in this realization. Figure 7.7.1-34[a] presents the seepage rate statistics along with the seepage rate for realization 2433. The seepage rate for realization 2433 is above the mean past 2,000 years and at the 95th percentile beyond 10,000 years. This high seepage rate in this realization, when combined with a greater concentration of iron oxyhydroxide colloids and higher solubility limits for neptunium and plutonium, results in high advective release from EBS and a larger dose.

In addition to the higher release from the EBS, fast breakthrough curves in the SZ are sampled for neptunium and plutonium. Figure 7.7.1-35[a] shows the SZ breakthrough curves for neptunium and plutonium for the four SZ regions for realization 2433. These curves, particularly for Region 1, can be compared to the 200 possible breakthrough curves for Region 1 used in the SZ model that are shown in *Saturated Zone Flow and Transport Model Abstraction* (SNL 2008 [DIRS 183750], Figures 6-9[a] and 6-11[a]). The breakthrough curves for both neptunium and plutonium in realization 2433 appear to be in the fastest 5 to 10 percent of the 200 breakthrough curves. The short travel time in the SZ results in little decay in the natural system so the high EBS releases contribute to high dose.

7.7.1.3[a] Igneous Intrusion Modeling Case

This section presents analyses of two single realizations selected from among the 3,000 realization base-case runs used to calculate the expected annual dose from the Igneous Intrusion Modeling Case for a one-million-year simulation (GoldSim filename: LA_v5.005_IG_003000_000.gsm; output DTN: MO0710ADTSPAWO.000 [DIRS 183752]). The 3,000 realizations are the combination of 300 epistemic uncertainty vectors and ten aleatory uncertainty vectors that specify the times of igneous intrusion events. In other words, each realization of this modeling case has one igneous intrusion event occurring at a specified time

with one given epistemic vector. The duration of the simulation for this modeling case is 1,000,000 years. The reader is referred to Sections 6.1.2 and 6.1.3 of the parent document for a discussion of how aleatory and epistemic uncertainties are treated and how expected annual dose is calculated for the Igneous Intrusion Modeling Case. Sections 6.5.1 of the parent document and 6.5.1[a] of this addendum provide details about the conceptual model, model abstraction, and TSPA-LA Model implementations for the Igneous Intrusion Modeling Case.

All WPs and DSs are assumed to have failed completely due to the igneous intrusion event so that the capabilities of both WP and DS to act as barriers to water flow are ignored. In addition, before the time of intrusion, only nominal corrosion is assumed for this modeling case, such that WPs could be breached by either SCC or by general corrosion and, thereby, subject radionuclides to potential release.

The mean annual dose and predominant radionuclides that contribute to it are shown for the base case on Figure 7.7.1-36[a]. This figure shows that the mean annual dose increases rapidly for the first 100,000 years to about 0.9 mrem, then decreases slightly to the value of 0.54 mrem at around 250,000 years, and then increases gradually for the remaining 750,000 years to a maximum of 0.89 mrem. The radionuclide that dominates dose early on (for the first 200,000 years) is ^{239}Pu, with its contribution decreasing as it undergoes radioactive decay. While the contribution from ^{239}Pu decreases, the contributions from ^{226}Ra, ^{242}Pu, and ^{237}Np increase. At around 200,000 years, ^{242}Pu overtakes ^{239}Pu as the radionuclide that dominates dose. Beyond 250,000 years, ^{226}Ra, ^{242}Pu, and ^{237}Np together account for more than two-thirds of the mean annual mean dose.

Expected annual dose from all 300 epistemic vectors is shown on Figure 7.7.1-37[a]. The expected annual dose of epistemic vector 286 is similar to the mean annual dose, which is why this epistemic vector was chosen for selecting the single realization used in the following analysis. Figure 7.7.1-38[a] presents the annual dose for the ten aleatory vectors that are associated with epistemic vector 286 and are represented by GoldSim realizations 2851 through 2860. Among these, GoldSim realization 2855, which has an igneous event occurring at 10,000 years, is chosen for the single realization analysis because its contribution to dose starts early. The model for GoldSim realization 2855 was run twice in order to first save information for all the percolation subregions and then to specifically save EBS cell-pathway details related to percolation subregion 3 under a seeping environment (GoldSim filenames: LA_v5.005_IG_003000_003.gsm and LA_v5.005_IG_003000_004.gsm; output DTN: MO0801TSPAMVAC.000 [DIRS 185080]).

This analysis of realization 2855 focuses on the four major contributors to dose mentioned above (^{239}Pu, ^{226}Ra, ^{242}Pu, and ^{237}Np) plus ^{234}U, whose transport behavior largely dominates the transport behavior of the decay product ^{226}Ra. Note that the annual dose for realization 2855 decreases slowly (Figure 7.7.1-38[a]), which differs somewhat from the late-time trend of expected annual dose for epistemic vector 286 (Figure 7.7.1-37[a]). This difference is due to the fact that the expected annual dose includes contributions from additional aleatory vectors with later igneous events.

Figure 7.7.1-39[a] shows the time history of total annual dose (summed over all radionuclides) along with the contributions to annual dose from the five radionuclides selected for the analysis

for realization 2855. A spike in total annual dose (~1,000 mrem) is noticeable immediately after the igneous intrusion event at 10,000 years. This spike is dominated by highly mobile radionuclides, primarily ^{99}Tc, ^{129}I, ^{14}C, and ^{36}Cl (none of which are shown on Figure 7.7.1-39[a]). Dose contributions from these four radionuclides decrease by about two orders of magnitude or more over the 10,000 years following the igneous event, so that by about 20,000 years after repository closure they contribute less than about 10 percent of the total annual dose (in this realization). For this reason, these four radionuclides are not analyzed in further detail in this section.

While dose contributions from these (and other) highly mobile radionuclides decrease, dose contributions from the four actinide radionuclides, ^{239}Pu, ^{237}Np, ^{234}U, and ^{242}Pu, increase until their contributions to total annual dose levels off between 28,000 and 130,000 years. After this, total annual dose decreases gradually for the duration of the simulation.

Igneous Intrusion—For GoldSim realization 2855, the igneous intrusion occurs at 10,000 years. The igneous intrusion fails all CSNF and CDSP WPs (total of 11,629 WPs) as well as the DSs. None of the WPs and DSs have failed by nominal corrosion processes prior to this event. Following the igneous intrusion, all WPs and waste forms experience high temperatures (peak expected temperature is 1,150°C) because of the heat of the magma. The high temperatures result in degrading all of CSNF instantaneously, oxidizing the UO_2 to U_3O_8, and making all non-uranium radionuclides available for release. Furthermore, because U_3O_8 has a high specific surface area (BSC 2004 [DIRS 169987], Section 6.2.2.2), the dissolution of U_3O_8 is also essentially instantaneous once contacted by water. The high temperature also results in rapid degradation of HLW glass. Five hundred years after the igneous event (i.e., a single timestep in the simulation during this time) WP temperature is calculated to have dropped to 52°C.

The various EBS environments affect waste form degradation and radionuclide mobilization differently for the Igneous Intrusion Modeling Case (discussed in Section 6.5.1.1.2 of the parent document) as compared to the Nominal Scenario Class (Section 6.3.4 of the parent document).

EBS Releases—The high degradation rates of CSNF and HLW allow the near-immediate release of their corresponding radionuclide inventories into solution. Because of solubility constraints, some radionuclides precipitate within the waste form domain of the EBS transport model. Following the igneous event, dissolved concentrations of neptunium, plutonium, and uranium from the CSNF waste form domain reach and are maintained at their solubility limits (Figure 7.7.1-40[a]). The solution (water) remains saturated with neptunium for about 40,000 years after the intrusion event while it is saturated with plutonium for about 200,000 years. The solution remains saturated with uranium throughout the simulation, owing to its large inventory. Dissolved radium concentrations, however, remain below the solubility limit in the CSNF waste form domain throughout the simulation. The dissolved concentration of radium increases early and is followed by a gradual decrease, due to the decay-chain ingrowth from ^{234}U (half-life = 246,000 yr) and subsequent decay of ^{226}Ra (half-life = 1,600 yr). The dissolved concentrations of neptunium and plutonium decrease rapidly once their precipitated solids have dissolved. As a result, their subsequent releases are not solubility controlled.

Gradual decreases in uranium, neptunium, and plutonium solubility limits (between 10,000 and 170,000 years) are caused by the gradual shift of pH towards neutral and a decrease of Pco_2 over

that period (Figure 7.7.1-41[a]). The sharp increase in the solubility limit for neptunium at 172,000 years (Figure 7.7.1-40[a]) occurs because the solubility controlling phase is changed from NpO_2 to Np_2O_5 following complete degradation of all steel that can act as a reductant (i.e., an electron donor) inside the waste form domain (Section 6.3.7.5 of the parent document for further discussion).

As discussed in Section 6.5.1.1.1 of the parent document, every WP and DS is rendered incapable of protecting its contents after an igneous intrusion event. As a result, high seepage fluxes flow through each WP, and these fluxes are set equal to the local percolation flux after an igneous intrusion (Section 6.5.1 of the parent document) and range from 0.18 to 3.54 m^3/yr. This leads to rapid releases of radionuclides from the WPs once the temperature drops below the boiling point of water (Figure 7.7.1-42[a]). Note that two types of mass release rates for ^{239}Pu and ^{242}Pu are presented in Figure 7.7.1-42[a]: (a) the release rate of mass dissolved and reversibly sorbed on colloids (denoted as aqueous) and (b) the release rate that also includes the mass irreversibly associated with the colloids (denoted as total). Among the four radionuclides for this analysis, ^{237}Np exhibits the highest release rate (approximately 550 g/yr), and its release rate decreases gradually as its inventory is depleted and its concentration declines. Releases of ^{242}Pu, ^{234}U, and ^{226}Ra have trends similar to that of ^{237}Np, whereas the release of ^{239}Pu decreases rapidly because of its relatively short half-life (2.41×10^4 years). Figure 7.7.1-42[a] also shows that most (greater than 90 percent) of ^{239}Pu and ^{242}Pu is transported as dissolved and reversibly sorbed on colloids, with the rest being transported irreversibly sorbed on colloids. For this reason, the irreversibly sorbed colloidal component of plutonium is not discussed in the rest of this analysis and the release rates of ^{239}Pu and ^{242}Pu referred hereafter only include the mass dissolved and reversibly sorbed on colloids.

Figure 7.7.1-43[a] shows the advective and diffusive release rates of major radionuclides from CSNF WPs. It shows that advection is the major transport mechanism for radionuclides released from WPs for the Igneous Intrusion Modeling Case. Diffusion contributes less than one percent of the total release from WPs except for ^{242}Pu at late time. Comparing Figure 7.7.1-43[a] with Figure 7.7.1-42[a] reveals that CSNF WPs are the dominant source for those major radionuclides.

Figure 7.7.1-44[a] presents the dissolved concentrations of neptunium, uranium, plutonium, and radium and their solubilities in the CSNF corrosion products domain for percolation subregion 3 under seeping environment. It shows that in the corrosion products domain, neptunium and plutonium concentrations maintain at their solubilities for a longer time than in the waste form domain (Figure 7.7.1-40[a]). However, unlike in the waste form domain, uranium concentration does not reach its solubility limit. Similar to the waste form domain, radium concentration does not reach its solubility limit. Moreover, dissolved concentrations of neptunium and plutonium decrease at slower rates than in the waste form domain because the corrosion products in the corrosion products domain gradually release neptunium and plutonium that had been sorbed onto corrosion product solids. The solubility controlled releases of ^{237}Np and ^{239}Pu are responsible for the 'plateau' in total dose between 28,000 and 130,000 years (Figure 7.7.1-39[a]).

Changes in radium solubility at 57,500 and 340,000 years are due to pH changes that cause the model to switch between two values of the radium solubility limit (Section 6.3.7.5.2 of the parent document). Changes in uranium solubility at those times also reflect changes in pH that cause

the model to switch between dissolved uranium concentrations being controlled by Na-boltwoodite solubility and schoepite solubility (Section 6.3.7.5.2 and Tables 6.3.7-56 and 6.3.7-57 of the parent document).

Natural System—Cumulative releases of ^{237}Np, ^{242}Pu, ^{234}U, and ^{226}Ra from the EBS, UZ, and SZ are presented in Figure 7.7.1-45[a]. Figure 7.7.1-45a[a] shows a small delay for ^{237}Np from the UZ and SZ of 500 years each (i.e., one timestep for each zone). This small delay is due to the fast transport predominately along the fracture pathways, with limited diffusion into the surrounding matrix. At the end of the simulation, 99 percent of neptunium that had been released from the EBS has migrated through the UZ, and 96 percent of that has migrated through the SZ. In other words, the UZ and SZ provide relatively minor retardation for ^{237}Np in this realization of the Igneous Intrusion Modeling Case. This is attributed to the relatively small K_d values assigned to neptunium. Similarly, ^{234}U is not substantially retarded by the UZ and SZ on Figure 7.7.1-45b[a]. The figure shows that the cumulative release of ^{234}U from the SZ after 330,000 years is higher than that from the EBS. This is not a numerical error but is caused by 'inventory boosting' performed at the UZ-SZ interface for transport through the SZ (Section 6.3.10.3 of the parent document).

Cumulative release of ^{242}Pu shown on Figure 7.7.1-45c[a] illustrates the relative influences that the UZ and SZ have on delaying plutonium release. The UZ delays plutonium release for a few thousand years, whereas plutonium release is delayed for more than 10,000 years by the SZ. At the end of the simulation, about 24 percent of ^{242}Pu that had been released from the EBS remains in the UZ, and 29 percent of ^{242}Pu that had been released from the UZ remains in the SZ. The UZ and SZ both retard ^{242}Pu significantly. This is attributed to the sorption of plutonium in the SZ volcanic matrix (as a result of fracture-matrix interactions) and alluvium.

The cumulative release history for ^{226}Ra is presented on Figure 7.7.1-45d[a], which indicates that a large fraction of ^{226}Ra released from the EBS does not exit the SZ. If radioactive decay and decay-chain ingrowth is ignored, then by 1,000,000 years, only 25 percent of ^{226}Ra that had been released from the EBS would have migrated through the UZ, and less than 0.1 percent of ^{226}Ra that had been released from the UZ would have migrated through the SZ. This substantial reduction in the mass of ^{226}Ra is caused by the high K_d values assigned to radium in the UZ and SZ (Tables 6.3.9-2 and 6.3.10-2 of the parent document) that serve to retard ^{226}Ra transport through the UZ and SZ. When this delay is combined with the short half-life of ^{226}Ra (1,600 years; Figure 6.3.7-4 of the parent document) it results in a significant decrease in the cumulative release from the SZ.

As pointed out previously, Figure 7.7.1-39[a] shows that the annual dose curve has a plateau that appears between 28,000 and 130,000 years. This plateau corresponds to the SZ groundwater concentration plateau of ^{237}Np and ^{239}Pu at the RMEI location for the same duration as shown on Figure 7.7.1-46[a]. The concentration plateaus correspond to the solubility controlled releases of neptunium and plutonium from the corrosion products domain shown on Figure 7.7.1-44[a]. Note that the SZ groundwater concentrations shown on Figure 7.7.1-46[a] are obtained by dividing the annual releases of radionuclides from the SZ by the 3,000 acre-ft/yr annual water usage, as per the regulatory requirements. Although the SZ groundwater concentration of ^{237}Np is higher than that of ^{239}Pu, the latter has a higher concentration dose conversion factor. As a result, ^{239}Pu dose is higher than ^{237}Np dose.

Figure 7.7.1-46[a] shows that for the first 500,000 years, the ^{234}U concentration increases with time and then decreases; so does the ^{226}Ra concentration. This suggests that ^{226}Ra concentration is largely controlled by ^{234}U concentration since the former is a decay product of the latter.

Igneous Intrusion Modeling Case: Outlier

For the purpose of analyzing an outlier realization for the Igneous Intrusion Modeling Case, epistemic vector 20 was chosen as shown on Figure 7.7.1-47[a] because it has the highest annual dose from about 50,000 years to about 300,000 years. Figure 7.7.1-48[a] shows the unweighted annual dose from 10 aleatory vectors, equivalent to GoldSim realizations 191 through 200, for epistemic vector 20. GoldSim realization 191 was chosen for further study, and the results are compared with GoldSim realization 2855 described earlier. In realization 191, the igneous event time is specified at 250 years and thereby occurs much earlier than for realization 2855, where it is specified at 10,000 years. Figure 7.7.1-49[a] shows the time history of annual dose and the contributions to annual dose from the selected radionuclides for realization 191. Four spikes in the total annual dose can be seen, with three prior to 10,000 years and the fourth being a broad peak past 10,000 years. The first spike (annual dose magnitude of about 1,100 mrem) occurs shortly after the igneous intrusion. This spike is caused by mobile radionuclides that travel unretarded through the engineered barrier and natural barrier system, such as ^{99}Tc, ^{129}I, and ^{14}C. The second spike (annual dose magnitude of about 400 mrem) occurs at 2,250 years shortly after a climate change from the monsoon to the glacial-transition climate. As shown in Figure 7.7.1-50[a], water flux through WPs increases due to the climate change, which causes higher advective releases and annual dose. The second spike is also caused by mobile radionuclides, such as ^{99}Tc, ^{129}I, and ^{14}C.

The third spike (annual dose magnitude of about 900 mrem) occurs at 4,500 years. Dose contribution from ^{79}Se dominants this spike. Selenium is moderately retarded in the UZ and SZ, as it has moderate K_d values in the UZ and SZ (Tables 6.3.9-2 and 6.3.10-2 of the parent document). ^{79}Se is not a major dose contributor in realization 2855 analyzed previously, nor in the base case (Figures 7.7.1-39[a] and 7.7.1-36[a]). Further analysis reveals that the sampled BDCF for ^{79}Se in realization 191 is 123 times higher than that in realization 2855 (a sampled value of 2.73 (mrem/yr)/(pCi/l) versus 2.22×10^{-2} (mrem/yr)/(pCi/l)). This is the primary reason for high ^{79}Se dose in realization 191.

The fourth spike (annual dose magnitude of about 6,900 mrem) occurs around 50,000 years with ^{239}Pu as the dominant radionuclide and the peak dose is about ten times higher than that in realization 2855 (Figure 7.7.1-39[a]). This is attributed to the higher solubility of plutonium in this realization, which is calculated to be about 0.105 mg/L in the CSNF waste form domain (Figure 7.7.1-51[a] compared to a value of about 0.005 mg/L for realization 2855 (Figure 7.7.1-40[a]). This difference (a factor of 21) is mainly caused by the difference in the sampled thermodynamic uncertainty values (the term ε_1 in Equation 6.3.7-13a of the parent document) for plutonium solubility (equivalent to GoldSim uncertain parameter Pu_Eps_1_low_a). In realization 191, the log of thermodynamic uncertainty is sampled to be 1.218 (at 96th percentile of the distribution), while for realization 2855, the sampled log value is -0.3428 (at 30th percentile of the distribution). The difference results in an increase in plutonium solubility by a factor of 36. Since there are other factors that modify the solubility, the actual

difference in plutonium solubility is smaller (21 times) than the difference in the sampled thermodynamic uncertainty.

The increase in ^{239}Pu dose after 10,000 years is due to climate change at 10,000 years leading to increased flow rate through the WP (Figure 7.7.1-50[a]) and faster travel times through the UZ and SZ. Annual dose contribution from ^{239}Pu decreases with time after 50,000 years, as the mass is depleted from the inventory and undergoes radioactive decay. Figure 7.7.1-51[a] shows that in the CSNF waste form domain, plutonium release is under solubility control until 156,000 years, while uranium release is under solubility control until 344,000 years. At later times, past 200,000 years, ^{242}Pu, ^{237}Np, ^{234}U, and ^{226}Ra overtake ^{239}Pu as the major dose contributors and show behavior similar to that of realization 2855.

7.7.1.4[a] Seismic Ground Motion Modeling Case for One Million Years

This section presents an analysis of a single realization from the 9,000 realization base-case run performed for calculating the expected dose from the Seismic GM Modeling Case (GoldSim filename: LA_v5.005_SM_009000_003.gsm; output DTN: MO0710ADTSPAWO.000 [DIRS 183752]) for the one-million-year long simulation. The expected annual dose is presented on Figure 7.7.1-52[a], where each of the 300 realizations represents expected annual dose for one epistemic uncertainty vector. The expected annual dose for each epistemic uncertainty vector is generated by taking an expectation over a sample of 30 aleatory uncertainty vectors. More details about the computational methodology is provided in Sections 6.1.2.4.4 and 7.3.2.6.2 of the parent document. A single epistemic vector is selected for further analysis in such a manner that the expected annual dose is broadly representative of the modeling case and similar in behavior to the mean annual dose curve (Figure 7.7.1-52[a]). A separate outlier realization analysis is not included for 1,000,000 year Seismic GM Modeling Case because the epistemic vector chosen for the detailed analysis has an expected annual dose near or above the 95th percentile and could be considered an outlier realization.

Epistemic uncertainty vector 155 is selected for further analysis. The thirty corresponding aleatory vectors (sampling sequences) are represented by GoldSim realizations 4621 through 4650 (Figure 7.7.1-53[a]). Of these, the aleatory vector 21 (sampling sequence 21), which is equivalent to GoldSim realization 4641, is selected for detailed analysis (solid red curve on Figure 7.7.1-53[a]). The GoldSim file for realization 4641 was run twice: first to save information for all the percolation subregions and then to specifically save details of the EBS cell pathway related to percolation subregion 3 for the seeping environment (GoldSim filenames: LA_v5.005_SM_009000_004.gsm and LA_v5.005_SM_009000_005.gsm; output DTN: MO0801TSPAMVAC.000 [DIRS 185080]).

The annual dose from realization 4641 is presented on Figure 7.7.1-54[a], along with contributions to dose from individual radionuclides. The annual dose profile shows four major peaks, two of which occur before 100,000 years and the other two around 300,000 years and 500,000 years. Prior to 500,000 years, the radionuclides that dominate dose are ^{99}Tc, ^{129}I, ^{79}Se, ^{239}Pu, and ^{242}Pu, after which dose is predominantly from ^{242}Pu, with minor contributions from ^{135}Cs and ^{237}Np. The annual dose increases steadily after 700,000 years. There is no dose prior to 24,500 years.

Seismic events are modeled as a Poisson process and are generated randomly at the specified rate of 4.287×10^{-4} yr^{-1} (equal to the difference between maximum annual exceedance frequency of 4.287×10^{-4} yr^{-1} and the minimum annual exceedance frequency of 1×10^{-8} yr^{-1}) (Section 6.6.1.3.2 of the parent document). Over the course of any simulation, several seismic events can occur with an average value of 429 total events (computed by multiplying the specified rate of the Poisson process, 4.287×10^{-4} yr^{-1}, by the simulation time period of one million years). For realization 4641, a total of 460 seismic events occur over the simulated duration (Figure 7.7.1-55[a]). The horizontal component of the peak ground velocity (PGV) corresponding to each seismic event (also shown on Figure 7.7.1-55[a]) is calculated from the mean bounded seismic hazard curve (Section 6.6 of the parent document) by uniformly sampling the annual exceedance frequency between the minimum and maximum values for each event.

The probability of damage from an event is calculated separately for the CDSP and CSNF packages due to the inclusion of a transportation, aging, and disposal canister in the CSNF packages, which increases their structural strength. Though the response surfaces for the probability of damage are different for CDSP and CSNF packages, they are both functions of the PGV and the residual stress threshold (RST) of Alloy 22. The PGV value varies with each seismic event (as shown on Figure 7.7.1-55[a]), whereas the RST of Alloy 22 is treated as an epistemic uncertainty and held constant over the realization. The RST can vary uniformly from 90 percent to 105 percent of the yield strength, and the value of 91.92 percent for epistemic vector 155 indicates a sample from the lower end of the distribution. A lower RST value typically results in a greater probability of damage to the WP during a given seismic event; however, the actual damage depends on a number of other conditions, such as whether the WP has intact internals or degraded internals, whether the DS framework and plate are intact or not, and whether the WP is covered by rubble or not. Each of these conditions is determined separately.

Based on the DS plate and framework fragility analysis (Section 6.6.1.3.5 of the parent document), which is a function of DS plate and framework thicknesses at the time of the event; the fraction of the drift filled by rubble (in lithophysal zones) at event time; and the PGV of the event, the DS framework is not calculated to fail until 90,485 years and the DS plate does not fail until 267,465 years (Figure 7.7.1-56[a]). (The failure times are taken from calculations done in GoldSim filenames: LA_v5.005_SM_009000_004.gsm and LA_v5.005_SM_009000_005.gsm; output DTN: MO0801TSPAMVAC.000 [DIRS 185080].) At the time of DS plate failure, the fraction of drift filled by rubble is still less than half (about 0.43). Note that the failure time of the DS from rubble fill (due to seismic events) is computed to be much earlier than the expected DS failure time from general corrosion only, which is computed to occur around 307,000 years.

The time of initial damage to the WP due to a seismic event is determined separately for CDSP and CSNF WPs (Section 6.6.1.3.8 of the parent document) and is calculated as the earliest of the following three failure times:

1. The time of initial damage to the intact WP moving freely beneath the intact DS. The probability of damage is based on intact WP-internals abstraction by assuming a 23-mm thickness of the WP OCB and is a function of PGV and RST.

2. The time of initial damage to the WP surrounded by rubble after the DS (either framework or plate) is failed. The probability of damage is based on the damage abstraction for the degraded WP internals surrounded by rubble and is a function of PGV, RST, and WP OCB thickness.

3. The time of initial damage to the WP by puncture after the DS plate is failed. The probability of damage is a function of PGV and WP OCB thickness.

For a CDSP WP, initial damage is caused by the seismic event at about 24,100 years, which is calculated from the damage abstraction for the intact WP moving freely beneath the intact DS. (The failure times are taken from calculations done in GoldSim filenames: LA_v5.005_SM_009000_004.gsm and LA_v5.005_SM_009000_005.gsm; output DTN: MO0801TSPAMVAC.000 [DIRS 185080].) The DS failure times are much later than the CDSP WP failure times. The PGV of the seismic event is about 0.7 m/s, and the probability of damage is computed to be about 0.22 for the sampled RST of 91.92 percent, based on results presented on Figure 6.6-11a of the parent document. To determine if damage occurs, the probability of damage is compared to a random number generated by sampling a uniform distribution between 0 and 1 for each seismic event; if the probability of damage exceeds the random number, the WP is calculated to be damaged. At the event time of about 24,100 years, the random number is 0.15 and so the CDSP WP is considered to be damaged. All CDSP WPs fail at this time, as there is no spatial variability for seismic damage (ignoring the small variation in WP thicknesses across various percolation subregions). The number of CDSP WPs failing in each percolation subregion for both seeping and non-seeping environments is shown on Figure 7.7.1-57[a].

For CSNF WPs, the first damage from a seismic event is calculated to be past the simulation time period. This is possible since the probability of a CSNF WP getting damaged directly from a seismic event is extremely small (Figure 6.6-10a of the parent document). Therefore, in this realization, CSNF WP breaches from SCC caused by nominal processes occur much earlier than breaches due to seismic damage within the simulated time period (Figure 7.7.1-58[a]). The breach times calculated by WAPDEG differ for each percolation subregion due to variability in corrosion processes and thermal profiles for the WP. The time of the first breach of CSNF WPs in the various percolation subregions is as follows: 188,000 years in percolation subregion 1; 168,000 years in percolation subregion 2; and around 204,000 years in percolation subregions 3, 4, and 5. Failure of additional CSNF WPs from nominal processes occur based on the WAPDEG calculated WP failure history for each percolation subregion. The CSNF WP failure time history for each percolation subregion, for both seeping and non-seeping environments, is shown on Figure 7.7.1-58[a]. Noticeable jumps in the number of failed WPs around 300,000 years and 500,000 years reflect coarse time discretization used by WAPDEG at late simulation time periods.

In order to compute the representative WP damaged area for a given percolation subregion for performing radionuclide transport calculations, a conservative approach is adopted when the WP failures first occur due to nominal processes and fail over time. Following the first WP failure, the WP damage abstraction for degraded internals is used and any damage from subsequent seismic events is added to the previous damaged area for the representative WP. This time varying cumulative damage area computed for the first failed WP is then applied to other WPs in

the percolation subregion once they fail by either nominal processes or seismic ground motion, thereby maximizing the area for radionuclide transport. Since all CDSP WPs simultaneously fail around 24,100 years from seismic damage, the damaged area of a WP increases from zero to an initial small area due to the first appearance of cracks. It then increases from subsequent seismic events that cause damage but remains relatively small, as shown for percolation subregion 3 (Figure 7.7.1-59[a]). The initial damage area increases sharply past 49,000 years, followed by a few more increases from events that cause damage. After failure of the DS plate (around 268,000 years), the WP is assumed to be surrounded by rubble, and the probability of damage decreases considerably, leading to no additional damage from subsequent seismic events—until the seismic event that occurs at about 850,000 years. However, past 200,000 years there are small, gradual increases in the opening area due to continuing SCC from nominal processes. Beyond 500,000 years, patches from general corrosion processes start to appear and the total opening area increases rapidly. The breach area history for the CSNF WPs is similar to that for CDSP WPs, except for the start time which is much later, as shown for the percolation subregion 3 on Figure 7.7.1-60[a]. Following the first stress corrosion crack failure from nominal processes around 204,000 years, the opening area increases discretely (from further SCC) as a result of subsequent seismic damages, although there is some small gradual increase in the opening area due to continuing SCC from nominal processes. Nevertheless, the breach area remains relatively small until general corrosion patches appear after about 600,000 years.

Calculations of the seismically damaged area that use the degraded internals abstraction are based on the thickness of the WP OCB (Figures 6.6-10 to 6.6-17 of the parent document), in addition to the sampled PGV and the RST value. Two end-member seismic-damage abstractions are generally used in the TSPA-LA Model. One is based on the 23-mm OCB thickness applied if the OCB thickness is greater than or equal to 23 mm. The second abstraction is based on the 17-mm OCB thickness applied if the OCB thickness is less than or equal to 17 mm (this happens rarely and typically near the end of the simulated time period). For OCB thicknesses between 23 mm and 17 mm, the damage is based on the linear interpolation between the two end-member damage abstractions. Inside-out corrosion of the OCB begins once the WP is breached, which accelerates thinning of the WP OCB and makes it more susceptible to both seismic damage and general corrosion patches. Profiles of mean thicknesses of WP OCB for both CDSP and CSNF WPs in percolation subregion 3 are shown on Figure 7.7.1-61[a], along with WP failure fractions. The initial thicknesses of both types of WP are the same but diverge due to the initiation of inside-out corrosion of all CDSP WPs following seismic damage around 24,100 years. On the other hand, the CSNF WPs do not begin to fail until after 200,000 years, and they typically fail over an extended period. Thus, failed CSNF WPs are, on average, thicker than failed CDSP WPs, making CSNF WPs less susceptible to seismic damage and general corrosion induced patch failures compared to CDSP WPs. This is the primary reason for the smaller opening area and longer time taken for patches to appear on CSNF WPs (Figure 7.7.1-60[a]) compared to CDSP WPs (Figure 7.7.1-59[a]).

Because general corrosion patches on the WPs (either CSNF or CDSP) do not appear until 500,000 years or later, all mass released from failed WPs until that time is by diffusion through stress corrosion cracks (because no advective water flow is allowed through stress corrosion cracks). ^{99}Tc is a major dose contributor, and its diffusive mass flux out of CDSP WPs for various percolation subregions is shown on Figure 7.7.1-62a[a]. Note that the relative magnitude of release rates among percolation subregions is proportional to the number of failed WPs in

each percolation subregion (Figure 7.7.1-57[a]). Releases of ^{99}Tc start when WPs are first damaged (around 24,100 years), then decrease over the next approximately 25,000 years as steady-state conditions are established. Release rates increase again around 49,500 years due to a sharp increase (about 30 fold) in the WP damage area (Figure 7.7.1-59[a]). Even though most of the HLW glass waste form has degraded by 40,000 years, including all of DSNF mass, not until about 55,000 years is most of the ^{99}Tc mass released from the WP. This delay reflects the role of small cracks in reducing the rate of release, despite the lack of a solubility controlling solid for ^{99}Tc and large concentration gradients across the WP.

In contrast, the diffusive mass flux of ^{242}Pu (a major dose contributor past 500,000 years) out of the failed CDSP WPs remains relatively constant (Figure 7.7.1-62b[a]). The release rate follows the WP OCB area opening curve, an indication that diffusive release of plutonium is proportional to the total WP opening area (Figure 7.7.1-59[a]). The slow relative release of ^{242}Pu is maintained throughout the simulation for a variety of reasons, including (a) longer half-life of ^{242}Pu (~ 375,000 years) compared to that of ^{99}Tc (210,000 years), (b) the dissolved concentration inside the waste form domain is limited by the solubility controlling mineral phase (Section 6.3.7.5 of the parent document) so that not all of the degraded mass is available for release, (c) sorption of ^{242}Pu in the corrosion products domain retards its transport and reduces the concentration gradient for diffusive flux, and (d) small diffusive areas associated with the WP OCB reduce the mass flux. Of these four factors, most important is sorption onto corrosion products. For example, in percolation subregion 3 for the seeping environment, 1,055 CDSP WPs fail around 24,100 years. Total initial ^{242}Pu mass in the CDSP inventory (combined HLW and DSNF masses) is approximately 38.65 g/pkg (grams per CDSP package) (from Table 6.3.7-5 of the parent document, with an adjustment based on uncertainty in the inventory). By using the decay rate of 1.85×10^{-6} yr^{-1}, the maximum mass of ^{242}Pu at the time of WP breach would be about 36.97 g/pkg, and about 35.31 g/pkg at 49,000 years, when breach area increases (Figure 7.7.1-59[a]). Based on the results of the transport calculation, the mass of ^{242}Pu sorbed onto corrosion products at 49,000 years is about 35.30 g/pkg, which accounts for just about all of the available mass. The mass is slowly released by desorption from corrosion products into the solution, thereby controlling both dissolved concentration (Figure 7.7.1-63[a]) and diffusive flux. Note that a mechanistic competitive sorption model that considers kinetic sorption and desorption is implemented for plutonium in the corrosion products domain (Section 6.3.8 of the parent document). As a result, variations in ^{242}Pu concentration within the corrosion products domain are moderated, even though upstream concentrations (in the waste form domain) can vary over a larger range based on time-varying degradation rates and solubility limits.

The diffusive flux of ^{99}Tc and ^{242}Pu from all five percolation subregions for CSNF WPs is shown on Figure 7.7.1-64a[a] and Figure 7.7.1-64b[a]. The release from percolation subregion 2 precedes releases from other percolation subregions (as expected) because CSNF WPs fail in percolation subregion 2 first (Figure 7.7.1-58[a]). Figure 7.7.1-60[a] shows the evolution of the CSNF WP OCB opening area for percolation subregion 3 in a seeping environment. The ^{99}Tc diffusive releases from CSNF WPs are sustained for a much longer time than are releases from CDSP WPs (compare Figure 7.7.1-64a[a] to Figure 7.7.1-62a[a]) due to the more gradual failure of CSNF WPs as shown on Figure 7.7.1-58[a]. However, once all CSNF WPs in a given percolation subregion have failed by nominal SCC (typically by about 550,000 years) and almost all of the CSNF waste form has degraded, the ^{99}Tc mass is depleted relatively quickly out of the WP, but still takes over 10,000 years to be fully released (equivalent to fewer than three model

timesteps at such late times). Compared to ^{99}Tc release, diffusive release of ^{242}Pu is more gradual and follows the breach area curve rather than the CSNF WP failure curve. The increase in diffusive releases after 800,000 years is caused by the patch opening that significantly increases the total WP breach area (Figure 7.7.1-60[a]) while the continued release of ^{242}Pu from CSNF WPs is maintained by sorption-desorption reactions with corrosion products. Figure 7.7.1-65[a] shows the example for percolation subregion 3 for the seeping environment, where most of the ^{242}Pu mass released from the inventory is sorbed on the corrosion products and then is gradually released by desorption, thereby controlling the dissolved concentration and diffusive release out of the WP (note that the curve showing the mass sorbed on corrosion products also includes the effects of radioactive decay).

The time histories for pH and ionic strength in the corrosion products domain for percolation subregion 3 for the seeping environment are shown on Figure 7.7.1-66[a]. The first sharp decline in ionic strength occurs around 380,000 years because that is the time when rubble completely fills the drift (a consequence of multiple seismic events, as shown on Figure 7.7.1-56[a]). At that time, the differential temperature and relative humidity time histories for high thermal conductivity rubble is imposed, leading to a small increase in relative humidity from 0.9956 to 0.9984. Since this increase in relative humidity corresponds to an equivalent increase in activity of water, it causes an appreciable decrease in ionic strength, indicating its high degree of sensitivity to relative humidity under vapor influx conditions (see Section 6.3.7.2.2 of the parent document for details on ionic strength abstraction). The second decline in ionic strength that occurs around 712,000 years is caused by water flowing through the WP after general corrosion patches have formed and exceeded a threshold of 0.1 L/yr, thereby leading to a change in the In-Package Chemistry Submodel (Section 6.3.7.2 of the parent document) from calculations based on vapor influx to calculations based on liquid influx. Despite the changes in ionic strength over the course of the simulation, pH in the corrosion products domain remains nearly constant as a result of buffering by surface complexation reactions.

Figure 7.7.1-67[a] compares (a) the concentration of ^{242}Pu that is associated reversibly and irreversibly with colloids to (b) the dissolved concentration in the WP (corrosion products domain) for both CDSP and CSNF WPs for the seeping environment in percolation subregion 3. The concentration of dissolved and reversibly sorbed ^{242}Pu mass on colloids (denoted as aqueous) overlays the dissolved concentration, indicating that the mass of ^{242}Pu reversibly associated with colloids is negligible. The concentration of various colloid types over time for both CDSP and CSNF WPs are shown on Figure 7.7.1-68[a]. Different types of colloids become stable at different times based on their stability relationships as illustrated on Figure 6.3.7-11 of the parent document. CSNF waste form colloids remain unstable throughout the simulation and therefore maintain a constant minimum concentration. The HLW glass waste form colloids become stable first, followed by uranium colloids while there is no advection through the WP and ionic strength remains relatively high. Following the opening of general corrosion patches and advent of advective flow, groundwater colloids and iron oxyhydroxide colloids become stable primarily because of the appreciable decrease in ionic strength (for example, as shown in Figure 7.7.1-66[a] for CSNF WP).

Both reversible and irreversible sorption of plutonium is modeled on HLW glass waste form colloids while only irreversible sorption is modeled on the iron oxyhydroxide colloids and CSNF

waste form colloids. Only reversible sorption of plutonium is modeled on the groundwater colloids and uranium colloids. The sampled plutonium K_d for HLW glass waste form colloids and groundwater colloids (both represented by smectite mineralogy) is about 1,700 mL/g, and the sampled plutonium K_d for uranium colloids is about 247 mL/g. Due to the combination of small colloid concentrations and relatively small sampled K_d for plutonium, the plutonium mass reversibly associated with colloids remains negligibly small compared to the mass in the dissolved state (Figure 7.7.1-67[a]). The concentration of ^{242}Pu irreversibly associated with HLW glass waste form colloids and iron oxyhydroxide colloids becomes significant at various times as shown on (Figure 7.7.1-67[a]).

Total EBS releases (i.e., summed over all percolation subregions) of ^{99}Tc and ^{242}Pu in the dissolved state, dissolved and reversibly associated with colloids (denoted as aqueous), and irreversibly sorbed on colloids for both CSNF and CDSP WPs are shown on Figure 7.7.1-69[a]. (The EBS release of ^{242}Pu mass irreversibly sorbed on CSNF waste form colloids is not shown as it is negligible due to the instability of those colloids.) The mass release of ^{99}Tc and ^{242}Pu (total) from CSNF WPs exceeds that released from CDSP WPs due to the greater number of CSNF WPs and larger inventory on a per package basis (Tables 6.3.7-1 and 6.3.7-5 of the parent document). It is interesting to note that, until the patches appear and advection starts, most of the ^{242}Pu mass released from the WP is in the dissolved state and very little is irreversibly associated with colloids (Figure 7.7.1-69[a]), even though the concentration of ^{242}Pu irreversibly associated with colloids is higher than the dissolved concentration in the WP (as shown by the example on Figure 7.7.1-67[a]). This is because prior to the opening of patches, since only diffusive release can occur through the WP, the colloid facilitated transport is limited by the diffusion coefficient of colloids, which is computed to be about 700 times smaller than that for the dissolved plutonium based on the sampled colloid particle diameter (SNL 2007 [DIRS 177407], Section 6.3.4.4). Once advection through the WP starts the transport of mass irreversibly associated with colloids becomes important.

The majority of the mass (combined for CSNF and CDSP WPs) that is passed from the EBS to the UZ at the repository horizon goes into fracture nodes in the UZ, rather than into the matrix nodes as shown on Figure 7.7.1-70[a] for ^{242}Pu. This is because the majority of the WPs in a given percolation subregion (except for percolation subregion 1) are in the seeping environment where drift seepage that flows out through the invert carries the mass advectively through the fractures, even though most of the mass is diffusing out of the WP. For percolation subregion 1, the fraction of mass going into the fractures is initially relatively small (about 0.4) but increases (to approximately 0.9) around 81,500 years. This behavior is due to the change in seepage flux, which remains relatively small (about 0.005 m^3/yr) until around 81,500 years and then increases to about 0.08 m^3/yr. This is because at this time, the nonlithophysal locations are considered to be collapsed from drift degradation based on the drift seepage model abstraction, resulting in the seepage flux for such locations to change from the non-collapsed drift seepage to the percolation flux (Section 6.3.3.1.2 of the parent document). The effect of this change is greatest for percolation subregion 1 because, compared to other percolation subregions, it has (a) the smallest ambient seepage rates prior to the drift collapse and (b) the highest fraction of nonlithophysal locations (about 32 percent).

The cumulative mass releases from EBS, UZ, and SZ are compared on Figure 7.7.1-71[a] for ^{99}Tc, ^{242}Pu (dissolved and reversibly sorbed on colloids; denoted as aqueous), and ^{242}Pu

(irreversibly sorbed on all colloids). The transport characteristics are quite different for ^{99}Tc and ^{242}Pu in the UZ and SZ domains as ^{99}Tc is transported without retardation; whereas ^{242}Pu (aqueous) experiences considerable retardation due to sorption onto the tuff matrix and alluvium (Table 6.3.9.2 and Table 6.3.10.2 of the parent document). Little retardation is apparent in the UZ and SZ domains for ^{242}Pu irreversibly sorbed onto colloids because the diffusive interaction between fractures and matrix continua for mass irreversibly sorbed onto colloids is not modeled and, once the mass is placed in the fracture continuum, it tends to stay there. Although a small fraction (0.00168) of irreversible mass associated with colloids travels unretarded through the UZ and SZ (designated as the 'fast fraction'; Section 6.3.8.3 of the parent document), almost all irreversible mass on colloids undergoes some retardation due to interaction between colloid particles and fracture surfaces. Despite this interaction, the mass irreversibly associated with colloids travels quickly through the UZ and SZ. As shown on Figure 7.7.1-71[a], almost all the mass released from the EBS, for both ^{99}Tc and ^{242}Pu (irreversibly sorbed onto colloids), is also released at the SZ model boundary within a relatively short period compared to the simulation time of 1,000,000 years. In contrast, the mass of ^{242}Pu (aqueous) released from the UZ and SZ model boundaries at the end of the simulation is appreciably smaller than that released from the EBS, indicating significant retardation (about 65 percent is released out of the UZ while only 31 percent is released out of the SZ). Since most of the mass is passed to the fracture nodes of the UZ, it diffuses from the fracture continuum into the matrix continuum due to fracture-matrix interaction in the UZ, with some mass also being transported into the matrix by advection due to lateral flow. Even though the free water diffusion coefficients in the UZ (as in EBS) vary by species (Table 6.3.9-3 of the parent document), the difference between ^{99}Tc and ^{242}Pu (aqueous) is relatively small (differ by a factor of 1.5) and can be ignored for most practical purposes. Thus, both ^{99}Tc and ^{242}Pu (aqueous) are equally likely to diffuse (assuming equal concentrations) from the fracture continuum into the matrix continuum. Because of sorption of ^{242}Pu in the UZ matrix, the concentration gradient between fracture and matrix is higher for ^{242}Pu than for ^{99}Tc, leading to greater diffusive flux of ^{242}Pu into the matrix and smaller cumulative release at the UZ-SZ boundary.

In the SZ domain, the mass released from each of the four UZ regions is passed to the corresponding SZ region. In each SZ region, a location is randomly selected as the starting point for transport and is manifested through sampling one of the 200 pre-generated SZ breakthrough curves for a given species (Section 6.3.10.2 of the parent document). Due to their different transport characteristics through volcanic units and alluvium, separate sets of breakthrough curves are available for ^{99}Tc, ^{242}Pu (dissolved and reversibly sorbed on colloids; denoted as aqueous), ^{242}Pu (fast traveling fraction irreversibly associated with colloids), and ^{242}Pu (slow traveling fraction irreversibly associated with colloids). The breakthrough curves are pre-generated as an impulse response function to a unit pulse and are convolved with the incoming UZ mass flux by using the convolution integral approach to produce the SZ mass flux at the location of the RMEI.

In this realization, SZ breakthrough curve number 122 was selected, and the breakthrough times of ^{99}Tc, ^{242}Pu (dissolved and reversibly sorbed on colloids; denoted as aqueous), and ^{242}Pu (slow traveling fraction irreversibly associated with colloids) are compared for all four zones on Figure 7.7.1-72[a]. The breakthrough curves for ^{242}Pu (fast traveling fraction irreversible on colloids) are not presented as very little mass is transported by them. The breakthrough of ^{99}Tc from all four SZ regions is much earlier than that for ^{242}Pu (aqueous) and for ^{242}Pu (slow

traveling fraction irreversible on colloids), with almost half of the mass input recovered after a few hundred years of travel in the SZ for ^{99}Tc compared to almost 100,000 years of travel time required for ^{242}Pu (aqueous) and 10,000 years of travel time required for ^{242}Pu (slow traveling fraction irreversible on colloids). However, the long tail noticeable in the breakthrough curve for ^{99}Tc for the remaining half of its input mass results from longitudinal and transverse dispersion in the volcanic units and alluvium due to fracture-matrix diffusive interactions in the dual porosity volcanic domain of the SZ transport model. The ^{242}Pu (aqueous) breakthrough is further impacted by sorption in both the volcanic matrix and alluvium. For SZ breakthrough curve 122, the initially sampled plutonium K_d for volcanic matrix units is approximately 120 mL/g, and the initially sampled plutonium K_d for the alluvium is 107 mL/g (SNL 2008 [DIRS 183750], Table A-1[b]). Both are modified in order to calculate effective K_d values but nevertheless result in considerable retardation. Nearly all the plutonium (>0.999 fraction) is transported in the dissolved phase, with a small fraction (<0.001) being transported via reversible sorption on the groundwater colloids. This is because the groundwater colloid concentration sampled is about 0.11 mg/L and the K_d for plutonium on the colloid is sampled to be about 6,560 mL/g, which when multiplied together, provides the fraction of the mass associated with colloids versus that transported in dissolved state. This fraction is equal to about 0.000722.

The release rates out of the SZ for ^{99}Tc, ^{242}Pu (dissolved and reversibly sorbed on colloids; denoted as aqueous), and ^{242}Pu (irreversibly associated with colloids for both fast and slow traveling fractions) are shown on Figure 7.7.1-73[a] for realization 4641, and all three essentially follow their release rates out of the EBS when combined over CDSP and CSNF WPs (Figure 7.7.1-69[a]). The SZ releases are converted into annual dose by taking the annual releases out of the SZ for each radionuclide, dissolving them in the 3,000 acre-ft of water (annual usage at RMEI as defined by the regulation) to compute the mass concentrations, converting the mass concentration into concentration of radioactivity (in curies per liter of water), and then multiplying with the corresponding BDCFs computed for the modern-interglacial climate (present-day climate). The end result of this calculation is shown on Figure 7.7.1-54[a].

7.7.1.5[a] Nominal Modeling Case

This section presents an analysis of a single realization out of the 300 realization base-case run performed for calculating the expected annual dose from the Nominal Scenario Class (GoldSim filename: LA_v5.005_NC_000300_000.gsm; output DTN: MO0710ADTSPAWO.000 [DIRS 183752]). The Nominal Scenario Class consists of a single modeling case that represents a set of possible repository futures from which are excluded (1) disruptive events and (2) early failures of DSs and WPs. Moreover, the Nominal Modeling Case serves as a 'reference system state' from which all other modeling cases are developed (Section 8.2.1 of parent document). The distribution of expected annual dose for 300 epistemic vectors that also implicitly account for aleatory uncertainties (such as time, location, and degree of damage to each WP) is shown on Figures 7.7.1-74a[a] (linear time) and 7.7.1-74b[a] (log time). Details about the calculation of the expected annual dose for this modeling case are described in Section 6.1.2.4.1 of the parent document.

The major radionuclides contributing to mean annual dose for this modeling case are shown on Figure 7.7.1-75[a]. Long-lived, highly-soluble, and mobile radionuclides, such as ^{99}Tc and ^{129}I, are the dominant dose contributors for most of the simulation, whereas long-lived,

sparingly-soluble, and strongly-sorbing radionuclides, such as ^{242}Pu, ^{135}Cs, and ^{237}Np become important dose contributors at later times when contributions from ^{99}Tc have declined.

Two minor peaks in the mean annual dose are apparent early on, at around 40,000 and 80,000 years (Figures 7.7.1-74[a]). These are the result of WPs failing by SCC from two realizations (out of the total of 300 realizations). After about 100,000 years, the mean annual dose steadily increases as a result of gradual WP failures. Step-wise increases in the mean annual dose noticeable around 200,000; 300,000; 500,000; and 700,000 years are due to increases in the number of WP failures (from SCC) calculated by the waste package degradation code WAPDEG V4.07 (STN:10000-4.07-01 [DIRS 181064]). WAPDEG calculates the corrosion rates at the timesteps provided in the WP thermal history input files from the multiscale thermohydrologic model (MSTHM) Abstraction (Section 6.3.2.3 of the parent document). The thermal history files have coarse temporal resolution past 100,000 years (due to small changes at late time periods) leading to evaluation of temperature at 200,000; 300,000; 500,000, 700,000; and 1,000,000 years. The stress corrosion crack growth rate is given by a power law function of stress intensity factor and repassivation slope n (Equation 6.3.5-14 of the parent document). The stress intensity factor is evaluated at the beginning of each WAPDEG timestep and is a function of the crack depth that drives the crack propagation. The large timesteps taken past 100,000 years combined with the sensitivity of the crack growth rate to the stress intensity factor, which is raised to the power $4n$, where n has a mean value of 1.165 (SNL 2007 [DIRS 181953], Table 8-15), can cause dramatic changes in the crack growth rate at each timestep. As a result, the crack growth rate can change from a small value for the timestep in which the crack initiates to a much larger value at the beginning of the next timestep, resulting in almost immediate penetration of many cracks and failure of WPs. An assessment of this temporal discretization for the Nominal Modeling Case is presented in Section 7.3.3.7[a].

Nominal Modeling Case—Realization 286

A single epistemic vector is selected for further analysis in such a manner that the expected annual dose is broadly representative of the modeling case and similar in behavior to the mean annual dose. Epistemic vector 286 is chosen for further analysis (Figure 7.7.1-76[a]), which is equivalent to GoldSim realization 286 (GoldSim filename: LA_v5.005_NC_000300_001.gsm; output DTN: MO0801TSPAMVAC.000 [DIRS 185080]).

Figure 7.7.1-77[a] shows the major radionuclides that contribute to the annual dose for realization 286 of the Nominal Modeling Case. Of these, ^{99}Tc and ^{129}I are the primary contributors with relatively minor contributions from ^{36}Cl, ^{79}Se, and ^{135}Cs. Between 250,000 and 300,000 years, the annual dose for realization 286 exhibits local step increases that result from a single CDSP WP failure in the non-seeping environment of percolation subregion 2 and two CDSP WP failures in the seeping environment of percolation subregion 2. All three CDSP WP failures are caused by SCC failure on the outer lids prior to the DS failure, which occurs at 304,000 years.

The three significant step increases in the annual dose at 300,000; 500,000; and 700,000 years for realization 286 (Figure 7.7.1-77[a]) result from the coarse time discretization employed in WAPDEG V4.07 software leading to increased WP failures from SCC shortly following those times. A more detailed explanation of the effect of large timesteps on crack propagation is

provided through an example calculation at the 500,000 and 700,000 year timesteps for percolation subregion 1, based on the sampled epistemic parameters for realization 286. The discussion will focus on incipient crack growth since they occur on every lid patch. Cracks due to weld flaws are ignored as they are much less frequent and are present on only a few WP lids in a given realization (Section 6.3.5.1.2 of the parent document). Incipient cracks initiate (nucleate) when general corrosion has penetrated to the depth at which the stress profile exceeds the threshold stress (critical depth). For realization 286 the threshold stress is sampled to be about 329 MPa (from a uniform distribution between 315.9 and 368.55 MPa; Table 6.3.5-3 of the parent document). Using the output table of stress versus depth generated by the SCCD V2.01 software (STN: 10343-2.01-01 [DIRS 181054]), evaluating at an angle of π radians (one of the five choices of angles), the critical depth is found to be approximately 6.5 mm (see file *WDStressO.fil* located in the output DTN: MO0801TSPAMVAC.000 [DIRS 185080] in the path: LA_v5.005_NC_000300_001 (Nominal Single)\ Additional_Information\ Supplemental_Work_for_Analysis\ WAPDEG_out_files_from_PS1ND_only_run). To initiate the stress corrosion cracks by 500,000 years (equivalent to thinning the WP OCB by 6.5 mm), the general corrosion rate is calculated to be around 13 nm/year (ignoring the temperature effects). This value is within the uncertainty range of general corrosion rate (Figure 6.3.5-6 of the parent document), which typically ranges from 2 to 15 nm/year over a cumulative probability range of 0.1 to 0.9 for the medium uncertainty curve selected in realization 286. Using the output table of stress intensity factor versus depth generated by SCCD V2.01 software at an angle of π radians, the stress intensity factor at 6.5 mm is found to be approximately 10.3 (MPa(√m)) (see file *WDKISCCO.fil* located in the output DTN: MO0801TSPAMVAC.000 [DIRS 185080] in the path: LA_v5.005_NC_000300_001 (Nominal Single)\ Additional_Information\Supplemental_Work_for_Analysis\WAPDEG_out_files_from_PS1ND_ only_run). The crack growth rate is then calculated from Equation 6.3.5-14 of the parent document to be 0.000005 mm/year (using the sampled value of 3.03×10^{-11} for A and 1.29 for n). This rate when applied over the 200,000 year timestep (from 500,000 years to 700,000 years) would result in a crack growth of 1 mm. At 700,000 years (beginning of new timestep) the stress intensity factor is re-evaluated based on the new crack depth, which is the sum of the critical depth at 500,000 years (6.5 mm), the crack growth over 200,000 year period (1 mm), and the additional general corrosion thinning over 200,000 year period (2.6 mm using a general corrosion rate of 13 nm/year). The new stress intensity factor, evaluated at the current depth of 10.1 mm, would be approximately 39.4 (MPa(√m)), which results in a crack growth rate of roughly 0.0054 mm/year and penetration of WP OCB (for remaining thickness of about 14.9 mm) in about 2,800 years after the start of the timestep. This calculation illustrates that the crack growth rates when recomputed over large time periods result in significant increase which in turn cause complete crack penetrations to occur shortly after the beginning of a new timestep leading to failure of large number of WPs.

Figures 7.7.1-78a[a] and 7.7.1-78b[a] illustrate the number and timing of WP failures within each percolation subregion for CDSP and CSNF WPs. These WP failures occur in both the non-seeping and seeping environments of each percolation subregion. Since there are about 2.4 times more CSNF WPs compared to CDSP WPs in the repository (8,213 CSNF WPs versus 3,416 CDSP WPs), relatively more CSNF WPs fail over the simulated duration. By the end of the simulation at 1,000,000 years, a total of 7,716 CSNF WPs have failed compared to a total of 3,227 failed CDSP WPs. The average WP failure area (breached area) time history for various

percolation subregions for CDSP and CSNF WPs are shown on Figures 7.7.1-79a[a] and 7.7.1-79b[a]. The breached area in all percolation subregions remains small throughout the simulation because WP failure is primarily from SCC. Only percolation subregion 1 for CSNF WPs has a (single) patch failure within the simulated time frame, which occurs past 950,000 years, leading to a small increase in area but even then the average breach area remains relatively small as the SCC failure area averaged over all failed WPs remains greater than the single patch failure area averaged over all the failed WPs. Thus, because only SCC failures occur on most WPs for the majority of the simulation, advective releases are negligible and radionuclides are primarily transported by diffusion out of the WP.

The rates at which ^{129}I, ^{79}Se, ^{135}Cs, and ^{242}Pu (dissolved and reversibly sorbed on colloids) are released over all percolation subregions from the EBS (as shown for waste form, WP, and invert), UZ, and SZ are shown on Figure 7.7.1-80[a] (for ^{129}I), Figure 7.7.1-81[a] (for ^{79}Se), Figure 7.7.1-82[a] (for ^{135}Cs), and Figure 7.7.1-83[a] (for ^{242}Pu). For ^{129}I and ^{79}Se, the curves that represent these release rates generally lie close to each other, which is indicative of each radionuclide being transported as a solute with little to no retardation through the engineered barrier and natural systems. The transport of ^{135}Cs (as solute and reversibly sorbed on the colloids) exhibits the same behavior through the EBS and the UZ but has significant retardation through the SZ. For ^{242}Pu (dissolved and reversibly sorbed on colloids), the mass released from the waste form is large relative to the mass released from the WP, invert, UZ, and SZ. This behavior reflects retardation due to sorption onto corrosion products inside the WP.

Figure 7.7.1-84[a] and Figure 7.7.1-85[a] compare the advective and diffusive releases of ^{129}I and ^{242}Pu (dissolved and reversibly sorbed on colloids) from all failed WPs in all percolation subregions. There is no advective release from CDSP WPs as there is no general corrosion patch failure. However, because there is corrosion patch failure for CSNF WPs in percolation subregion 1 past 950,000 years, there is some advective release, but it is still negligible compared to diffusive release. The advective release for ^{242}Pu (dissolved and reversibly sorbed on colloids) is not shown as it is below the cut-off scale for the plot. The step increase in diffusive releases coincides with the step increases in WP failures, but beside the step changes, the diffusive release remains steady for ^{129}I and shows gradual increase for ^{242}Pu that is dissolved and reversibly sorbed on colloids. This is attributed to the relatively steady rate of WP failures between the step changes (Figure 7.7.1-78[a]). Thus, although more WPs are failing with time, the rate of WP failure remains relatively steady, thereby maintaining steady releases of ^{129}I even after accounting for large diffusive flux due to high concentration gradient. The release of ^{242}Pu, in contrast, in addition to being similarly affected by the rate of WP failure, is also impacted by relatively low aqueous solubility and sorption on the corrosion products inside the WP, which reduce the concentration gradient. Combined with a small breach area per package (Figure 7.7.1-79[a]), these factors cause ^{242}Pu to be released slowly from each failed WP. As a result, as more WPs fail through time, the ^{242}Pu release rate increases gradually. Releases from CSNF WPs dominate that of CDSP WPs because (a) comparatively more CSNF WPs are failed and (b) there is comparatively larger inventory for the radionuclides of interest on a per package basis in a CSNF WP. Note that results for ^{99}Tc, ^{36}Cl, and ^{79}Se are not shown separately as they demonstrate similar transport characteristics as ^{129}I.

As previously shown on Figures 7.7.1-80[a] through 7.7.1-83[a], the release rates of ^{129}I are quite different from those for ^{242}Pu but are generally similar to ^{99}Tc, ^{36}Cl, and ^{79}Se. ^{129}I is transported

as an unretarded species through the EBS, UZ and SZ, and nearly all of the mass released from the waste form travels quickly through the EBS (WP and invert), UZ, and SZ. The mass fraction of ^{129}I passed to the UZ matrix and fracture continuum from the EBS at the repository level is shown on Figure 7.7.1-86[a]. The fraction of mass released to UZ fracture increases from percolation subregion 1 to 5, in proportion to the seepage fraction assigned to various percolation subregions (Section 6.3.3.1.3 of the parent document). The seepage fraction determines the fraction of WPs assigned to the seeping environment versus the non-seeping environment within a percolation subregion. Since ^{129}I is neither sorbed nor limited by solubility, the diffusive mass release from the WP remains largely a function of waste form degradation rate and concentration inside the WP. The change in the WP to invert concentration gradient between non-seeping environment and seeping environment due to flow through the invert has limited effect on the diffusive releases of ^{129}I per failed WP. Thus the fraction of ^{129}I mass passed to UZ fracture for a given percolation subregion is proportional to the number of failed WPs in a seeping environment compared to the non-seeping environment and thus directly related to the seepage fraction, which increases from percolation subregion 1 to 5. [Note: Although no water is modeled to flow advectively through the WPs due to the presence of stress corrosion cracks, the in-drift seepage in the seeping environments flows around the WPs (and DSs) to the invert and, thus, the diffusive releases out of the WP are carried primarily by advection from the invert into UZ fracture continuum with less mass release into the matrix continuum. In the non-seeping environment the transport through the invert is primarily by diffusion into the matrix continuum due to large effective diffusive area of the matrix continuum (Section 6.3.8.3 of the parent document).]

The mass fraction of ^{242}Pu (dissolved and reversibly sorbed on colloids) passed to the UZ matrix and fracture continuum from the EBS at the repository level is shown on Figure 7.7.1-87[a]. In contrast to the mass fraction of ^{129}I, a relatively larger fraction of ^{242}Pu is passed into the fractures, indicating a disproportionately larger contribution from WPs located in the seeping environments compared to the non-seeping environment. This is because highly sorbed species such as ^{242}Pu have a lower concentration in the WP than a nonsorbing species such as ^{129}I, and the diffusive flux is primarily controlled by concentration gradient between the WP and the invert. In the seeping environment the flow through the invert causes the concentration gradient to increase (due to reduction in distance to the effective zero concentration boundary from the WP) leading to disproportionately larger diffusive mass flux from the seeping environment than the non-seeping environment per failed WP. As a result, most of the ^{242}Pu mass released in a given percolation subregion is from the contribution of WPs in the seeping environment that are released to the UZ fracture continuum.

Transport through the SZ for each radionuclide is governed by sampling a breakthrough curve from 200 pre-generated breakthrough curves applicable to each radionuclide. The breakthrough curves are abstractions of more complex SZ flow and transport modeling studies. Each epistemic realization randomly samples a number from 1 to 200, and that sampled number represents the set of species-specific breakthrough curves to be used in that particular realization. For realization 286, breakthrough curve set 33 is selected. Solute transport of ^{129}I and ^{79}Se in the SZ is relatively quick due to no retardation modeled for ^{129}I and limited retardation for ^{79}Se (sampled K_d of about 8.3 mL/g and 6.7 mL/g in the SZ volcanic matrix and alluvium, respectively) as shown by release rates for SZ when compared to UZ in Figures 7.7.1-80[a] and 7.7.1-81[a]. In contrast, dissolved ^{242}Pu (with sampled K_d of about 84 mL/g for SZ volcanic

matrix and 87 mL/g for SZ alluvium) and, to a much greater extent, dissolved ^{135}Cs (with sampled K_d of about 5986 mL/g for SZ volcanic matrix and 563 mL/g for SZ alluvium) undergo sorption while being transported through the SZ and hence are retarded (Figures 7.7.1-83[a] and 7.7.1-82[a]).

^{242}Pu is one of the radionuclide species that is transported both dissolved and reversibly sorbed on colloids and irreversibly associated with fast traveling and slow traveling fraction of colloids. Figure 7.7.1-88[a] shows the contribution to the mean annual dose of ^{242}Pu (dissolved and reversibly sorbed on colloids; denoted as aqueous) and associated irreversibly with colloids (for both traveling fast and slow). While colloidal ^{242}Pu exists as a species in the natural system, its contribution to the mean annual dose is very small and the majority of the dose is from the dissolved ^{242}Pu.

Nominal Modeling Case: Outlier

For the purpose of analyzing an outlier realization for the Nominal Modeling Case, epistemic vector 85 (equivalent to GoldSim realization 85) was chosen as shown on Figure 7.7.1-89[a] because it has the highest annual dose at 1,000,000 years. As shown on Figure 7.7.1-90[a], ^{242}Pu is the major radionuclide contributor to the dose past 700,000 years. The release rates for ^{242}Pu from the waste form, WP, invert, UZ, and SZ are shown on Figure 7.7.1-91a[a]. For realization 85, the release of ^{242}Pu from the waste form starts earlier and occurs within a shorter time frame leading to an order of magnitude higher release rates compared to the gradual release for realization 286 (Figure 7.7.1-83[a]) that occurs over extended time periods. This difference in waste form release rate stems primarily from the difference in WP failure rates due to SCC on the outer lids of the WP from nominal processes. As shown on Figure 7.7.1-91b[a] for realization 85, the CSNF WP failure in all percolation subregions starts past 160,000 years and by about 500,000 years, all WPs are failed. In comparison, for realization 286, the CSNF WP failures (Figure 7.7.1-78b[a]) occur over a longer time frame starting around 300,000 years and continuing until the end of simulation at 1,000,000 years.

For realization 85, the peak release of ^{242}Pu from waste form occurs around 300,000 years. But due to sorption of plutonium on the corrosion products inside the WP, significant retardation of ^{242}Pu occurs inside the WP, and the peak release out of the WP is delayed until around 900,000 years indicating long residence times inside the WP on the order of 500,000 to 600,000 years. Because the WP release rates control the release behavior out of the UZ and SZ (Figure 7.7.1-91a[a]), it indicates that sorption and resulting retardation is the primary control on annual dose. The release rate of ^{242}Pu for realization 286 shows similar behavior (Figure 7.7.1-83[a]) as the sorption inside the WP reduces the release rate. However, because the peak waste form release does not occur until around 800,000 years, the peak release from the WP is not seen within the simulated time period as it is anticipated that the peak releases from the WP would be delayed by 500,000 to 600,000 years.

Thus, due to a combination of earlier WP failure start times and faster failure rate, the mass released from the waste form is also mostly released from the WP within the simulated time period. This results in a higher annual dose magnitude for realization 85.

7.7.1.6[a] Human Intrusion Modeling Case

This section presents an analysis of a single realization from the 9,000 realization base-case run performed for calculating the expected dose for the Human Intrusion Modeling Case for the 1,000,000-year simulation duration (Base Case GoldSim Run filename: LA_v5.005_HI_009000_000.gsm; output DTN: MO0710ADTSPAWO.000 [DIRS 183752]). The expected annual dose is presented in Figure 7.7.1-92[a], where each of the 300 realizations represents expected annual dose for one epistemic uncertainty vector. The expected annual dose for each epistemic uncertainty vector is generated by taking an expectation over a sample of 30 aleatory uncertainty vectors (for more details on the computational methodology, refer to Section 6.1.2.5 of the parent document). A single epistemic vector is selected for further analysis such that its expected annual dose is broadly representative of the modeling case and similar in behavior to the mean annual dose curve (Figure 7.7.1-92[a]).

The epistemic uncertainty vector 277 is selected for further analysis. The 30 corresponding aleatory sampling vectors for the selected epistemic vector correspond to GoldSim realizations 8281 through 8310 (Figure 7.7.1-93[a]). The annual dose from the 30 aleatory vectors falls into two groups: (1) the group with higher dose represents those realizations in which a CSNF WP is selected, and (2) the group with lower dose represents those realizations in which a CDSP WP is selected. The specific realization selected for further analysis is GoldSim realization 8309 (Figure 7.7.1-93[a]), which is chosen from the first group (representing releases from a CSNF WP). Realization 8309 represents aleatory uncertainty vector 29, in which the CSNF WP breached from a human intrusion event is located in percolation subregion 4 of the EBS and where the mass from the UZ borehole is passed to SZ source region 1 (GoldSim filename: LA_v5.005_HI_009000_002.gsm; output DTN: MO0801TSPAMVAC.000 [DIRS 185080]).

In the stylized Human Intrusion Modeling Case, a borehole pathway is modeled as being drilled directly through a single DS and WP vertically down to the water table. The time of this intrusion, which is assumed to result from exploratory drilling for ground water, is fixed at 200,000 years. Once the WP is breached, the waste form degrades by nominal degradation processes and the radionuclides are transported from the WP under nominal conditions to the vertical UZ borehole pathway, such that the mass is released at the water table for transport through the SZ to the RMEI at the regulatory boundary. The vertical borehole pathway is modeled as being 190 meters in length and conceptualized as a dual-porosity medium consisting of a discrete vertical fracture surrounded by matrix consisting of rubble from partial collapse of the borehole. The fracture is assumed to be open so that the water that flows in the borehole moves through the fracture pathway. Also, the radionuclide mass released from the WP (by diffusion and advection) is passed to the fracture pathway where it undergoes vertical advection within the fracture and lateral diffusion into the surrounding matrix due to fracture-matrix interaction. No retardation of colloids or solute is modeled on the fracture surface although species-dependent sorption coefficients are applied in the matrix (for additional details, refer to Section 6.7 of the parent document).

The major radionuclides contributing to annual dose for realization 8309 are shown on Figure 7.7.1-94[a], along with the total annual dose. ^{99}Tc and ^{129}I are the early major dose contributors (before 300,000 years), following the WP breach at 200,000 years, whereas ^{242}Pu becomes the dominant dose contributing radionuclide later on (with minor contribution from

^{237}Np, ^{135}Cs, ^{79}Se, and ^{233}U). The early contribution to dose from ^{99}Tc and ^{129}I occurs because they travel unretarded through the WP, UZ borehole pathway, and SZ. By contrast, ^{242}Pu, ^{237}Np, ^{135}Cs, and ^{233}U are retarded in these transport pathways to varying degrees and therefore contribute to dose much later. Because ^{99}Tc and ^{242}Pu are the dominant radionuclides with very different transport properties, they have been chosen for further analysis.

The cumulative mass release of ^{99}Tc and ^{242}Pu from the waste form inventory following the failure of one CSNF WP is shown on Figure 7.7.1-95[a]. The waste form starts degrading following the breach at 200,000 years, and due to the relatively slow CSNF degradation rate (about 6.9×10^{-5} yr^{-1}), it is almost fully (0.99 fraction) degraded by 268,000 years. The rate at which ^{99}Tc is released from the waste form domain and the corrosion products domain of the WPs is shown on Figure 7.7.1-96[a]. Because the dissolved concentration of ^{99}Tc is not limited by a solubility controlling solid, the mass of ^{99}Tc released from the degrading waste form is quickly transported out of the WPs by advection and diffusion. In this realization, the volumetric water flux through the WP (and going to the UZ borehole) is calculated to be about 8.7×10^{-4} m^3/yr (which is equivalent to the calculated percolation rate of about 26.9 mm/yr for the drilled borehole cross-sectional area of 0.0324 m^2 [Table 6.7-5 of the parent document]). Diffusive releases are higher than advective releases through the WP (in both waste form and corrosion products domains) because of the implementation of a zero concentration boundary just outside the WPs to maximize the concentration gradient. Almost all of the ^{99}Tc mass is released by about 300,000 years, as indicated by the negligibly small release rates past this time period (Figure 7.7.1-96[a]). The waste form degradation primarily controls the release of ^{99}Tc out of the WPs. After the ^{99}Tc mass is made available for transport, it is released out of the WPs without appreciable delay.

The ^{242}Pu mass release from the waste form domain and the corrosion products domain of the WP are shown on Figure 7.7.1-97[a]. ^{242}Pu is modeled as being transported both as dissolved and reversibly sorbed on colloids (denoted as aqueous) and as irreversibly sorbed onto iron oxyhydroxide colloids and waste form colloids. Note that CSNF waste form colloids remain unstable throughout the simulation (and are set to a minimum defined concentration) so they contribute negligibly to the total mass released, whereas iron oxyhydroxide colloids remain unstable for a short period, until about 220,000 years, and contribute to the mass release afterwards. The diffusive release of ^{242}Pu (dissolved and reversibly sorbed on colloids) exceeds advective releases as most of the ^{242}Pu mass remains in dissolved state, with very little being reversibly sorbed onto groundwater and uranium mineral colloids. However, the mass that is irreversibly sorbed on the iron oxyhydroxide colloids is predominantly transported by advection (Figure 7.7.1-97[a]) due to the small diffusion coefficient of colloids. The concentration of ^{242}Pu that is dissolved, and that which is irreversibly sorbed onto iron oxyhydroxide colloids, are both shown on Figure 7.7.1-98[a] for the waste form domain and the corrosion products domain. The dissolved concentration in the waste form domain is limited by the solubility of plutonium dioxide (PuO_2) in the waste form domain for several hundred thousand years following the breach. Because the solubility of PuO_2 is low, most ^{242}Pu mass from the degraded waste form is precipitated early in the waste form domain. Plutonium is gradually depleted from the waste form domain by diffusion and advection, and not until 748,000 years is enough mass depleted to cause the plutonium concentration inside the waste form domain to drop below the solubility limit. The dissolved concentration of ^{242}Pu in the corrosion products domain remains small initially, as ^{242}Pu is sorbed onto corrosion products whose mass increases over time from

degradation of steel. By 320,000 years, all of the steel in the corrosion products domain is degraded, and the maximum sorption capacity for the corrosion products domain is reached. As ^{242}Pu continues to be transported from the waste form domain to the corrosion products domain, the dissolved concentration of ^{242}Pu in the corrosion products domain starts to build up after 320,000 years, reaching the solubility limit in that domain, which is maintained until all ^{242}Pu mass has been depleted in the waste form domain and the concentration of ^{242}Pu drops at 748,000 years (Figure 7.7.1-98[a]). The concentration of ^{242}Pu in the corrosion products domain after this time is maintained by ^{242}Pu mass desorbing from the corrosion products. The concentration of ^{242}Pu that is irreversibly sorbed onto iron oxyhydroxide colloids also keeps increasing until about 748,000 years and then declines slowly as iron oxyhydroxide colloids are transported out, predominantly by advection (Figure 7.7.1-97[a]). Because the concentration of ^{242}Pu irreversibly sorbed onto iron oxyhydroxide colloids is not limited by solubility, it exceeds the dissolved concentration within a short period. Nevertheless, because the diffusion coefficient of colloids is calculated to be much smaller than the diffusion coefficient of dissolved plutonium (by a factor of about 700), the diffusive mass flux of ^{242}Pu (aqueous), which is mostly dissolved mass, exceeds the advective mass flux of ^{242}Pu irreversibly sorbed onto iron oxyhydroxide colloids (Figure 7.7.1-97[a]).

The mass released from the WP is passed into the UZ borehole that consists of dual porosity fracture and matrix media. The borehole is modeled using the GoldSim pipe element pathway, where only 1-D transport is considered. All of the mass released from the WP is placed in the fracture where it advects vertically downwards and diffuses laterally into the surrounding matrix medium. The volumetric flux of water applied to the fracture pathway is the same as that applied to the WP (about 8.7×10^{-4} m^3/yr; equivalent to the percolation rate of about 26.9 mm/yr), which results in an average linear velocity of about 82 m/yr through the fracture medium, considering the fracture plan area of 4.2×10^{-4} m^2, fracture saturation of 0.025, and no infill material in the fracture. Thus, for a species where fracture-matrix interaction is ignored, the travel time through the borehole length of 190 m should be less than 3 years.

The mass release of ^{99}Tc from the borehole virtually overlays the mass release from the WP (Figure 7.7.1-99[a]), indicating negligible delay. This is expected as no retardation is modeled for ^{99}Tc. Although fracture-matrix interaction could cause a minor delay in the ^{99}Tc breakthrough time, those effects are not apparent because of large timesteps taken past 204,000 years. The long tail in the ^{99}Tc release past 300,000 years, after most of the mass has been released, results from fracture-matrix interaction in the SZ where the mass is released back into the fractures from the matrix. The release rate from the SZ is comparable with that of the WP and UZ borehole releases early on, indicating fast transport through the SZ.

The release rates for the dissolved and reversibly sorbed ^{242}Pu (denoted as aqueous) from the WP, UZ borehole, and SZ are shown on Figure 7.7.1-100[a]. The release rates out of the borehole are considerably smaller than the incoming release rates from the WP. This is attributed to retardation in the matrix once the mass diffuses into the matrix from the fractures. The K_d for plutonium in the matrix is sampled to be about 115 mL/g (0.115 m^3/kg), which results in an effective retardation of about 1,550 (using the matrix bulk density of 1,980 kg/m^3 and matrix water content of 0.15). Because of the sorption, the dissolved concentration of ^{242}Pu in the matrix medium is reduced, thereby increasing the diffusive gradient (and diffusive flux) from the fracture to the matrix, thus limiting the mass available for advective transport through the

fracture. The release rates out of the SZ are lower than that for the UZ borehole due to further retardation in the SZ volcanic and alluvium units.

The cumulative mass releases from the WP, UZ borehole, and SZ for the ^{99}Tc, ^{242}Pu (aqueous), and ^{242}Pu (irreversibly sorbed on colloids) is shown on Figure 7.7.1-101[a]. The cumulative releases of ^{99}Tc out of WP, UZ, and SZ virtually overlay, indicating negligible retardation. Similarly, negligible retardation is indicated for ^{242}Pu (irreversibly sorbed on colloids) as the cumulative releases out of WP, UZ, and SZ virtually overlap. The fracture-matrix diffusive interaction for the mass irreversibly sorbed on colloids is not modeled in the UZ borehole and the SZ pathway due to the small diffusion coefficient of colloids. Thus, the mass of ^{242}Pu irreversibly sorbed on colloids that is introduced into the UZ borehole fracture stays in the fracture and is advected out quickly. In the SZ, some retardation of the colloids due to interaction with the fracture surfaces is modeled but the affects are not apparent due to the large timesteps taken. In contrast, the cumulative mass released from the UZ borehole for ^{242}Pu (aqueous) indicates that at the end of the simulation (one-million years), only a negligibly small fraction (<0.004) of the mass released from the WP is released out of the UZ borehole and, of the mass released from the UZ borehole, only about half is released out of the SZ. It is interesting to note that even though ^{242}Pu (aqueous) release is higher out of the WP compared to the release of irreversibly sorbed ^{242}Pu mass on colloids, due to retardation of ^{242}Pu (aqueous) in the UZ borehole, the release of ^{242}Pu irreversibly sorbed on colloids becomes relatively larger out of the UZ borehole.

The ^{242}Pu mass irreversibly sorbed on colloids coming out of the UZ borehole is partitioned into a fast traveling fraction and a slow traveling fraction before being passed to the SZ. Almost all of the ^{242}Pu mass irreversibly sorbed (99.8 percent) travels as a slow fraction in the SZ with some retardation of the colloid particles in the volcanic units and alluvium while the remaining travels unretarded as a fast fraction. All of the mass from the UZ borehole is passed into the SZ Source Region 1, consistent with the sampled aleatory uncertainty in this realization.

The mass release out of the SZ for ^{99}Tc, ^{242}Pu (aqueous), ^{242}Pu (irreversible on colloids traveling slowly), and ^{242}Pu (irreversible on colloids traveling fast) is shown on Figure 7.7.1-102[a]. The long tail in the ^{99}Tc release past 300,000 years, after most of the mass has been released, results from fracture-matrix interaction in the SZ where the mass is released back into the fractures from the matrix. Following the depletion of ^{99}Tc mass, the release rates from the slow traveling fraction of ^{242}Pu mass irreversibly sorbed on colloids becomes dominant.

The SZ releases are converted into annual dose by taking the annual releases out of the SZ for each radionuclide, dissolving them in the 3,000 acre-ft of water (annual usage at RMEI as defined by the regulation) to compute the mass concentrations, converting the mass concentration into a concentration of radioactivity (in curies per liter of water), and then multiplying with the corresponding BDCFs computed for the modern-interglacial climate (present-day climate). The end result of this is Figure 7.7.1-94[a], where dose for total ^{242}Pu (combined for mass in dissolved state, reversibly associated with colloids, and irreversibly associated with colloids) is shown.

Human Intrusion Modeling Case: Outlier

For the purpose of analyzing an outlier realization for the Human Intrusion Modeling Case, epistemic vector 181 was chosen as shown in Figure 7.7.1-103[a] because it has the highest annual dose between 300,000 and 800,000 years. Figure 7.7.1-104[a] displays the annual dose from 30 aleatory vectors associated with epistemic vector 181. The aleatory vector 15 (equivalent to GoldSim realization 5415) is chosen for further analysis due to its high dose. In this realization a CSNF WP, located in percolation subregion 3, is breached by the human intrusion and the mass is released through the UZ borehole pathway to the SZ source region 3.

The major dose contributing radionuclides for realization 5415 are shown in Figure 7.7.1-105[a]. Of these, the relative dose contribution from ^{242}Pu is by far the highest from 300,000 years until the end of the simulation. Although ^{242}Pu is also the dominant dose contributing radionuclide for realization 8309 described earlier (Figure 7.1.1-94[a]), its dose contribution relative to other radionuclides is much higher in realization 5415.

Figure 7.7.1-106[a] compares the dissolved ^{242}Pu concentrations in the waste form and corrosion product domains along with the plutonium solubilities in the respective domains for realization 5415. Although plutonium solubilities and dissolved concentrations are similar to those for realization 8309, the concentrations of ^{242}Pu associated irreversibly with iron oxyhydroxide colloids in the corrosion products domain is significantly higher. This is due to sampling higher iron oxyhydroxide colloid concentration (GoldSim epistemic uncertainty parameter Conc_Col_FeOx_SS_Sampled_a). For realization 5415, colloid concentration is sampled at 20.49 mg/L (at 98 percentile of the distribution) compared to a sampled value of 0.23 mg/L (at 64 percentile) for realization 8309. This two orders of magnitude difference in iron oxyhydroxide colloid concentration is proportional to the concentration of ^{242}Pu associated irreversibly with iron oxyhydroxide colloids. This is the main reason for the outlier behavior observed at later times for this realization as the irreversibly sorbed mass is transported through the UZ and SZ. The volumetric flux through the WP and UZ borehole in realization 5415 ($= 7.6 \times 10^{-4}$ m^3/yr) is similar to that for realization 8309 ($= 8.7 \times 10^{-4}$ m^3/yr).

7.7.1.7[a] Seismic Ground Motion Modeling Case for 10,000 Years

This section presents an analysis of a single realization from the 9,000 realization base-case run performed for calculating the expected dose for the Seismic GM Modeling Case for the 10,000-year simulation duration (GoldSim filename: LA_v5.005_SM_009000_001.gsm; output DTN: MO0710ADTSPAWO.000 [DIRS 183752]). The expected annual dose is presented on Figure 7.7.1-107[a], where each of the 300 realizations represent expected annual dose for an epistemic uncertainty vector. The expected annual dose for each epistemic uncertainty vector is generated by taking an expectation over a sample of 30 aleatory uncertainty vectors that specify both the time of the seismic damage and the fractional damaged area of the WP.

The computational methodology for dose from the 10,000-year Seismic GM Modeling Case is different from that of the one-million-year case. Unlike the latter, where the sequence of seismic events are generated randomly and the damaged area of the WP is determined based on the computed PGV along with other parameters, the former is based on determining the dose response by specifying the WP damage time and the damaged area. This dose response function

is used by Equation 6.1.2-22 of the parent document to compute the expected dose by taking the expectation over various damage areas and damage times. Because of this computational requirement, for each epistemic vector, the dose response functions for 30 aleatory uncertainty vectors are considered by specifying six discrete damage times (at 200; 1,000; 3,000; 6,000; 12,000; and 18,000 years) over each of the five fractional WP damage areas (10^{-7}, 10^{-6}, 10^{-5}, 10^{-4}, and 10^{-3}) (Table 6.6-3[a]). In addition, the consequences of seismic ground motion events are approximated by examining only the occurrence of SCC damage to CDSP WPs under intact DS without considering rockfall and without considering the effects of corrosion processes in thinning the WP OCB and DS. As a result, only diffusive releases from the CDSP WPs can occur. Furthermore, because the drift degradation is not considered, the thermal-hydrologic processes in the EBS remain the same as under nominal condition. For more details on the computational methodology, refer to Sections 6.1.2.4.4 and 7.3.2.6.1 of the parent document.

A single epistemic vector (out of a sample size of 300 epistemic vectors) is selected for further analysis in such a manner that the expected annual dose is broadly representative of the modeling case and similar in behavior to the mean annual dose curve. After consideration, epistemic vector 155 is chosen for further evaluation (Figure 7.7.1-107[a]). The thirty corresponding aleatory vectors (sampled for the given epistemic vector) are represented by GoldSim realizations 4621 through 4650 (Figure 7.7.1-108[a]). Of these, the eighth aleatory vector, which is equivalent to GoldSim realization 4628, is selected for further analysis (dashed red curve). In this aleatory vector, the seismic damage time is specified at 1,000 years and the fractional damaged area of the CDSP WP is specified at 10^{-5}. The GoldSim file for realization 4628 is run twice to first save information for all the percolation subregions and then to specifically save EBS cell-pathway details related to percolation subregion 3 for the non-seeping environment (GoldSim filenames: LA_v5.005_SM_009000_008.gsm and LA_v5.005_SM_009000_009.gsm; output DTN: MO0801TSPAMVAC.000 [DIRS 185080]).

The total annual dose from realization 4628 is presented on Figure 7.7.1-109[a] along with the individual dose from major dose contributing radionuclides. The dominant radionuclides are ^{99}Tc, ^{129}I, ^{14}C, ^{36}Cl, and ^{79}Se, with negligible contributions from remaining radionuclides. The annual dose increases rapidly following the WP damaging event at 1,000 years, reaching a maximum around 2,000 years and then declining gradually with time as the radionuclide mass is depleted. The bump noticeable around 2,000 years is a result of climate change from monsoonal to glacial-transition climate that occurs at 1,950 years. The dose behavior for ^{99}Tc, ^{129}I, ^{14}C, and ^{36}Cl is observed to be nearly identical to each other and results from their similar transport characteristics through the EBS, UZ, and SZ as these radionuclides are transported without any solubility control and without undergoing any sorption. The relative differences in dose among them are primarily due to their different masses in the inventory, decay rates, and BDCFs. The transport of ^{79}Se is somewhat different from the rest as ^{79}Se is retarded in the UZ and SZ despite having no solubility controlling mineral phase. Hence, for the purpose of describing the transport behavior of major dose contributing radionuclides, only ^{99}Tc (the highest dose contributor among radionuclides that have similar transport characteristics) and ^{79}Se are considered in the following discussion.

All CDSP WPs in all five percolation subregions fail at 1,000 years in this realization. The number of packages in a given percolation subregion is proportional to the repository area occupied by that percolation subregion. As a result, 40 percent of the WPs belong to percolation

subregion 3, 25 percent each to percolation subregions 2 and 4, and 5 percent each to percolation subregions 1 and 5. In each percolation subregion, the number of WPs is further distributed among seeping and non-seeping environments based on the seepage fraction for that percolation subregion. The number of failed CDSP WPs for all percolation subregions distinguished by seeping and non-seeping environments is shown on Figure 7.7.1-110[a]. Note that for a given percolation subregion, most of the WPs fall in the non-seeping environment due to small calculated seepage fraction. For example, the seepage fraction for percolation subregion 3 is about 0.33, so only 33 percent of the WPs assigned to percolation subregion 3 belong to the seeping environment, the remaining (67 percent) belong to the non-seeping environment. The seepage fraction for a given percolation subregion remains constant over the simulation duration and is based on the determination of fraction of seeping locations at 10,000 years in the given percolation subregion.

Since the DSs remains intact and only SCC on the CDSP WP surface due to vibratory ground motion is modeled, no advective transport of radionuclides can occur through the WP. The only release mechanism out of the WP is by diffusion along the diffusive pathways inside the WP and through the cracks on the WP OCB to the invert. Since the fractional damage area to the WP OCB, in this realization, is specified to be 10^{-5}, it is equivalent to the diffusive area of 3.26×10^{-4} m^2 (note that the outer surface area of the CDSP WP is set to be 32.6 m^2), which is applied only over the WP OCB thickness (computed to be 0.0301 m, the distance from outside the inner vessel to the outside of the OCB). Inside the WP the diffusive areas and diffusive lengths for the discretized transport domains are different and are described in Section 6.3.8 of the parent document.

The diffusive releases of ^{99}Tc from the failed CDSP WPs for various percolation subregions (combined over seeping and non-seeping environments) are shown on Figure 7.7.1-111[a]. The diffusive release for percolation subregion 3 is the highest, as expected, due to greatest number of failed WPs among various percolation subregions. Although the number of failed WPs is the same among percolation subregions 2 and 4 and among percolation subregions 1 and 5, the relative peak releases are different because of higher seepage fractions for percolation subregion 4 (compared to 2) and 5 (compared to 1), leading to greater proportion of WPs being placed in a seeping environment. Diffusive release from a WP placed in a seeping environment, compared to a non-seeping environment, tends to be higher due to changed boundary conditions as drift seepage water flows through the invert and removes the mass. This has the effect of moving the zero concentration boundary closer to the WP, thereby increasing the concentration gradient from the WP to the invert. The diffusive releases of ^{79}Se from failed CDSP WPs for various percolation subregions are similarly affected as ^{99}Tc (Figure 7.7.1-112[a]). The magnitudes, however, are much smaller for ^{79}Se due primarily to lower inventory mass per failed CDSP WP (about 12.5 g) compared to ^{99}Tc (of about 960 g per failed CDSP WP), thus leading to lower concentrations in the WP and lower diffusive gradient. In addition, the free water diffusion coefficients among the two radionuclides are slightly different (^{99}Tc has a free water diffusion coefficient of 1.95×10^{-9} m^2/s while that for ^{79}Se is 1.04×10^{-9} m^2/s), which could also cause minor differences in release.

Within percolation subregion 3, the diffusive and advective mass fluxes of ^{99}Tc from the EBS are compared on Figure 7.7.1-113[a] for the seeping and non-seeping environments. Even though the releases from the WP are only diffusive, because of flow in the invert, the advective flux

from EBS is greater in the seeping environment. For the non-seeping environment, the diffusive flux from EBS is greater than the advective flux that results from imbibition flow in the invert. Since the total mass flux for the non-seeping environment is greater than that for the seeping environment for percolation subregion 3 (due to larger number of failed WPs in the non-seeping environment), the results for the non-seeping environment are analyzed in more detail.

The dissolved concentrations of ^{99}Tc out of the various transport domains in the EBS are shown in Figure 7.7.1-114[a]. The concentrations in the HLW and DSNF waste form subdomains and in the majority of the corrosion products domain overlap as a result of fast transport of ^{99}Tc inside the WP due to the large diffusive areas modeled. As shown on Figure 7.7.1-114[a], the HLW glass is almost completely degraded by about 4,000 years. However, the ^{99}Tc mass in the waste form and corrosion products domain is not fully depleted and the concentration declines gradually. This is attributed to the small diffusive area of 3.26×10^{-4} m^2 applied to the transport cell representing the OCB thickness of 0.031 m within the corrosion products domain. This small diffusive area reduces the diffusive conductance across the WP OCB cell pathway and thus exerts a strong influence on the mass transport and concentrations in the surrounding cells that are part of the EBS transport finite difference network (Section 6.3.8 of the parent document). As a result, the concentration in the WP OCB cell is considerably reduced compared to the upstream waste form cells. The diffusive mass flux of ^{99}Tc across various cell pathways is compared on Figure 7.7.1-115[a], which shows the reduction in diffusive flux across the WP OCB, thereby causing retention of appreciable mass in the WP for thousands of years following the breach. The diffusive release out of the upstream cell representing the corrosion products domain (except WP OCB cell) virtually overlaps that of the downstream WP OCB cell due to harmonic averaging of the cell properties for computing the diffusive conductance between the adjoining cells (see Equation 6.3.8-28 of the parent document). Since the diffusive area of the downstream WP OCB cell (3.26×10^{-4} m^2) is orders of magnitude smaller than that of the upstream cell (29.7 m^2; Section 6.3.8.2.3 of the parent document), the diffusive conductance between the two cells (within a finite difference network of cells) is controlled by the WP OCB cell.

The initial sharp increase in concentration noticeable on Figure 7.7.1-114[a] is due to the delayed onset of transport following the breach at 1,000 years as the relative humidity remains below the threshold value of 95 percent (required to initiate transport) until 1,080 years. As a result, almost 80 years of HLW mass is accumulated from degradation prior to the onset of release. Similarly, because all of the DSNF mass is degraded instantaneously following the WP breach, it is also all available for release after 1,080 years. The characteristics of diffusive release and concentrations for ^{79}Se (not shown) are similar to that for ^{99}Tc, except for the magnitudes, and also show the strong influence of reduced diffusive area of the WP OCB in controlling the mass flux out of the WP.

The mass released from the EBS (for each percolation subregion summed over the seeping and non-seeping environments) is passed to the UZ by partitioning the mass into the fracture and matrix nodes of the UZ transport model at the repository horizon. The fraction of ^{99}Tc and ^{79}Se mass that is passed to the fractures is shown on Figures 7.7.1-116[a] and 7.7.1-117[a]. In almost all percolation subregions (except for percolation subregion 1), the mass fraction going into the fracture (compared to the matrix) is greater than 0.5 initially following the breach and then reduces rapidly. This is because initially the mass flux from the seeping environment is greater

than the non-seeping environment (due to increased concentration gradient between the WP and invert due to flow through the invert), which is predominantly passed into the UZ fracture continuum. Eventually, the mass contribution from the non-seeping environment increases (since more WPs are failed in the non-seeping environment) and more mass diffuses into the UZ matrix continuum due to the larger effective diffusive area connection between the matrix and the invert. After 4,000 years, steady state conditions are established once the HLW waste form is fully degraded and the release is controlled by the small diffusive area through the WP OCB. Among various percolation subregions, the fraction of mass released into the fracture is proportional to the seepage fraction. Thus, percolation subregion 5 (seepage fraction of 0.44) has relatively greater mass going into the fractures than percolation subregion 1 (seepage fraction of 0.16). As a result, the sharp increase noticed around 2,000 years due to climate change is most pronounced in percolation subregion 5 and least in percolation subregion 1.

The cumulative release over all percolation subregions from various transport domains from the engineered and natural barrier systems are shown on Figure 7.7.1-118[a] for ^{99}Tc and Figure 7.7.1-119[a] for ^{79}Se. For ^{99}Tc, considerable delay in release occurs out of the WP compared to the release out of the waste form due to the small diffusive area in the WP OCB. Marginal delay is noticed in the invert early on (as shown by EBS release) due to transient conditions as the concentrations build up in the invert. After a few thousand years, the mass released from the EBS matches that released from the WP indicating the limited barrier capability of the invert for a non-sorbing radionuclide with no solubility control. The cumulative release curve for the UZ indicates considerable delay compared to the release from the EBS. This is attributed to the majority of the mass entering the UZ in the matrix nodes and undergoing slower transport. Due to fracture-matrix interaction, the mass that is released into the matrix continuum is transferred into the fracture continuum and quickly carried out via advection. Thus, although most of the mass enters the UZ through matrix nodes, most of it is released out of the fracture nodes at the UZ-SZ interface over the simulated time period. Despite this, only about 75 percent of the mass released from the EBS is released out of the UZ by 10,000 years, indicating appreciable UZ barrier capability in delaying the mass release once the mass enters the matrix. Some delay in the SZ is also observed due to the effects of longitudinal dispersion and fracture-matrix diffusive interaction; however, by 10,000 years, about 90 percent of the mass released from the UZ is released out of the SZ model boundary. The breakthrough curves for ^{99}Tc in the SZ for all four regions are shown on Figure 7.7.1-120[a]. The breakthrough occurs quickly and, by 200 years following the mass input, almost half the mass gets released out of the SZ. The long tail that extends for thousands of years indicates a high degree of dispersion due to the fracture-matrix interaction as the mass that initially diffused into the SZ matrix moves back into the fracture and is eventually transported out.

The cumulative releases for ^{79}Se (Figure 7.7.1-119[a]) show similar behavior to ^{99}Tc for the release from the waste form, WP, and EBS. Due to the small diffusive area in the WP OCB, the release out of the WP is delayed and magnitude is reduced compared to the release out of the waste-form domain. However, in contrast to ^{99}Tc, the transport of ^{79}Se is significantly retarded in the UZ and SZ. This is because of reversible sorption of ^{79}Se in the UZ and SZ volcanic matrix and SZ alluvium. The sampled K_d for the UZ tuff matrix is about 9.3 mL/g (for zeolitic units), 7.4 mL/g (for devitrified units), and 4 mL/g (for vitric units). The sampled K_d for the SZ matrix in the volcanic units is about 16.4 mL/g and that for the SZ alluvium is about 13.4 mL/g. The SZ alluvium K_d is further modified by multiplying by the ratio of effective porosity (sampled value of 0.22) to the total porosity (0.3), thus leading to the effective SZ alluvium K_d of 9.8 mL/g. In the UZ matrix, even with small sampled K_d values, the retardation is significant as the concentration gradient from the matrix to the fracture is further reduced due to sorption in the matrix. By 10,000 years, only about 41 percent of the total mass released from the EBS is released out of the UZ. In the SZ, the delay is even more pronounced as only about 20 percent of the mass that enters from UZ is released out of the SZ model boundary by 10,000 years. Figure 7.7.1-120[a] shows the breakthrough curves from the four SZ regions indicating significant retardation for ^{79}Se, with median delay of around 20,000 years. Compared to the transport of unretarded species such as ^{99}Tc, the effective retardation factor of ^{79}Se in the SZ, for this realization, is about 100 (based on the ratio of median travel times of ^{79}Se to ^{99}Tc).

The release rates out of the SZ model boundary for ^{99}Tc and ^{79}Se are shown on Figure 7.7.1-121[a] for realization 4628. The SZ releases are converted into annual dose by taking the annual releases out of the SZ for each radionuclide, dissolving them in the 3,000 acre-ft of water (annual usage at RMEI as defined by the regulation) to compute the mass concentrations, converting the mass concentration into concentration of radioactivity (in curies per liter of water), and then multiplying with the corresponding BDCFs computed for the modern-interglacial climate (present-day climate). The end result of this is Figure 7.7.1-109[a].

7.7.1.8[a] Summary of Single-Realization Analyses

The single-realization analyses of the seven modeling cases described above provide useful insights into interactions among several submodels under a variety of thermal, mechanical, chemical, and physical conditions in and around the repository. These analyses assist in understanding the coupling among the EBS, UZ, and SZ transport models when calculating annual dose to the RMEI in a given realization. Within each transport model domain, the interaction of various submodels (and their abstractions) under a given set of physicochemical conditions is described in detail, providing confidence that the submodels are coupled as intended and that their behaviors can be explained in a logical manner, leading to the dose calculations. In addition to explaining the interaction of submodels, the transport behaviors of major dose contributing radionuclides are also described and highlighted in the various modeling cases. For some modeling cases, outlier realization analysis is presented to highlight various processes or weighting factors that exert control on the magnitude of dose. In all cases, early releases following WP breach are dominated by non-sorbing and solubility-unlimited radionuclides, such as ^{99}Tc and ^{129}I, whereas later releases are dominated by longer-lived, solubility-limited radionuclides that tend to sorb more strongly, such as ^{242}Pu, ^{237}Np, and ^{239}Pu.

7.7.2[a] Comparison with Simplified TSPA Analysis

A Simplified Analysis has been developed to evaluate repository performance utilizing simplified representations of the mathematical equations that describe radionuclide mass transfer rates. This analysis, called Simplified TSPA Analysis, is described in detail in Appendix L of the parent document. The analysis results are compared to the TSPA-LA Model results to generally corroborate the maximum dose levels. The Simplified TSPA Analysis has its bases in the process- and abstraction-level modeling captured in supporting analysis and model reports. Thus, it represents the same conceptualization of the repository system and its underlying technical bases to those of the TSPA-LA Model. However, detailed analysis, checking, and review activities identified an unintended inconsistency between the distribution coefficients (K_d) used for the TSW units in the UZ used in the simplified analysis (Appendix L of parent document) and those used in the TSPA-LA Model that was not previously documented in the parent document. The UZ K_d distributions are set to the values for vitrified tuff in the simplified analysis (Appendix L of the parent document). These values are consistent with vitrified tuffs at the base of the TSW but inconsistent with the TSW units between the repository and the basal units, which make up much of the TSW below the repository, and are comprised of devitrified tuffs. The K_d distributions for vitrified and devitrified tuff are similar for all radionuclides excluding ^{126}Sn and ^{135}Cs, which show significant differences (Table 6.3.9-2 and Table L-41 of the parent document). Since ^{126}Sn and ^{135}Cs are minor contributors to dose (Section 8.1[a]) despite the differences in the K_d distributions, the basic results of the two models (i.e., dose over time and contribution to dose of dominant radionuclides) can be compared for individual modeling cases.

Models of the degradation of the engineered barriers were developed for the nominal, seismic ground motion, and igneous intrusion conditions. This was done to allow for comparisons with the modeling cases evaluated with the TSPA-LA Model. The Simplified TSPA Analysis is a different system level mathematical model, and the results can be used to generally corroborate the TSPA-LA Model v5.005 maximum dose.

7.7.2.1[a] Waste Package Early Failure Modeling Case

In the Simplified TSPA Analysis, a 500 realization simulation of the Waste Package EF Modeling Case was conducted over a 1,000,000-year period. A comparison of the Simplified TSPA Analysis results considering all realizations and the TSPA-LA Model results using v5.005 for this modeling case at 200,000 years; 400,000 years; 600,000 years; 800,000 years; and 1,000,000 years following repository closure is shown on Figure 7.7.2-3[a]. This comparison is identical to the results documented in Section 7.7.2.1 of the parent document and shows that the Simplified TSPA Analysis results in annual doses that are similar in magnitude to, but higher than, those of the TSPA-LA Model.

7.7.2.2[a] Nominal Modeling Case

The Nominal Modeling Case accounts for the WPs that fail under nominally expected conditions because of general corrosion and SCC and for the DSs that fail under nominally expected conditions because of general corrosion.

Figure 7.7.2-6[a] shows a comparison of the mean annual dose between the two models. The difference in the time that SCC begins between the Simplified TSPA Analysis and the TSPA-LA Model results in the difference in the annual dose histories. In a sense, the annual dose from the Simplified TSPA Analysis is translated outward in time by a few hundred thousand years.

This comparison is identical to the results documented in Section 7.7.2.2 of the parent document and shows that the general trend in the annual dose between the two models is very similar and the peak mean annual dose calculated using the Simplified TSPA Analysis is within approximately half of an order of magnitude as that calculated by the TSPA-LA Model.

7.7.2.3[a] Seismic Ground Motion Modeling Case

The Seismic GM Modeling Case evaluates repository performance for those WPs that fail due to the ground motion damage associated with the seismic event. This case begins with the Nominal Modeling Case discussed above and includes the effect of seismic events over a 1,000,000-year period. In the Simplified TSPA Analysis, the occurrence of seismic events is modeled using the approach presented in Section L2.1 of the parent document. The effects of seismic events on rockfall/drift degradation and seepage are modeled as presented in Sections L2.2 and L2.5 of the parent document, respectively. The effects of seismic ground motion on the performance of the DS and WP is modeled as presented in Sections L2.7.2 and L2.8.3 of the parent document, respectively.

The mean annual dose results for the Simplified TSPA Analysis are similar to those from the TSPA-LA Model. Figure 7.7.2-9[a] shows a comparison of the Simplified TSPA Analysis results and the TSPA-LA Model results for the Seismic GM Modeling Case at 200,000 years; 400,000 years; 600,000 years; 800,000 years; and 1,000,000 years following repository closure. There is generally a positive trend in the annual dose for the TSPA-LA Model results whereas the Simplified TSPA Analysis is variable with time. The two models show a similar peak mean annual dose; the Simplified TSPA Analysis is within approximately half an order of magnitude lower as that calculated by the TSPA-LA Model. However, the earlier peak dose in the Simplified TSPA Analysis reflects the differences in the sampling technique used in the Simplified TSPA Analysis and the lower rate of general corrosion results in 40 percent of the realizations having no WP failures over the 1,000,000-year simulation period, as documented in Section 7.7.2.3 of the parent document. Another notable difference occurs at 200,000 years. Figure 7.7.2-9[a] shows a significant reduction between the TSPA-LA Model v5.005 results and the Simplified TSPA Analysis. This is a result of differences between version 5.000 and 5.005 of the TSPA-LA Model as discussed in Section 7.3.1.5.6[a] of this addendum. Overall, for all other time periods the comparison presented in this addendum is nearly identical to the comparison of results documented in Section 7.7.2.3 of the parent document.

7.7.2.4[a] Igneous Intrusion Modeling Case

The Igneous Intrusion Modeling Case evaluates repository performance for the disruptive event where a volcanic dike intersects the repository. In the Simplified TSPA Analysis, a 1,000,000-year simulation was conducted where a single igneous intrusion event was assumed to randomly occur over the simulation period in each of 500 realizations. All WPs are assumed to be completely failed when the event occurs.

The mean annual dose results for the Simplified TSPA Analysis are similar to those from the TSPA-LA Model. Figure 7.7.2-12[a] shows a comparison of the Simplified TSPA Analysis results and the TSPA-LA Model v5.005 results for this modeling case at 200,000 years; 400,000 years; 600,000 years; 800,000 years; and 1,000,000 years following repository closure. There is generally a positive trend in the annual dose for the TSPA-LA Model results whereas the Simplified TSPA Analysis is variable with time. The results of the Simplified TSPA Analysis are similar in magnitude as those generated by the TSPA-LA Model with the Simplified TSPA Analysis yielding slightly higher mean annual doses. The comparison presented in this addendum differs slightly from the comparison of results documented in Section 7.7.2.4 of the parent document in that the results presented using version 5.005 of the TSPA-LA Model are generally lower that version 5.000 over all time periods after approximately 100,000 years. This difference can be attributed to the corrected distribution for the SZ longitudinal dispersivity as documented in Section 7.3.1.5.4[a] of this addendum.

7.7.3[a] Comparison with Electric Power Research Institute Analysis

No change.

7.7.3.1[a] Introduction and Purpose

This section gives a brief confirmation of the comparison between the EPRI TSPA Analysis and the TSPA-LA Model using v5.005 results. The purpose of this comparison is to confirm a summary presented in Section 7.7.3 of the parent document. The previous analysis showed the EPRI TSPA Analysis compared reasonably well with the TSPA-LA Model, and differences can be related to the different treatment of seepage, inventory, and EBS failure characteristics.

Section 7.7.3 of the parent document presents a comparison between the EPRI TSPA Analysis and the TSPA-LA Model considering the overall features of the dose history curves, together with evaluating the apparent differences between the two models. It is not necessary to reproduce that discussion in this addendum as the summary and conclusions will not change. Rather, only a brief comparison of the mean annual dose results using v5.005 is presented as confirmation of the comparison between the EPRI TSPA Analysis and the TSPA-LA Model.

7.7.3.2[a] Overview of the TSPA Models

No change.

7.7.3.3[a] Unsaturated Zone Flow

No change.

7.7.3.4[a] Engineered Barrier System Environment

No change.

7.7.3.5[a] Waste Package and Drip Shield Degradation

The EBS Corrosion Model is used in the EPRI TSPA Analysis to compute failure distributions for different components of the EBS, which comprise three versions for the nominal, seismic and

igneous scenarios. The EBS Corrosion Model accounts for various failure mechanisms and uncertain parameters that are sampled using Monte Carlo simulations to produce mean failure distribution curves for the DS, WP, and cladding. These mean failure distribution curves are used as input in the near-field model, which is described in greater detail in Appendix M. The current TSPA-LA Model does not take credit for cladding; that is, radionuclides can be released as soon as the WP starts to fail. The EPRI TSPA Analysis accounts for cladding failure for dripping and non-dripping conditions following WP failure.

In the EPRI TSPA Analysis, the computed failure distribution curves for the nominal scenario for the WP are shown on Figure 5-7 in Apted and Ross (2005 [DIRS 182229]), indicating onset of WP failures before 100,000 years. The EPRI TSPA Analysis only considers 8,160 CSNF WPs, of which 5,304 WPs fail after 1,000,000 years (Senger 2008 [DIRS 185124]). In the TSPA-LA Nominal Scenario Class, the probabilistic projections of WP breaches exhibit a few realizations with a SCC occurring before 100,000 years (Section 8.2.1[a]). However, as Figure 7.7.3-2[a] indicates, the bulk of the WP failure occurs after about 200,000 years with 6,256 WPs failed after 1,000,000 years.

As a confirmation of the comparison presented in Section 7.7.3.5 of the parent document, the mean WP and DS failure curves for the TSPA-LA Nominal Scenario Class are shown on Figure 7.7.3-2[a] using TSPA-LA Model v5.005. These results are identical to those presented on Figure 7.7.3-2 of the parent document.

7.7.3.6[a] Waste Form Degradation and Mobilization

No change.

7.7.3.7[a] Engineered Barrier System Flow and Transport

No change.

7.7.3.8[a] Unsaturated Zone Transport

No change.

7.7.3.9[a] Saturated Zone Transport

No change.

7.7.3.10[a] Biosphere

No change.

7.7.3.11[a] Mean Annual Dose Comparison—Nominal Case

The computed mean radionuclide doses for the EPRI nominal scenario is given on Figure 5-10 in Apted and Ross (2005 [DIRS 182229]). In comparison, the results from TSPA-LA Model v5.005 for the computed mean annual doses for the combined Nominal Scenario Modeling Case and the Waste Package EF Modeling Case are shown on Figure 7.7.3-3[a]. The results presented in this addendum are identical to the comparison of results documented in Section 7.7.3.11 of the parent document. These results corroborate the detailed analysis of the

comparison presented in Section 7.7.3.11 of the parent document. In general, the results presented in this addendum confirm the main features of the dose release curves for the EPRI nominal scenario compares reasonably well with the TSPA-LA Model. The differences can be related mostly to differences in seepage and in the different implementation of the inventory and EBS failure characteristics. This is partly due to the fact that the EPRI TSPA Analysis uses earlier analysis and/or model report results.

7.7.4[a] Performance Margin Analysis

The PMA calculations presented in Section 7.7.4 and Appendix C of the parent document paralleled those of the TSPA-LA Model (Section 8) but focused on scrutinizing the impact of select conservatisms embedded in the TSPA-LA Model components and submodels (utilized by the modeling cases to calculate annual doses). The PMA is intended to estimate the cumulative impact of the conservatisms in the TSPA-LA Model and, thereby, indicate the potential performance margin embedded in the TSPA-LA Model's dose-risk projections. Thus, the PMA is an important validation activity supporting the TSPA-LA Model. The PMA evaluates and confirms the conservative nature of the TSPA-LA Model and it provides confidence that there are no non-conservatism remaining in the analysis. The results included in this addendum are used to update the conclusions of the PMA presented in the parent document.

7.7.4.1[a] Projections of the TSPA-LA Performance Margin

The objective of the PMA is to quantitatively evaluate the impact of the major explicit and implicit conservatisms in the TSPA-LA Model. This section provides a comparison of the total dose calculated by TSPA-LA Model v5.000, TSPA-LA Model v5.005, and the PMA presented in Appendix C of the parent document. This comparison confirms the conclusion of the analysis presented in Section 7.7.4.1 of the parent document.

Performance Margin in the Total Mean Annual Dose for 10,000 Years Postclosure

A comparison of the total mean annual dose history for the PMA and the TSPA-LA Model is shown on Figure 7.7.4-7a[a]. Figure 7.7.4-7a[a] shows that there is essentially no difference that exists between the mean annual dose estimates calculated by the two TSPA-LA Model versions for the first 10,000 years postclosure. Figure 7.7.4-7a[a] also shows that the following general observations about the performance margin projections for the first 10,000 years postclosure are the same as presented in Section 7.7.4 of the parent document:

- The PMA total mean annual doses are generally lower by nearly an order of magnitude over the first 10,000 years compared with the total mean annual dose from the TSPA-LA Model.

- The peak PMA total mean annual doses calculated over 10,000 years are lower by over an order of magnitude over the largest total mean annual dose from the TSPA-LA Model.

- Total mean annual doses calculated for 10,000 years are dominated by projected releases for the Igneous Intrusion Modeling Case (Appendix C, Figure C7-7, of the parent document).

Performance Margin in the Total Mean Annual Dose after 10,000 Years through the Period of Geologic Stability

A comparison of the total mean annual dose history for the PMA and the TSPA-LA Model is shown on Figure 7.7.4-7b[a]. For the 1,000,000-year simulation, the mean annual dose calculated by using TSPA-LA Model v5.005 is noticeably lower than TSPA-LA Model v5.000 from an approximate period of 120,000 years through about 300,000 years after postclosure (Figure 7.7.4-7b[a]). From this comparison plot, the following general observations can be drawn about the PMA out to 1,000,000 years postclosure:

- The PMA total mean annual doses are generally lower by nearly an order of magnitude over the first 100,000 years instead of 200,000 years as documented in the parent document and compared with the total mean annual dose from the TSPA-LA Model.

- The peak PMA total mean annual doses calculated over 1,000,000 years are lower by a factor of two over the largest total mean annual dose from the TSPA-LA Model as documented in the parent document.

The differences between the PMA results presented in the parent document to those in this addendum can be related mostly to an update to the implementation of the Seismic Ground Motion damage abstraction, as documented in Section P3 of Appendix P in the parent document. The probability of seismic damage is provided for two end-member states of the WP—one with intact internals and one with fully degraded internals. In TSPA-LA Model v5.000, once any WP is breached by a nominal process in a given percolation subregion (e.g., from first occurrence of stress corrosion cracks located on the outer lids), the probability of seismic damage is switched from the intact internals abstraction to the fully degraded internals abstraction, which increases the chance of seismic damage occurring while the DS is intact. This probability is then applied to all the WPs in the given percolation subregion, which is conservative, as most of the WPs have not yet failed by the nominal processes and should be using the intact internals damage probability. As a result, CSNF WPs fail earlier (Figure 8.1-5b of the parent document), beginning at approximately 150,000 years postclosure, and acquire greater damage area than expected, between approximately 200,000 and 300,000 years postclosure. The removal of this conservative implementation for seismic ground motion damage from v5.000 to v5.005 of the TSPA-LA Model results in fewer WPs damaged during a seismic event between approximately 200,000 and 300,000 years postclosure (Figure 8.1-5b[a]). This difference accounts for the smaller performance margin observed from approximately 200,000 to 300,000 years postclosure between the PMA and TSPA-LA Model v5.005 results presented in this addendum.

Scenario Specific Insights about the Performance Margin

Additional important insights about the performance margin can be gained by disaggregating the total mean annual dose into the total mean annual dose curves for the individual modeling cases and conducting a systematic evaluation of the effects of the changes incorporated into the PMA. This detailed analysis is included in Appendix C of the parent document; however, one notable change is documented in this addendum.

A comparison between the observations listed above for the PMA and the TSPA-LA Model results yields some notable differences. With regards to TSPA-LA Model v5.000 results, the Seismic GM Modeling Case dominates the total mean annual dose for the 10,000-year time period; whereas for 1,000,000 years, the Seismic GM and Igneous Intrusion Modeling Cases are the dominant contributors to the total mean annual dose to the RMEI (Figure 8.1-3, Section 8.1.1.2, of the parent document). However, in TSPA-LA Model v5.005 results while the Seismic GM Modeling Case still dominates the total mean annual dose for the 10,000-year time period, over the 1,000,000-year period the Igneous Intrusion Modeling Case dominates the total mean annual dose until approximately 700,000 years postclosure when the Seismic GM and Igneous Intrusion Modeling Cases contribute nearly equally to the total mean annual dose (Section 8.1.1.2[a]). In the PMA results, the Igneous Intrusion Modeling Case dominates the total mean annual dose for the time period of 10,000 years (Figure C7-7f of the parent document). For the time period after 10,000 years and through the period of geologic stability, the Igneous Intrusion Modeling Case dominates the total mean annual dose with a small contribution from the Seismic GM Modeling Case beginning around 225,000 years (Figure C7-8f of the parent document). These differences are primarily due to a lower incidence of WP failure (Appendix C6.8 and C7.2) and a reduction in the seismic induced WP SCC crack damage in the PMA Model (Appendix C6.8 and C7.2). The remaining cases combined have a negligible contribution for both the PMA and TSPA-LA Model total mean annual dose results.

7.7.4.2[a] Summary of the TSPA-LA Performance Margin

The results in this addendum confirm that the specified objectives of the PMA are met as follows:

1. The PMA results confirm that submodel conservatisms propagated through the TSPA-LA Model are also conservative with respect to the total system performance measures (e.g., total mean annual dose).

2. Relative to the TSPA-LA Model results, the peak PMA total mean annual dose is lower by over an order of magnitude for the 10,000-year time period and lower by a factor of two for the time period after 10,000 years.

3. The evaluated conservatisms did not introduce any inappropriate risk dilution in the TSPA Model results presented in support of the LA. This was demonstrated by the absence of higher peak mean annual doses relative to the TSPA-LA Model for the PMA results for both the probabilistic projections of the total dose histories and the projected total mean dose.

The assessment of the potential performance margin embedded in the TSPA-LA Model results is presented in detail in Appendix C of the parent document.

7.8[a] NATURAL ANALOGUES

No change.

7.9[a] TECHNICAL REVIEWS SUMMARY

No change.

7.10[a] SUMMARY OF MODEL CONFIDENCE BUILDING

The purpose of Section 7.10[a] is to summarize the additional validation activities documented in this addendum. Concluding remarks are presented in Section 7.10.10[a].

7.10.1[a] Validation Strategy

No change.

7.10.2[a] Code and Input Verification

For the results presented in this addendum, additional code and input verification testing was documented, including: (1) verification of the integrated system software (GoldSim) that is the software platform for the TSPA-LA Model used in this addendum, and (2) verification of model inputs from the TSPA Input Database. GoldSim V9.60.300 (STN: 10344-9.60-03 [DIRS 184387]) was qualified per IM-PRO-004. Additional submodels used in the Human Intrusion Scenario were verified. Coupling between the Human Intrusion submodels was examined by verifying that the information generated by one submodel is fed correctly to successive submodels and that this information does not exceed the applicable range of the successive submodel. The code and input verification was conducted to provide additional confidence in the software and the input used in the TSPA-LA Model and to comply with the requirements of SCI-PRO-006 *Models*, Section 6.3.2. In other words, these activities were conducted to verify that the computer codes and model inputs that originated from an outside source (analysis and/or model reports), or generated internally within the TSPA-LA Model, are implemented correctly.

The activities in Section 7.2 of the parent document and the additional work presented in Section 7.2[a] of this addendum demonstrate that the system software for TSPA-LA Model v5.005 is appropriate and valid, that input is correct and verified, that the internal transfer of information within the model is correct and within the valid range of successive submodels, and that submodels are valid per their respective source analysis and/or model reports. In other words, incorporation of information and submodels from other sources into TSPA-LA Model v5.005 has not altered the validity of the information or the submodels or both as demonstrated in the parent document for TSPA-LA Model v5.000.

7.10.3[a] Model Stability Testing

Demonstration of stability of TSPA-LA Model v5.005 is essential to validation and confidence building of the model results. As discussed in Section 7.3 of the parent document, the TSPA-LA Model computes mean annual dose in four steps: (1) selection of values for epistemic parameters and aleatory uncertainties; (2) numerically solving a complex, coupled system of differential equations describing radionuclide decay, flow, transport, and other physical processes; (3) integration over aleatory uncertainty, carried out either by quadrature or Monte Carlo techniques; and (4) integration over epistemic uncertainty, conducted by a Monte Carlo

technique. Section 7.3 of the parent document discusses the details of how the stability of the TSPA-LA Model is verified through implementation of the four steps during the TSPA-LA Model computations. TSPA-LA Model stability verification involved five different analyses: (1) statistical stability of mean annual dose, (2) numerical accuracy of expected annual dose, (3) temporal stability, (4) spatial stability, and (5) stability of a FEHM particle tracking model. A summary of each of these stability tests and their results obtained from them are provided in Section 7.10.3 of the parent document. Two additional analyses were presented in this addendum, one for statistical stability and one for temporal stability.

Statistical Stability

The TSPA-LA Model v5.005 changes are minor, the same LHS size (300) was used for TSPA-LA Model v5.000, and the uncertainty in total expected annual dose is driven by the same uncertain inputs. Thus, it is reasonable to conclude that TSPA-LA Model v5.005 also produces a statistically stable estimate of the total mean annual dose based upon the evaluation of the statistical stability presented in the parent document. However, an additional illustration of the accuracy of the estimate of the total mean annual dose for TSPA-LA Model v5.005, using a bootstrap sampling procedure to generate confidence intervals, is presented.

Numerical Accuracy of Expected Annual Dose

No change.

Temporal Stability

This addendum includes an update to the evaluation of temporal stability of the TSPA-LA Model Human Intrusion Scenario. This update was necessary due to the change in the timestepping scheme used in the Human Intrusion Scenario in TSPA-LA Model v5.005. The simulations were conducted by reducing the TSPA-LA Model timestep size to examine the timestep size sensitivity. The annual dose from the TSPA-LA Model calculations with different timestep sizes were compared graphically to determine the effect of refining the timesteps. The details of the approach and results are provided in Section 7.3.3 of the parent document. The results of this analysis show a better resolution using the base-case timestep scheme than previously documented in the parent document. The test results for the Human Intrusion Modeling Case confirm that the timestep scheme used for dose calculation in this modeling case is adequate.

In addition, a new evaluation of the temporal stability of the TSPA-LA Model Nominal Modeling Case is presented in Section 7.3.3.7[a]. The temporal discretization used to determine general corrosion rates is influential to the annual dose resulting from nominal corrosion processes. Simulation was conducted with shorter timesteps for the calculation of the crack growth rate, which removes the jumps in the number of WP failures by SCC, which in turn is reflected in the expected annual dose curves for the alternative scheme. However, this similarity in statistics for expected annual dose for the two timestep schemes indicates that the Nominal Modeling Case is sufficiently stable with respect to temporal discretization.

Spatial Stability

No change.

Stability of FEHM Particle Tracking Model

No change.

7.10.4[a] Uncertainty Characterization Review and Sensitivity Analyses

No change.

7.10.5[a] Surrogate Waste Form Validation

The analyses presented in Section 7.5 of the parent document and Section 7.5[a] of this addendum show that the use of surrogates to represent naval spent fuel is appropriate. Both analyses of NSNF show that mean annual dose from NSNF is bounded by that from the Zircaloy-clad CSNF surrogate.

7.10.6[a] Corroboration of Abstraction Results with Validated Process Models

No change.

7.10.7[a] Corroboration of Results with Auxiliary Analyses

The auxiliary analyses are an important aspect of determining whether the TSPA-LA Model is yielding reasonable results (e.g., that the model is producing the results that would be expected). Additional discussions of the results for some of the verification and validation testing activities presented in Section 7.7 of the parent document are presented in Section 7.7[a] for four different sets of auxiliary analyses: (1) single realization analysis (Section 7.7.1[a]), (2) updated comparison of the results of TSPA-LA Model v5.005 with a Simplified TSPA Analysis (Section 7.7.2[a]), (3) updated comparison of the results of TSPA-LA Model v5.005 with the TSPA independently developed by EPRI (Section 7.7.3[a]), and (4) updated PMA comparison to TSPA-LA Model v5.005 (Section 7.7.4[a]). A summary of the additional discussion included in this addendum is provided below.

Single Realization Analysis

The single realization analyses presented in the parent document and in Section 7.7.1[a] of this addendum comprise a comprehensive explanation detailing how the transport of key radionuclides is affected by coupling various submodels of the EBS, UZ, and SZ domains in the TSPA Model, following the WP failure under varying physical-chemical-thermal-mechanical conditions, and providing confidence that these model components are working as expected and the aggregate TSPA-LA Model results (in terms of dose) are reflective of the model components. Through examination and explanation of key aspects affecting the release of radionuclides, it is demonstrated that the TSPA-LA Model is functioning as intended and that the submodels are coupled correctly to yield the system level results. Repeating these analyses in this addendum

provides confidence that TSPA-LA Model v5.005 is functioning as designed and helps confirm the validation of the model.

The parent document includes single realization analyses of four modeling cases: (1) Waste Package EF Modeling Case (Section 7.7.1.1), (2) Drip Shield EF Modeling Case (Section 7.7.1.2), (3) Igneous Intrusion Modeling Case (Section 7.7.1.3), and (4) Seismic GM Modeling Case (1,000,000 years) (Section 7.7.1.4). Details of the analyses and ensuing results are repeated in this addendum and discussed in Sections 7.7.1.1[a] through 7.7.1.4[a]. Three additional modeling cases: (1) Nominal Modeling Case (Section 7.7.1.5), (2) Human Intrusion Modeling Case (Section 7.7.1.6), and (3) Seismic GM Modeling Case (10,000 years) (Section 7.7.1.7) are included in this addendum. The results confirm that the changes from TSPA-LA Model v5.000 to TSPA-LA Model v5.005 had little impact on the results presented using v5.000 and, therefore, support the demonstration of model validation and add to the confidence in the TSPA-LA Model results.

Comparison with Simplified TSPA Analysis

A comparison of the TSPA-LA Model results to a stand-alone Simplified TSPA Analysis was conducted and documented in Section 7.7.2 and Appendix L of the parent document. Section 7.7.2 of the parent document provides a detailed discussion on the comparative results for the individual modeling cases for the Simplified TSPA Analysis and the TSPA-LA Model, including the minor differences in the prominence of certain radionuclides and mean annual doses calculated by the two approaches. A comparison of the updated results presented in this addendum with the Simplified TSPA Analysis was provided in Section 7.7.2[a].

The results presented in Section 7.7.2[a] comparing the TSPA-LA Model v5.005 results and the Simplified TSPA Analysis corroborate the conclusions presented in the parent report.

Comparison with EPRI TSPA Analysis

A limited comparison of the EPRI TSPA Analysis results with those of TSPA-LA Model v5.005 is documented in this addendum. Detail of the similarities and differences between the EPRI TSPA Analysis and TSPA-LA Model v5.000 is discussed in Section 7.7.3 of the parent document with additional detail provided in Appendix M of the parent document.

The results documented in Section 7.7.3[a] identify the general similarities as well as the differences between the results from the two models detailed in Section 7.7.3 of the parent document.

Performance Margin Analysis

A comparison of TSPA-LA Model v5.005 results with the PMA was conducted to confirm the quantitative evaluation of the differences in repository performance due to significant explicit and implicit conservatisms embedded in the TSPA-LA Model submodels documented in Section 7.7.4 and Appendix C of the parent document. The conservatisms were evaluated to (1) confirm that they are conservative with respect to the mean annual dose of the TSPA-LA Model; (2) quantify the extent to which they, individually and collectively, overestimate the projected annual dose; and (3) assess that the evaluated conservatisms did not introduce any inappropriate

risk dilution in the TSPA-LA Model results presented in support of the LA. The details of approach and results of the PMA are presented in Section 7.7.4 of the parent document with additional supporting material in Appendix C of the parent document. Summarizing here, the results show that the margin evaluated in the PMA as documented in the parent document are indeed conservative with respect to the total system performance measures (e.g., peak mean annual dose) as the largest doses calculated in the PMA for 10,000 years and 1,000,000 years are lower than the doses used in the compliance demonstration presented in Section 8[a] of this addendum. The additional analyses confirm that the largest calculated PMA mean annual doses are lower by over an order of magnitude and a factor of two over the largest mean annual dose relative to the TSPA-LA Model (Section 8[a]) for the time periods of 10,000 years and 1,000,000 years, respectively. Further, this PMA confirms that the significant conservatisms did not introduce risk dilution in the TSPA-LA Model results, as demonstrated by the absence of higher peak doses in the comparison of the projected total mean annual dose for the PMA relative to TSPA-LA Model v5.005. The differences in the relative contributions to the total mean annual dose from each of the scenario modeling cases between the PMA and the TSPA-LA Model indicate that the reduction in the selected conservative assumptions embedded in these TSPA-LA Model components provides a performance margin in the projected annual dose predictions presented in Section 8 of the parent document and Section 8[a] of this addendum.

7.10.8[a] Corroboration of Results with Natural Analogues

No change.

7.10.9[a] Technical Reviews Summary

No change.

7.10.10[a] Conclusions

The comparison of TSPA-LA Model v5.005 results to the validation activities that were presented in the parent document were conducted to verify that modifications to parameter values and submodel implementations detailed in Sections 4[a] and 6[a] of this addendum did not adversely affect the overall validation of the TSPA-LA Model. Additionally, only the validation and confidence building activities presented in the parent document that may have been affected by the changes from v5.000 to v5.005 have been updated in this addendum. Section 7[a] also includes additional discussion of the results for some of the verification and validation testing activities presented in the parent document that are used to enhance confidence in the TSPA-LA Model results. All results presented in this section utilized TSPA-LA Model v5.005 and confirmed that the updated model is within the range of validation previously documented in the parent document.

Changes were made to the TSPA-LA Model to address the issues presented in Appendix P of the parent document and to address unintended conservatisms in the TSPA-LA Model, as indicated in Appendix P[a] of this addendum. As documented in Appendix P of the parent document, and confirmed in the updated validation activities presented in this addendum, only Section P3 identified an issue in the TSPA-LA Model v5.000 that had the potential to significantly change the total expected annual dose results (Appendix P of the parent document). Although the

TSPA-LA Model v5.005 expected annual dose results confirm a significant decrease over the time period between approximately 100,000 to 300,000 years, the activities presented in Section 7 of the parent document, and the additional results documented in Section 7[a] of this addendum, confirm: (1) the GoldSim code functions as intended; (2) inputs were accurately implemented in the TSPA-LA Model; (3) the TSPA-LA Model is numerically, temporally, and spatially stable; and (4) the resultant dose calculations are appropriate for their intended use.

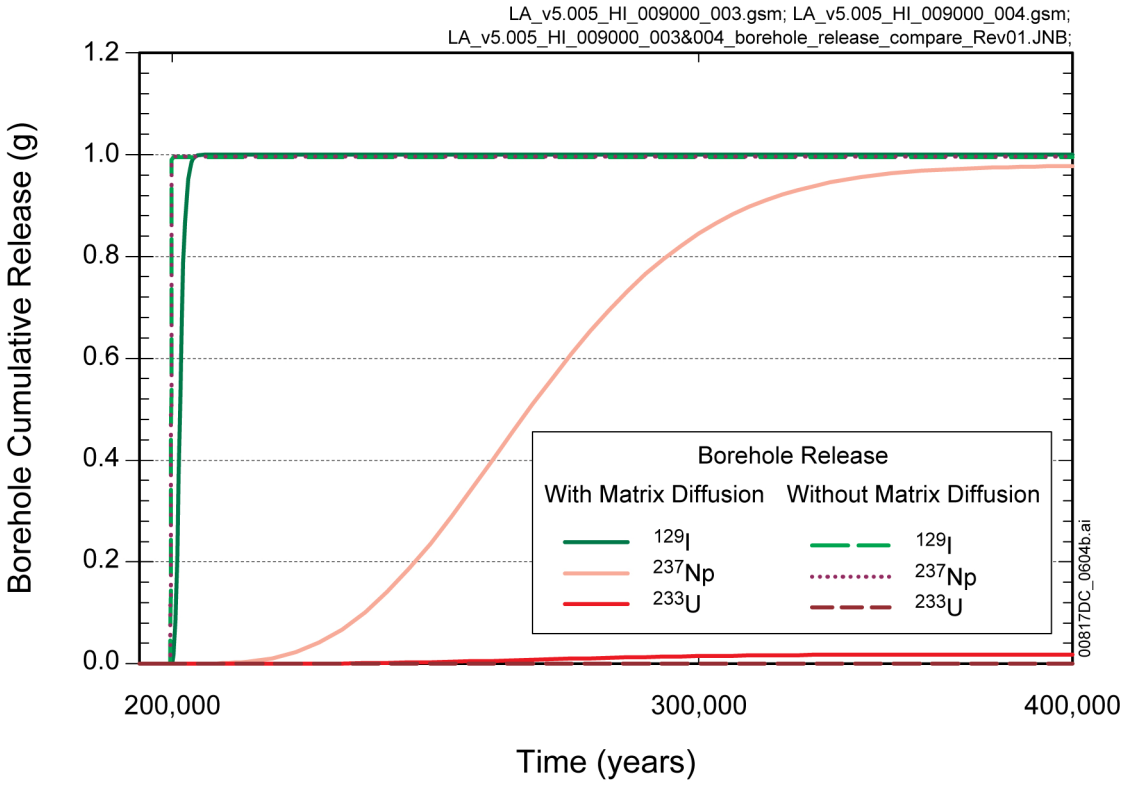

Source: Output DTN: MO0801TSPAMVAC.000 [DIRS 185080].

Figure 7.2-17[a]. Cumulative Releases of ^{129}I, ^{237}Np, and ^{233}U from the Human Intrusion Borehole Based on Simulations Considering and not Considering Matrix Diffusion

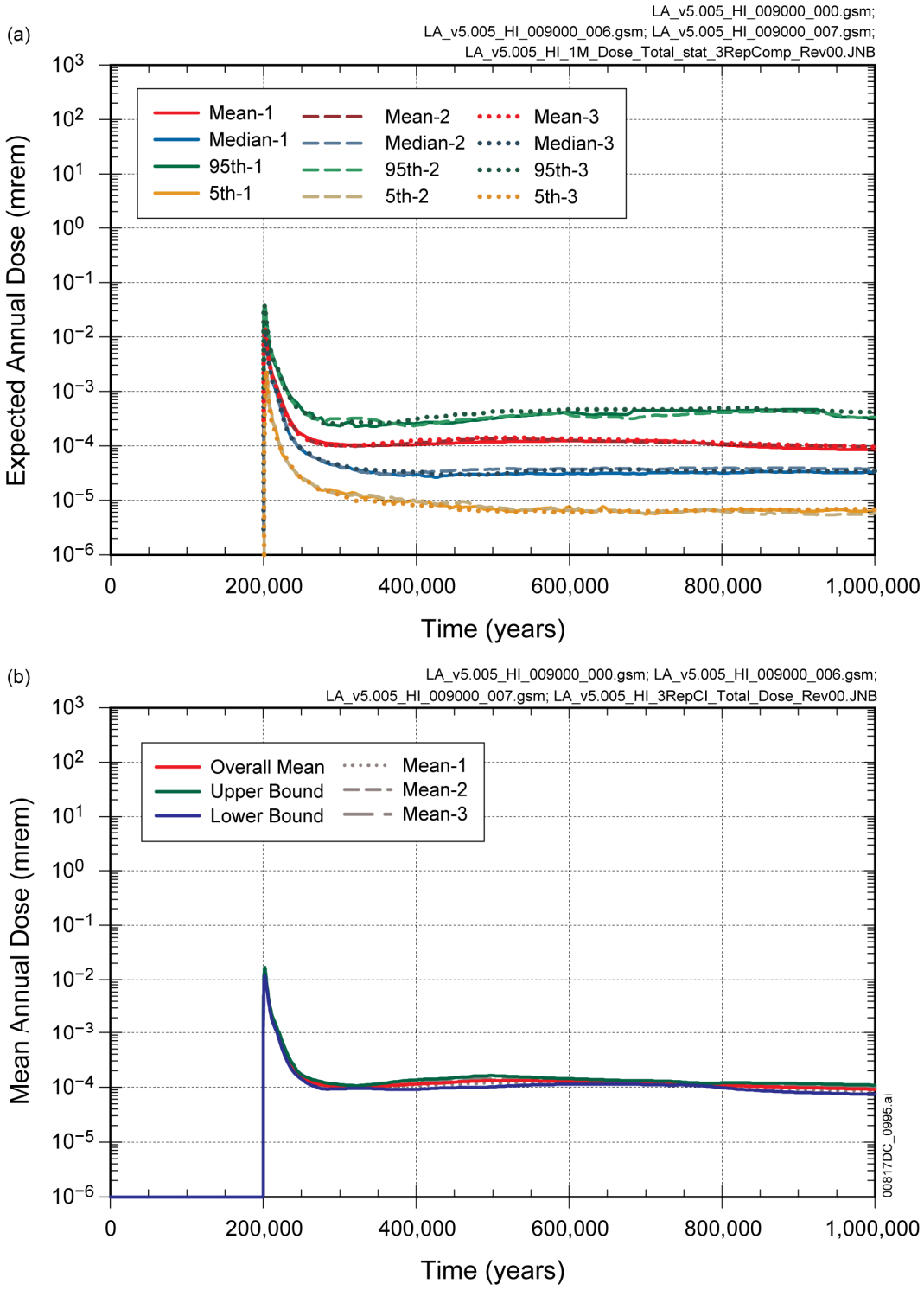

Source: Output DTNs: MO0710ADTSPAWO.000 [DIRS 183752]; and MO0801TSPAADSA.000 [DIRS 185078].

Figure 7.3.1-14[a]. Stability of Human Intrusion Scenario: (a) Comparison of Expected Annual Dose for Three Replicates and (b) Confidence Interval around Mean Annual Dose

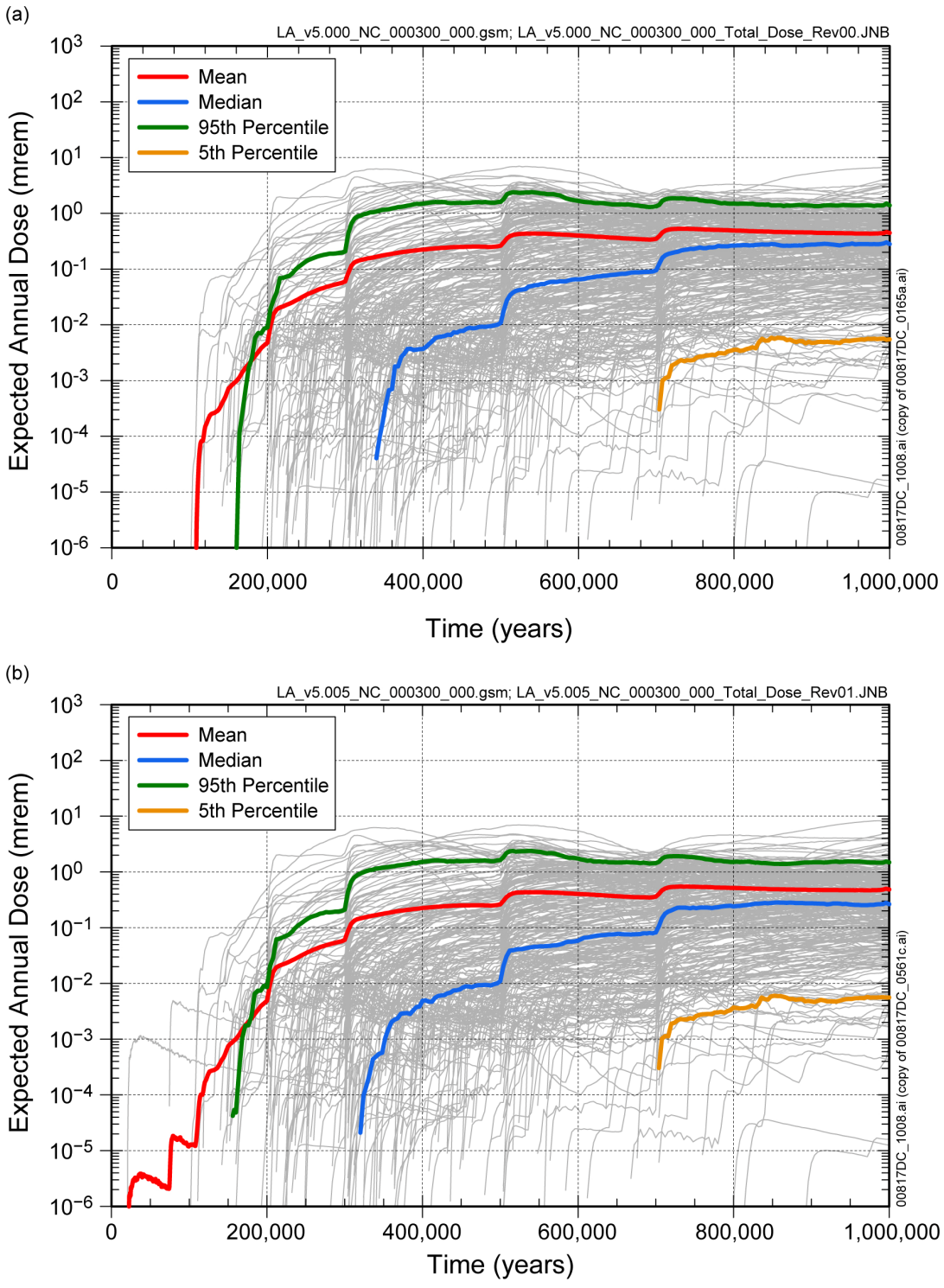

Source: Output DTNs: MO0709TSPAREGS.000 [DIRS 182976]; and MO0710ADTSPAWO.000 [DIRS 183752].

Figure 7.3.1-17[a]. Expected Annual Dose for 1,000,000 Years for the Nominal Modeling Case from (a) TSPA-LA Model v5.000 and (b) TSPA-LA Model v5.005

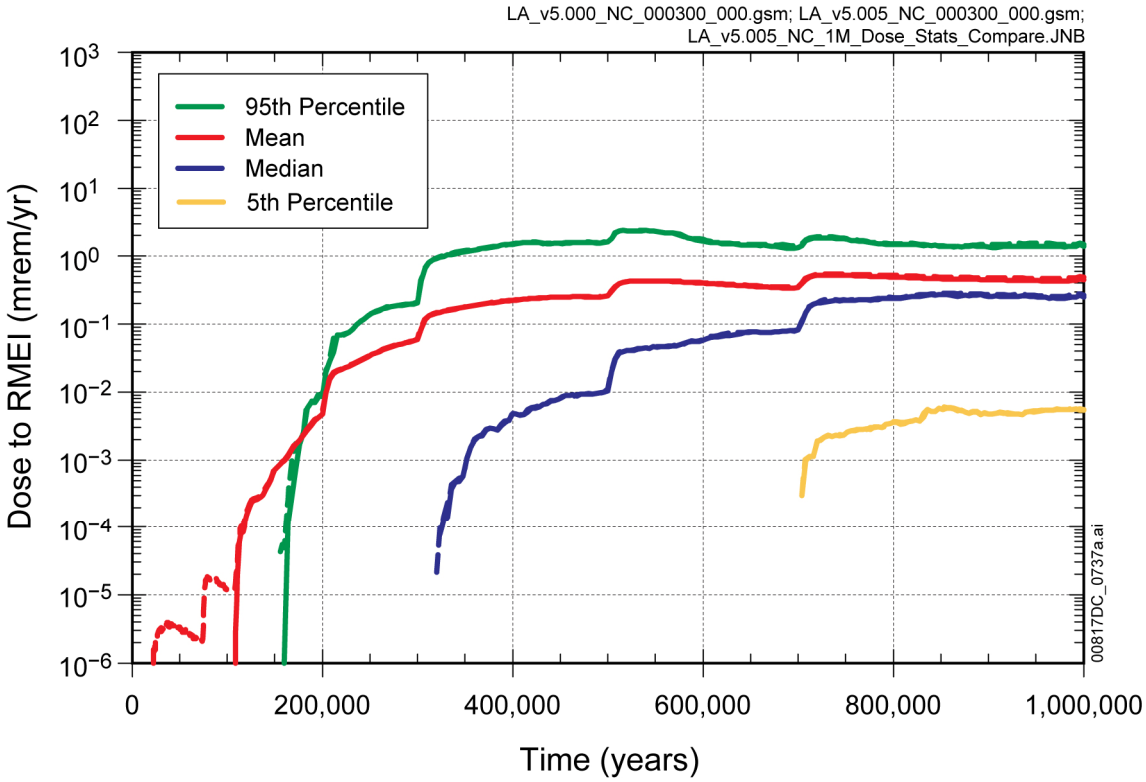

Source: Output DTNs: MO0710ADTSPAWO.000 [DIRS 183752]; and MO0709TSPAREGS.000 [DIRS 182976].

NOTE: Solid lines indicate TSPA-LA Model v5.000 and dashed lines indicate TSPA-LA Model v5.005.

Figure 7.3.1-18[a]. Comparison of Statistics for Expected Annual Dose in the Nominal Modeling Case between TSPA-LA Model v5.000 and TSPA-LA Model v5.005

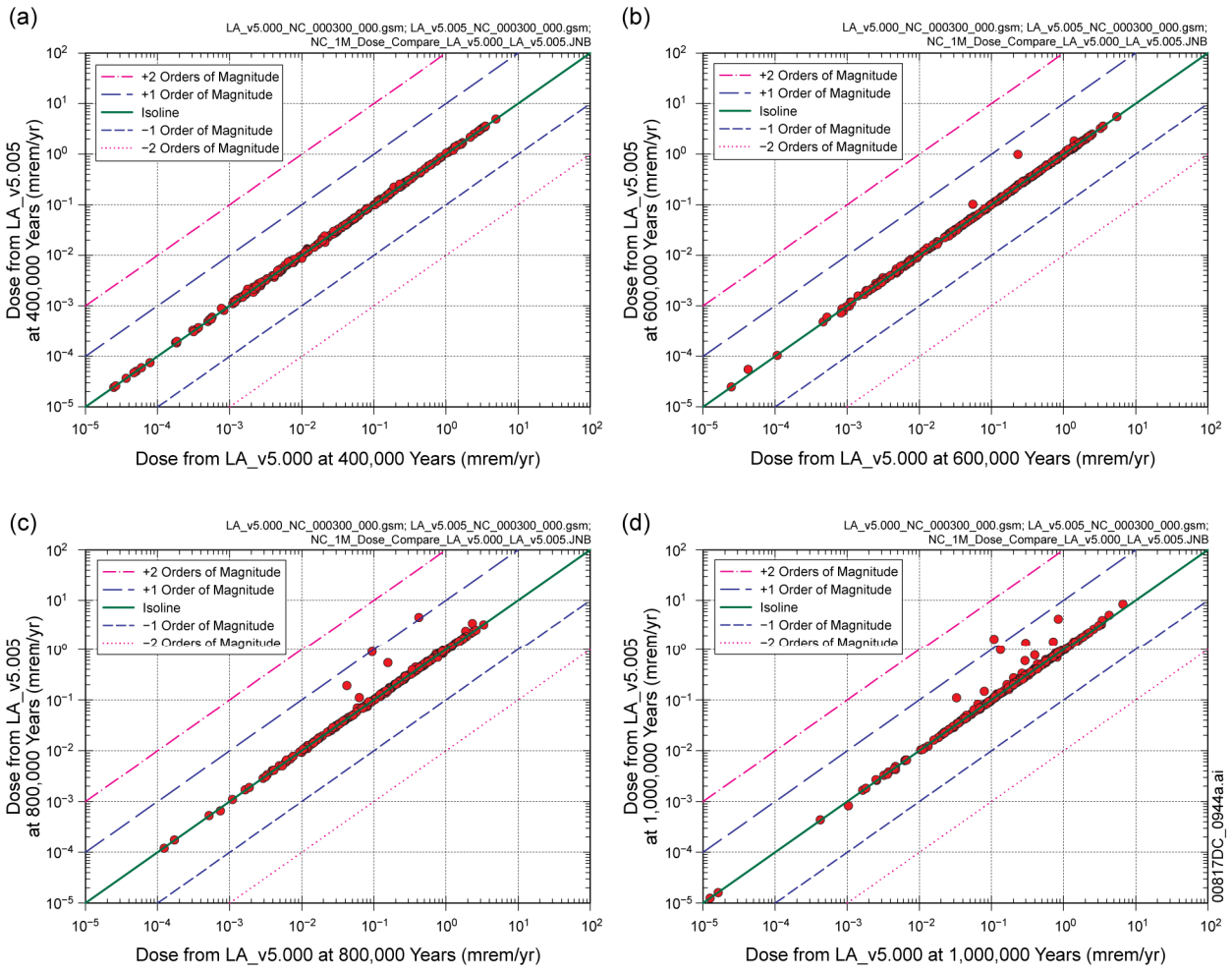

Source: Output DTNs: MO0710ADTSPAWO.000 [DIRS 183752]; and MO0709TSPAREGS.000 [DIRS 182976].

Figure 7.3.1-19[a]. Comparison of Expected Annual Dose for Individual Sample Elements in the Nominal Modeling Case between TSPA-LA Model v5.000 and TSPA-LA Model v5.005 at (a) 400,000; (b) 600,000; (c) 800,000; and (d) 1,000,000 Years

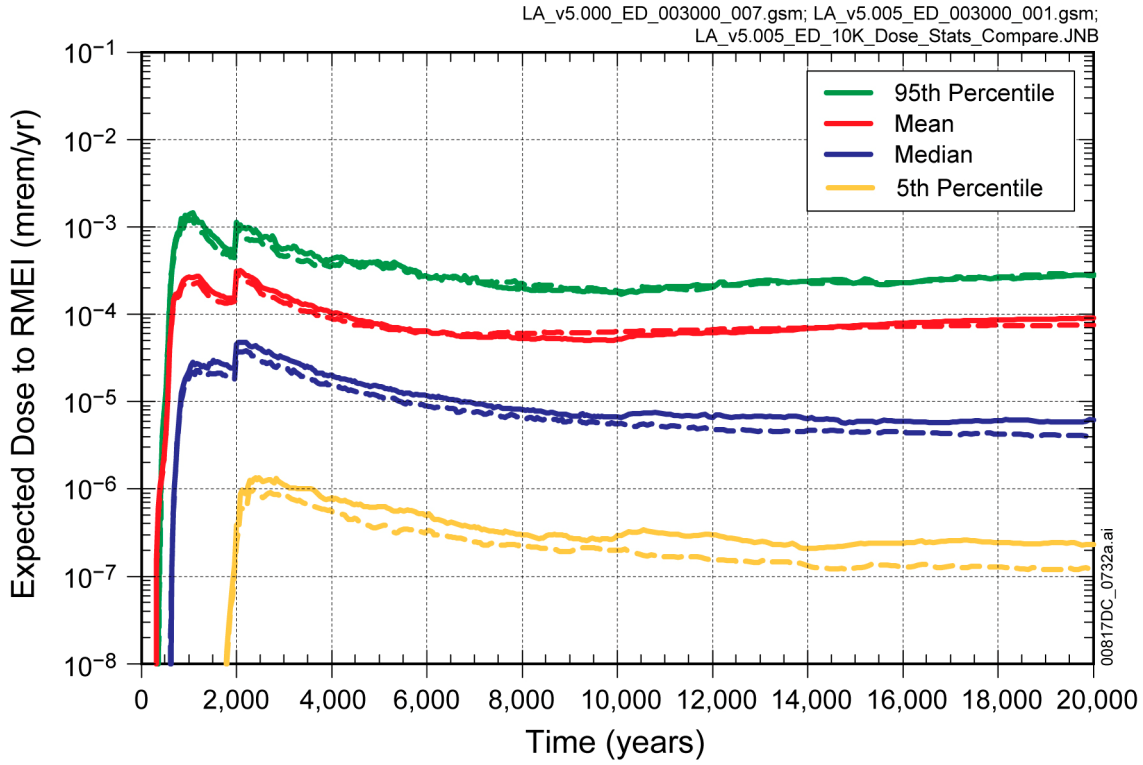

Source: Output DTNs: MO0710ADTSPAWO.000 [DIRS 183752]; and MO0709TSPAREGS.000 [DIRS 182976].

NOTE: Solid lines indicate TSPA-LA Model v5.000 and dashed lines indicate TSPA-LA Model v5.005.

Figure 7.3.1-20[a]. Comparison of Statistics for Expected Annual Dose over 20,000 Years in the Drip Shield Early Failure Modeling Case between TSPA-LA Model v5.000 and TSPA-LA Model v5.005

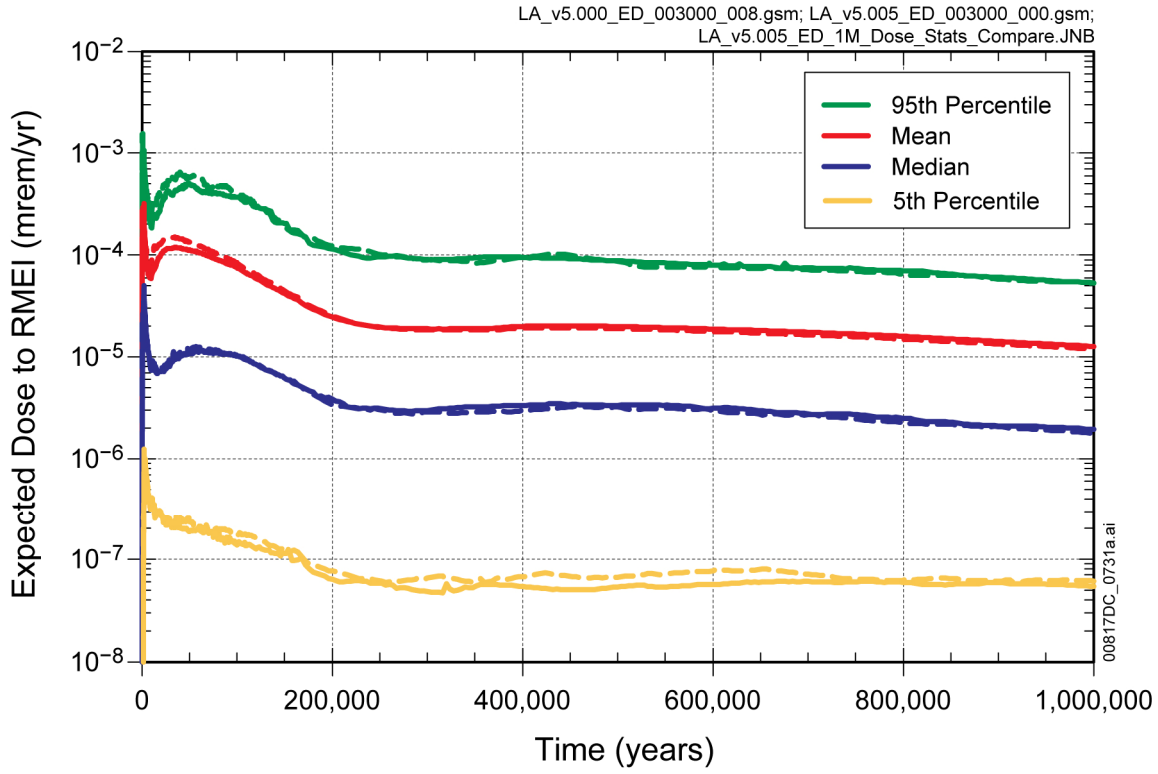

Source: Output DTNs: MO0710ADTSPAWO.000 [DIRS 183752]; and MO0709TSPAREGS.000 [DIRS 182976].

NOTE: Solid lines indicate TSPA-LA Model v5.000 and dashed lines indicate TSPA-LA Model v5.005.

Figure 7.3.1-21[a]. Comparison of Statistics for Expected Annual Dose over 1,000,000 Years in the Drip Shield Early Failure Modeling Case between TSPA-LA Model v5.000 and TSPA-LA Model v5.005

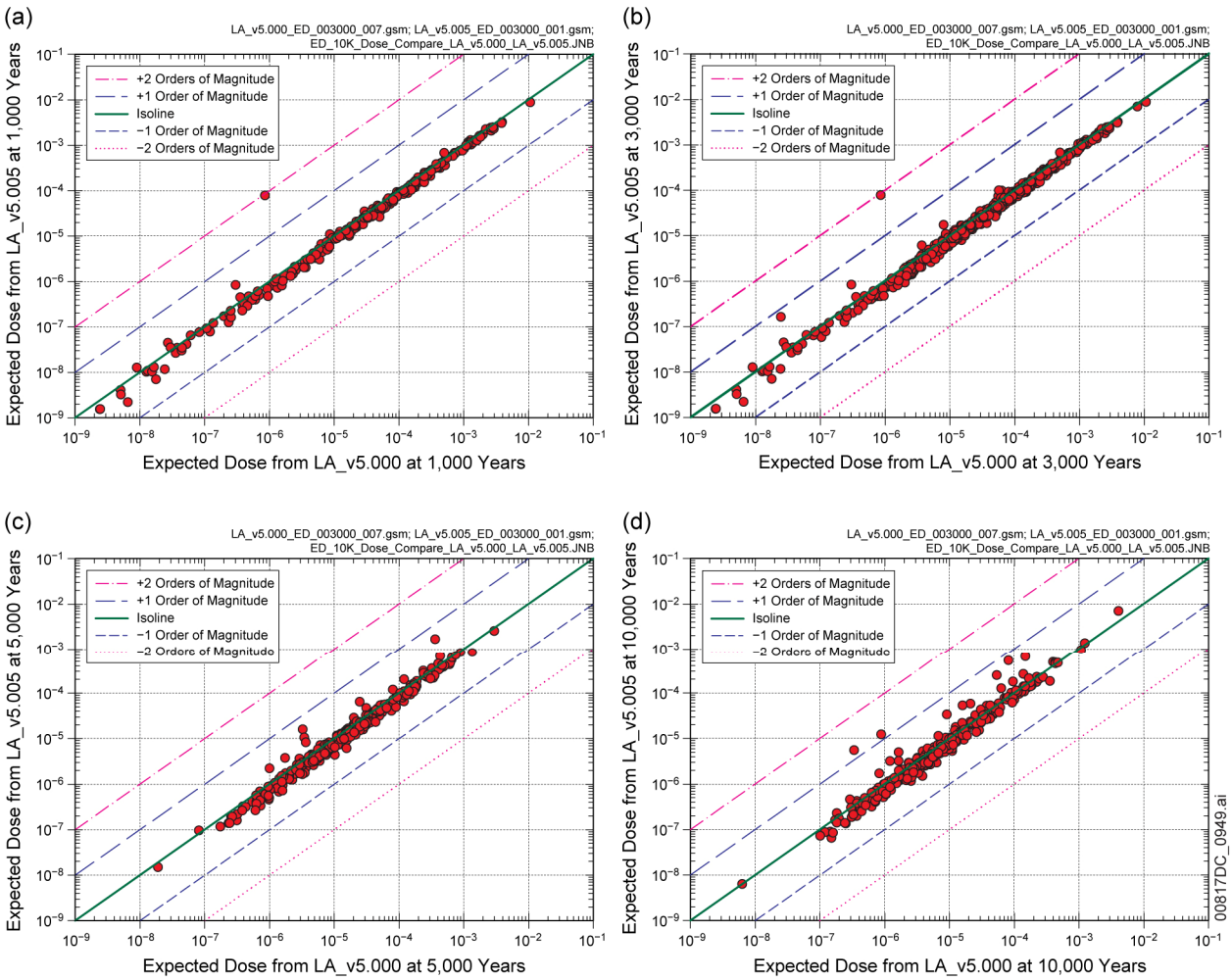

Source: Output DTNs: MO0710ADTSPAWO.000 [DIRS 183752]; and MO0709TSPAREGS.000 [DIRS 182976].

Figure 7.3.1-22[a]. Comparison of Expected Annual Dose for Individual Sample Elements in the Drip Shield Early Failure Modeling Case between TSPA-LA Model v5.000 and TSPA-LA Model v5.005 at (a) 1,000; (b) 3,000; (c) 5,000; and (d) 10,000 Years

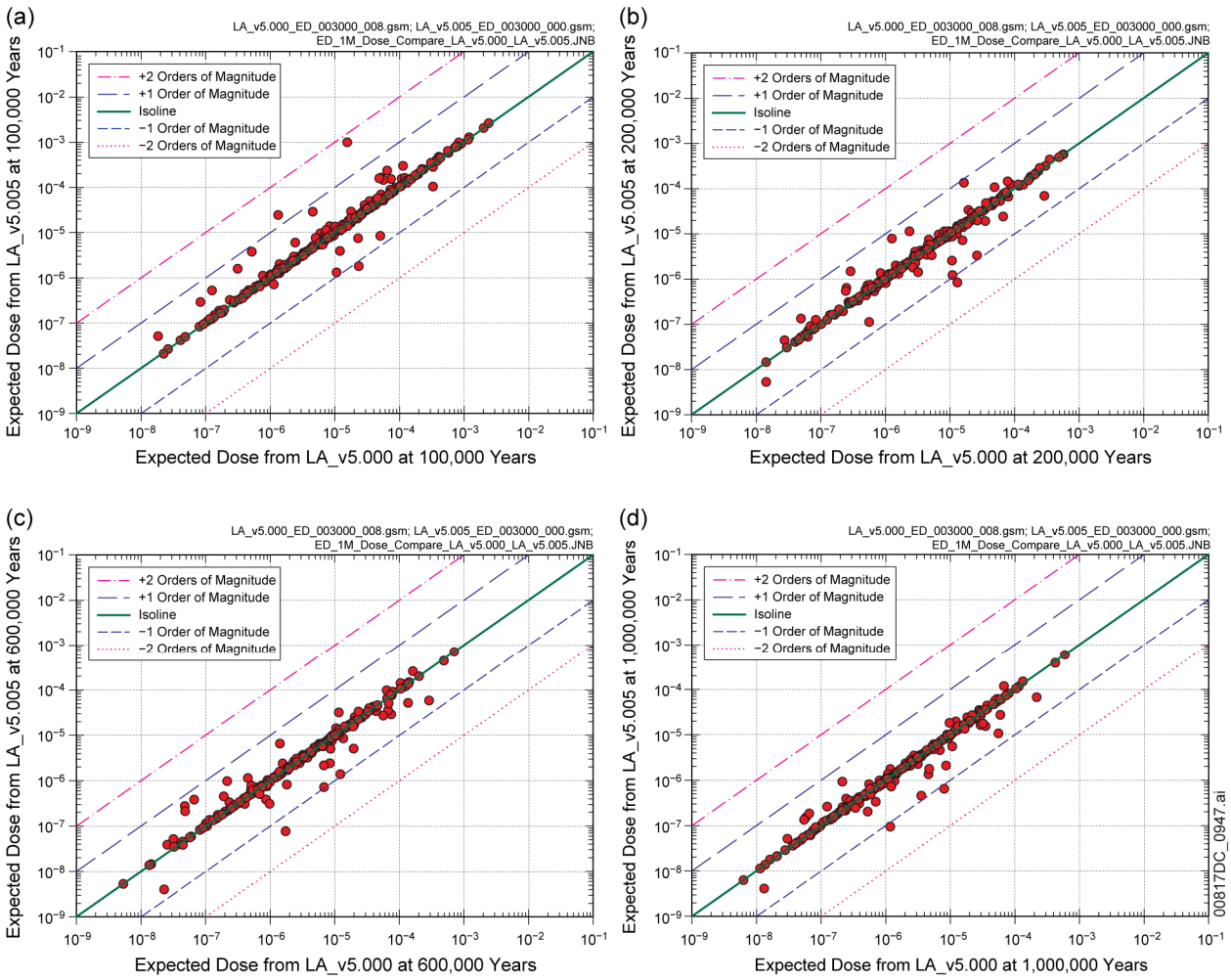

Source: Output DTNs: MO0710ADTSPAWO.000 [DIRS 183752]; and MO0709TSPAREGS.000 [DIRS 182976].

Figure 7.3.1-23[a]. Comparison of Expected Annual Dose for Individual Sample Elements in the Drip Shield Early Failure Modeling Case between TSPA-LA Model v5.000 and TSPA-LA Model v5.005 at (a) 100,000; (b) 200,000; (c) 600,000; and (d) 1,000,000 Years

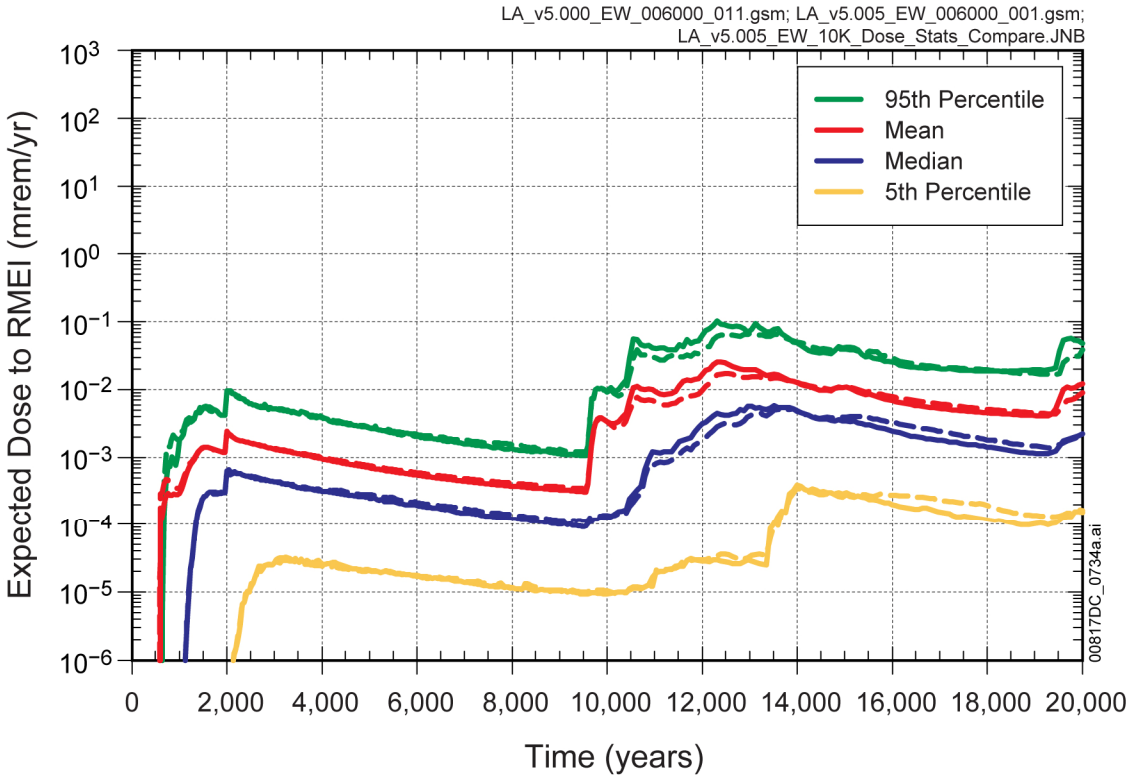

Source: Output DTNs: MO0710ADTSPAWO.000 [DIRS 183752]; and MO0709TSPAREGS.000 [DIRS 182976].

NOTE: Solid lines indicate TSPA-LA Model v5.000 and dashed lines indicate TSPA-LA Model v5.005.

Figure 7.3.1-24[a]. Comparison of Statistics for Expected Annual Dose over 20,000 Years in the Waste Package Early Failure Modeling Case between TSPA-LA Model v5.000 and TSPA-LA Model v5.005

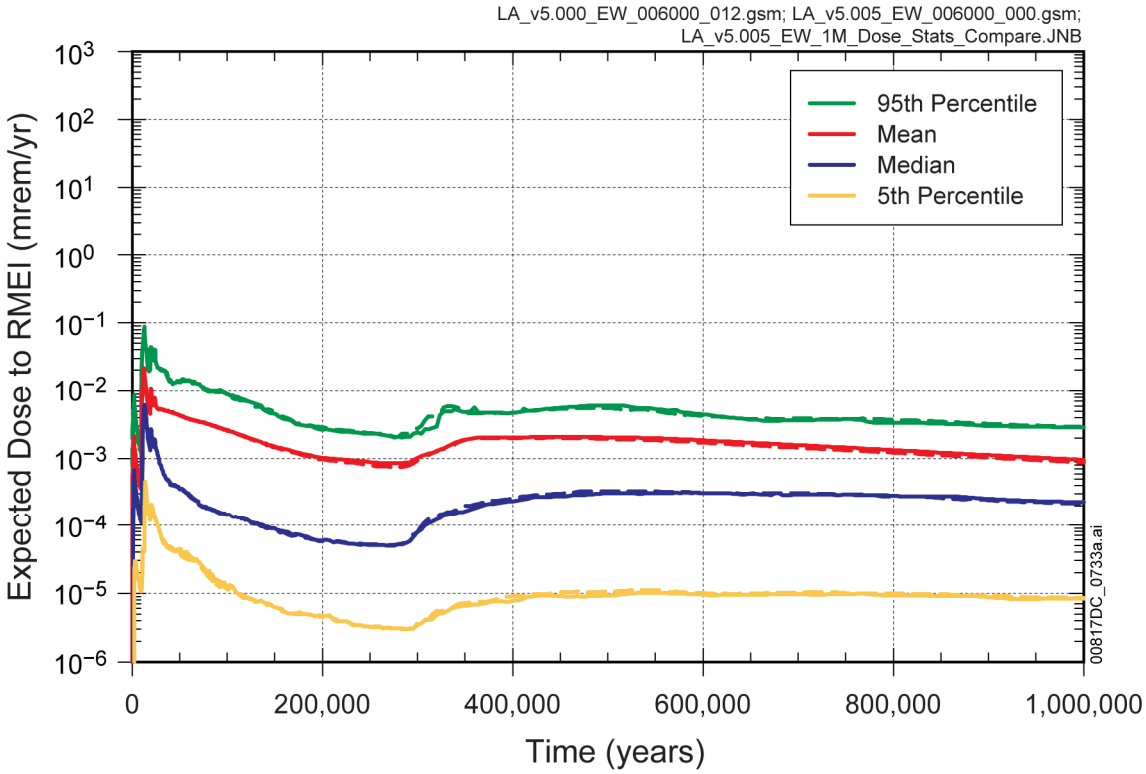

Source: Output DTNs: MO0710ADTSPAWO.000 [DIRS 183752]; and MO0709TSPAREGS.000 [DIRS 182976].

NOTE: Solid lines indicate TSPA-LA Model v5.000 and dashed lines indicate TSPA-LA Model v5.005.

Figure 7.3.1-25[a]. Comparison of Statistics for Expected Annual Dose over 1,000,000 Years in the Waste Package Early Failure Modeling Case between TSPA-LA Model v5.000 and TSPA-LA Model v5.005

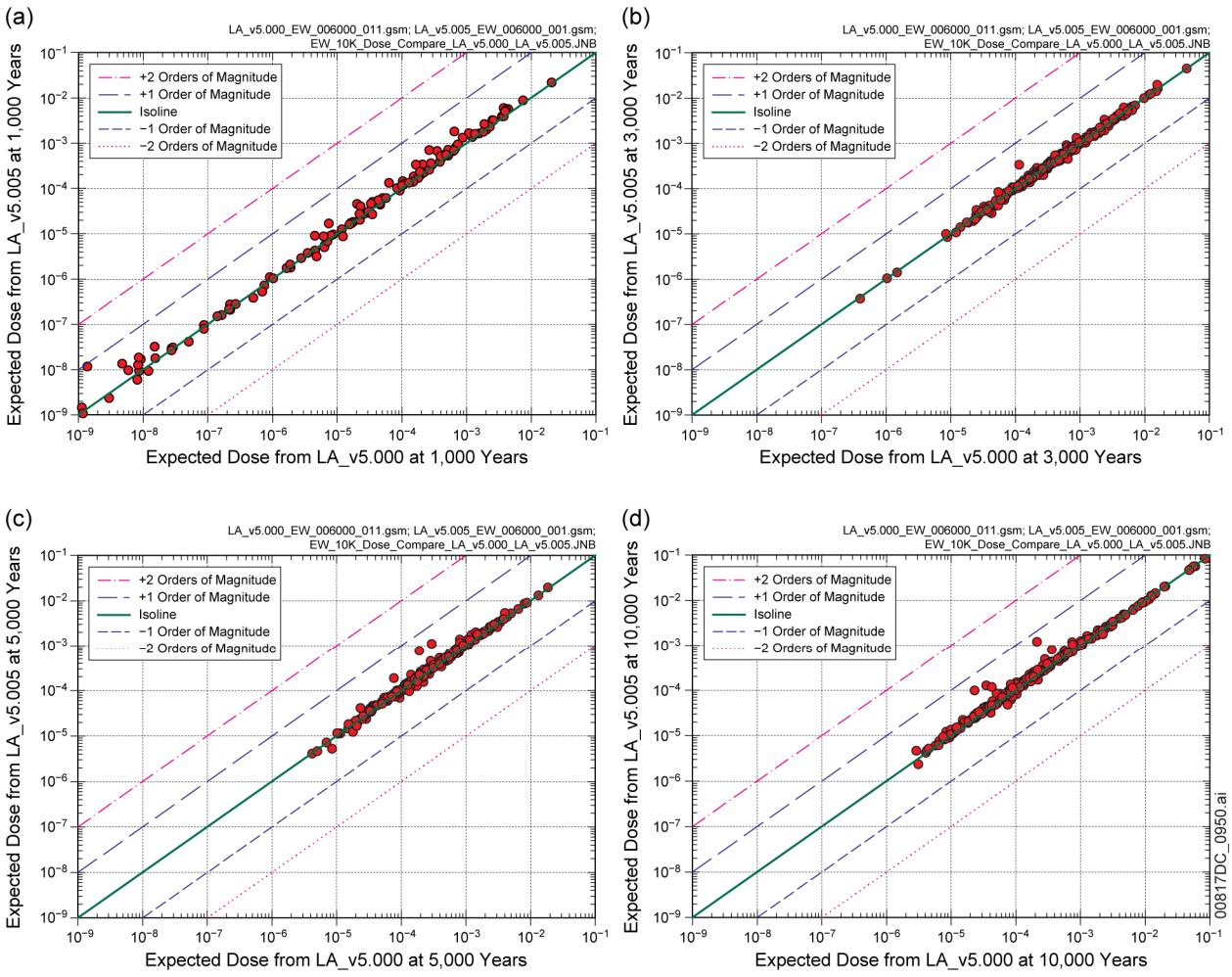

Source: Output DTNs: MO0710ADTSPAWO.000 [DIRS 183752]; and MO0709TSPAREGS.000 [DIRS 182976].

Figure 7.3.1-26[a]. Comparison of Expected Annual Dose for Individual Sample Elements in the Waste Package Early Failure Modeling Case between TSPA-LA Model v5.000 and TSPA-LA Model v5.005 at (a) 1,000; (b) 3,000; (c) 5,000; and (d) 10,000 Years

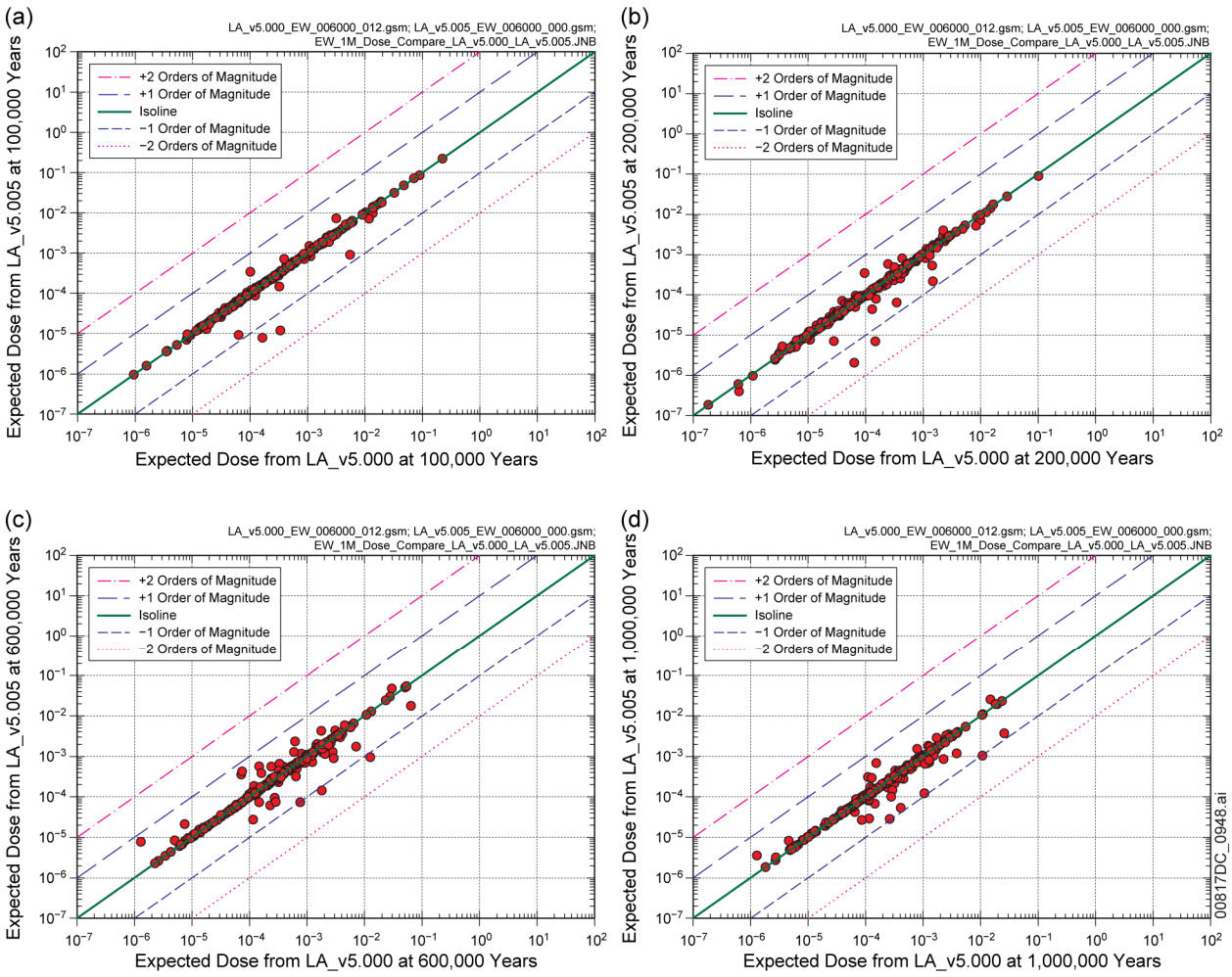

Source: Output DTNs: MO0710ADTSPAWO.000 [DIRS 183752]; and MO0709TSPAREGS.000 [DIRS 182976].

Figure 7.3.1-27[a]. Comparison of Expected Annual Dose for Individual Sample Elements in the Waste Package Early Failure Modeling Case between TSPA-LA Model v5.000 and TSPA-LA Model v5.005 at (a) 100,000; (b) 200,000; (c) 600,000; and (d) 1,000,000 Years

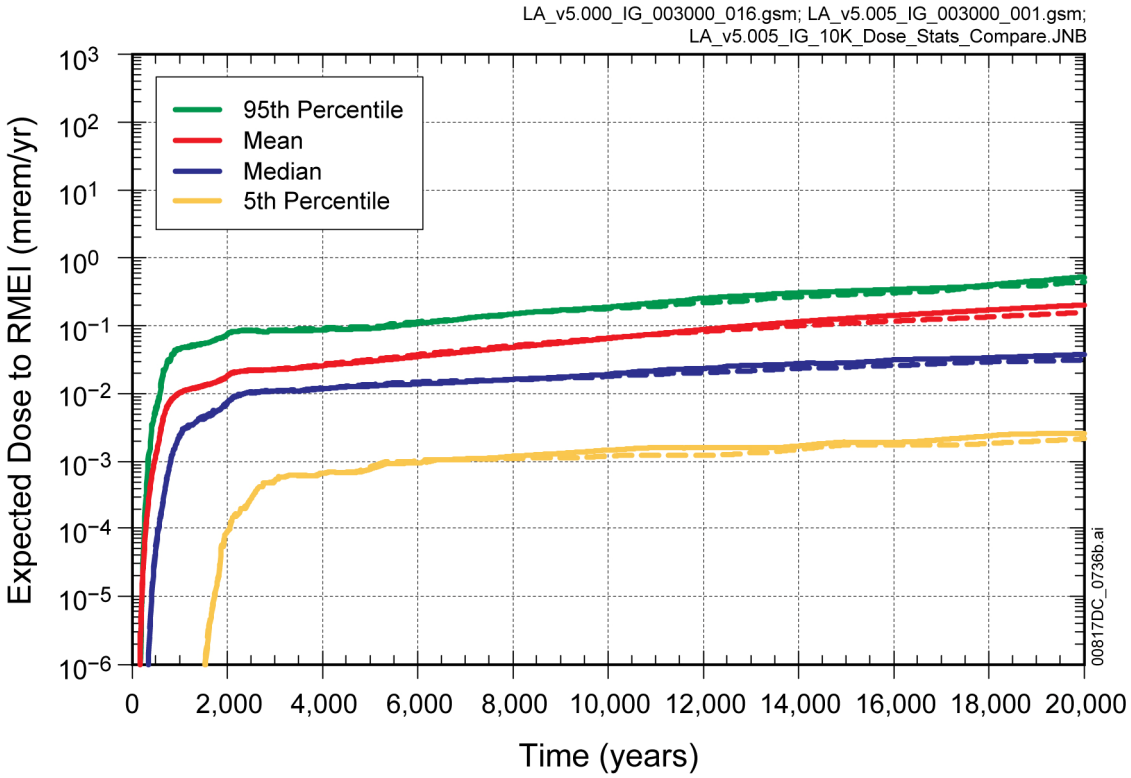

Source: Output DTNs: MO0710ADTSPAWO.000 [DIRS 183752]; and MO0709TSPAREGS.000 [DIRS 182976].

NOTE: Solid lines indicate TSPA-LA Model v5.000 and dashed lines indicate TSPA-LA Model v5.005.

Figure 7.3.1-28[a]. Comparison of Statistics for Expected Annual Dose over 20,000 Years in the Igneous Intrusion Modeling Case between TSPA-LA Model v5.000 and TSPA-LA Model v5.005

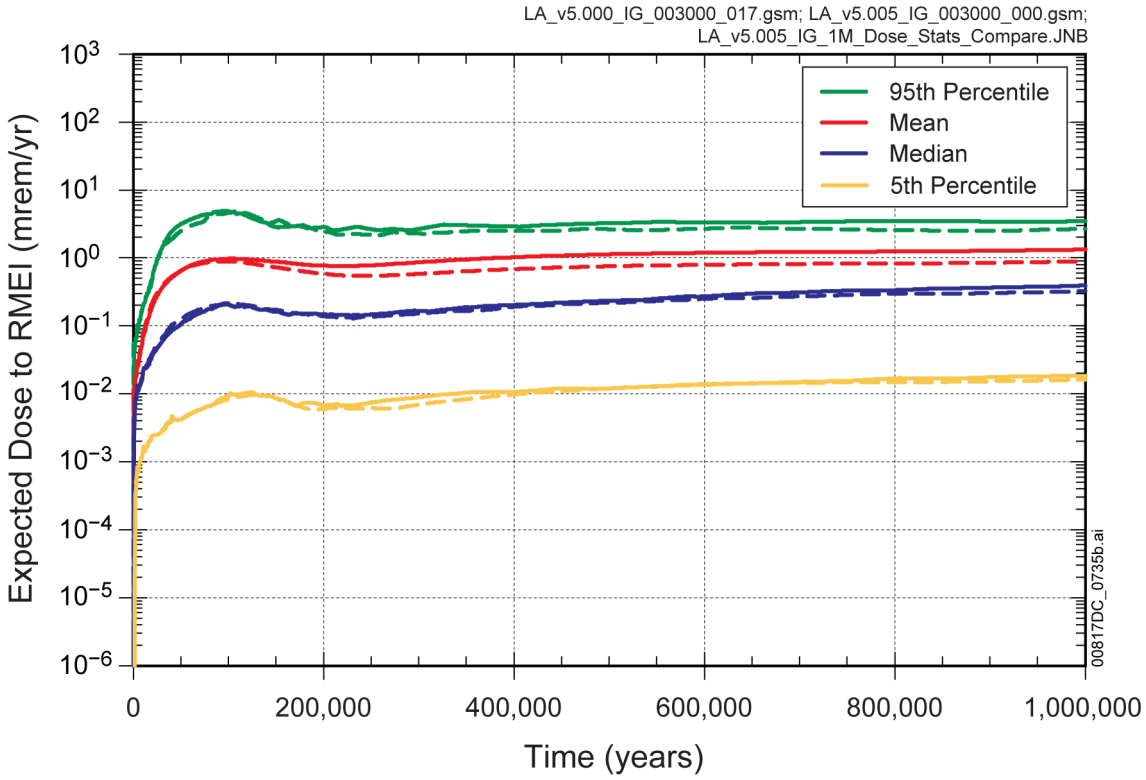

Source: Output DTNs: MO0710ADTSPAWO.000 [DIRS 183752]; and MO0709TSPAREGS.000 [DIRS 182976].

NOTE: Solid lines indicate TSPA-LA Model v5.000 and dashed lines indicate TSPA-LA Model v5.005.

Figure 7.3.1-29[a]. Comparison of Statistics for Expected Annual Dose over 1,000,000 Years in the Igneous Intrusion Modeling Case between TSPA-LA Model v5.000 and TSPA-LA Model v5.005

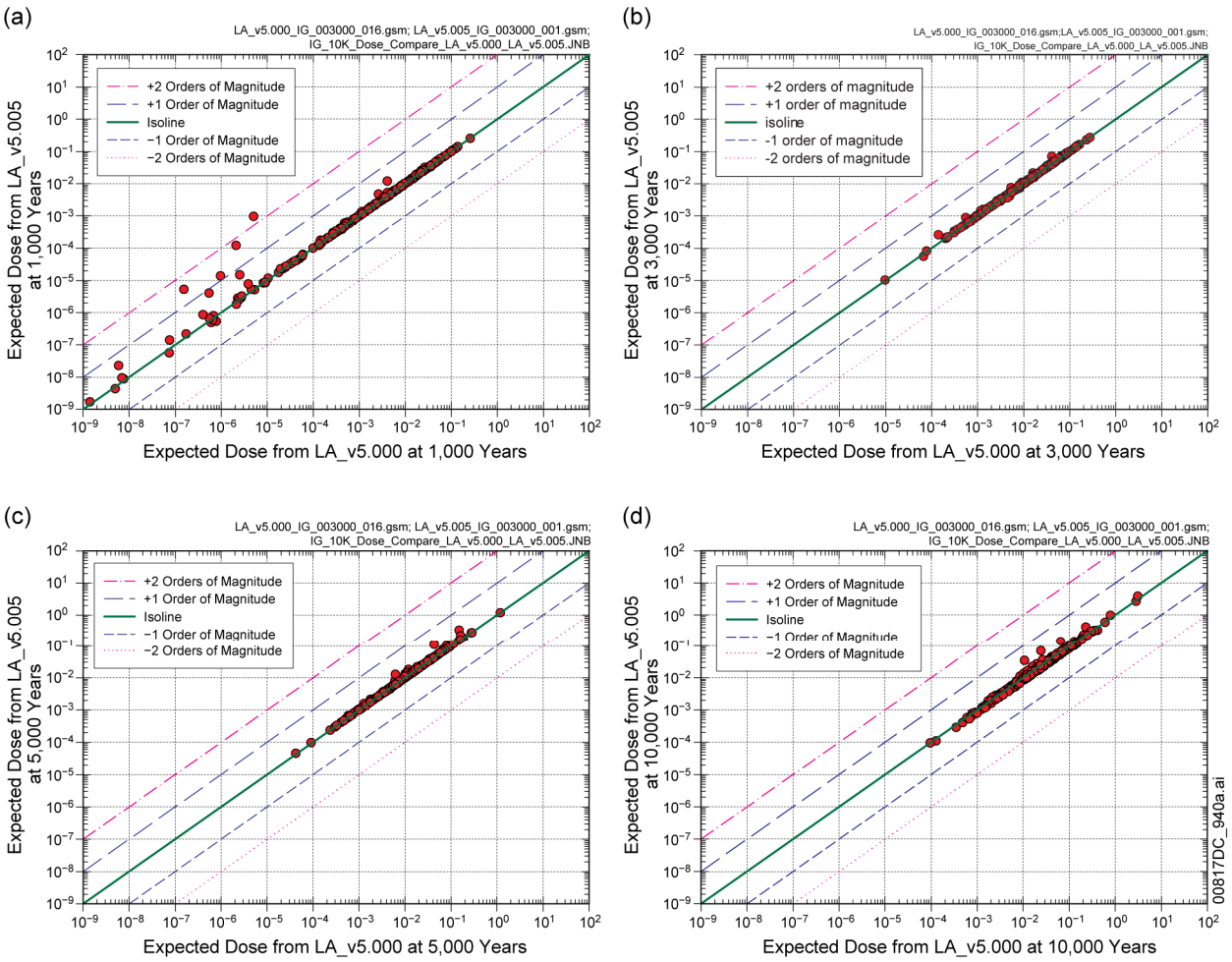

Source: Output DTNs: MO0710ADTSPAWO.000 [DIRS 183752]; and MO0709TSPAREGS.000 [DIRS 182976].

Figure 7.3.1-30[a]. Comparison of Expected Annual Dose for Individual Sample Elements in the Igneous Intrusion Modeling Case between TSPA-LA Model v5.000 and TSPA-LA Model v5.005 at (a) 1,000; (b) 3,000; (c) 5,000; and (d) 10,000 Years

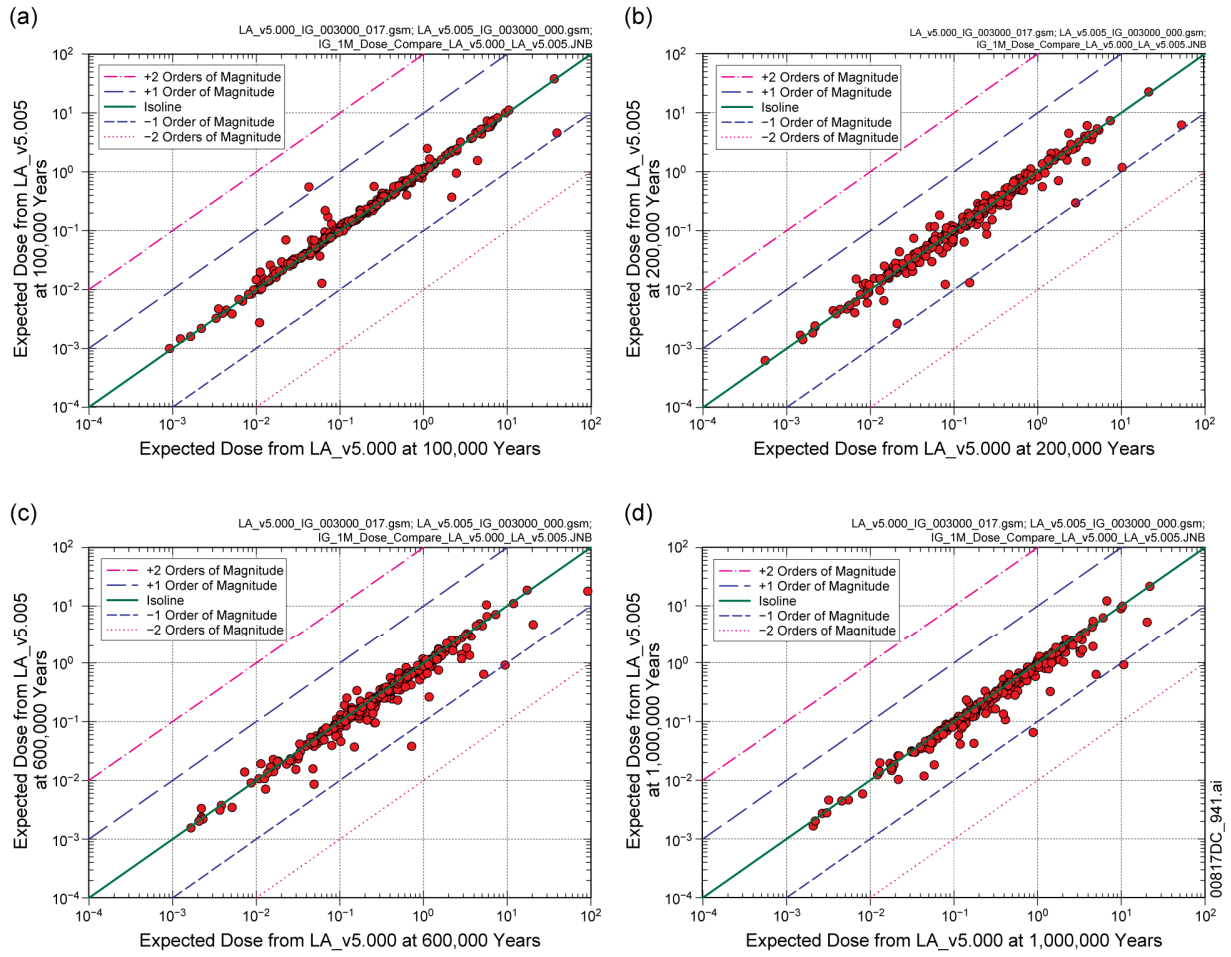

Source: Output DTNs: MO0710ADTSPAWO.000 [DIRS 183752]; and MO0709TSPAREGS.000 [DIRS 182976].

Figure 7.3.1-31[a]. Comparison of Expected Annual Dose for Individual Sample Elements in the Igneous Intrusion Modeling Case between TSPA-LA Model v5.000 and TSPA-LA Model v5.005 at (a) 100,000; (b) 200,000; (c) 600,000; and (d) 1,000,000 Years

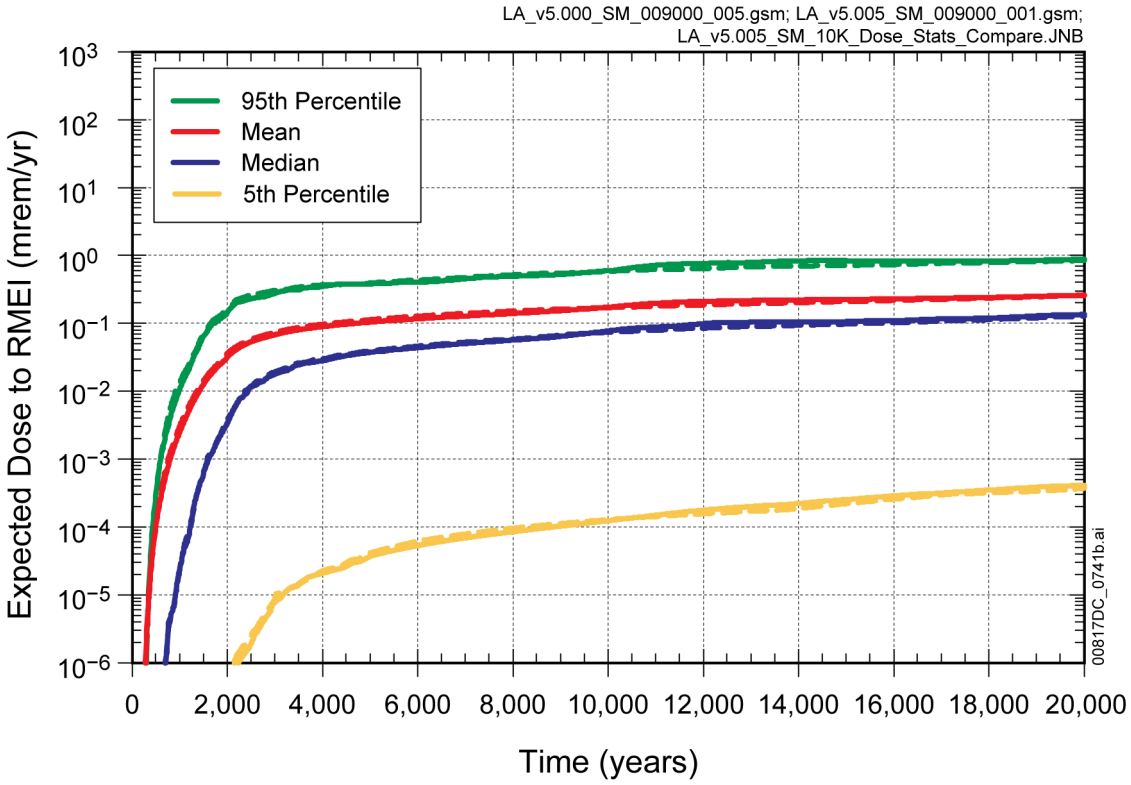

Source: Output DTNs: MO0710ADTSPAWO.000 [DIRS 183752]; and MO0709TSPAREGS.000 [DIRS 182976].

NOTE: Solid lines indicate TSPA-LA Model v5.000 and dashed lines indicate TSPA-LA Model v5.005.

Figure 7.3.1-32[a]. Comparison of Statistics for Expected Annual Dose over 20,000 Years in the Seismic Ground Motion Modeling Case between TSPA-LA Model v5.000 and TSPA-LA Model v5.005

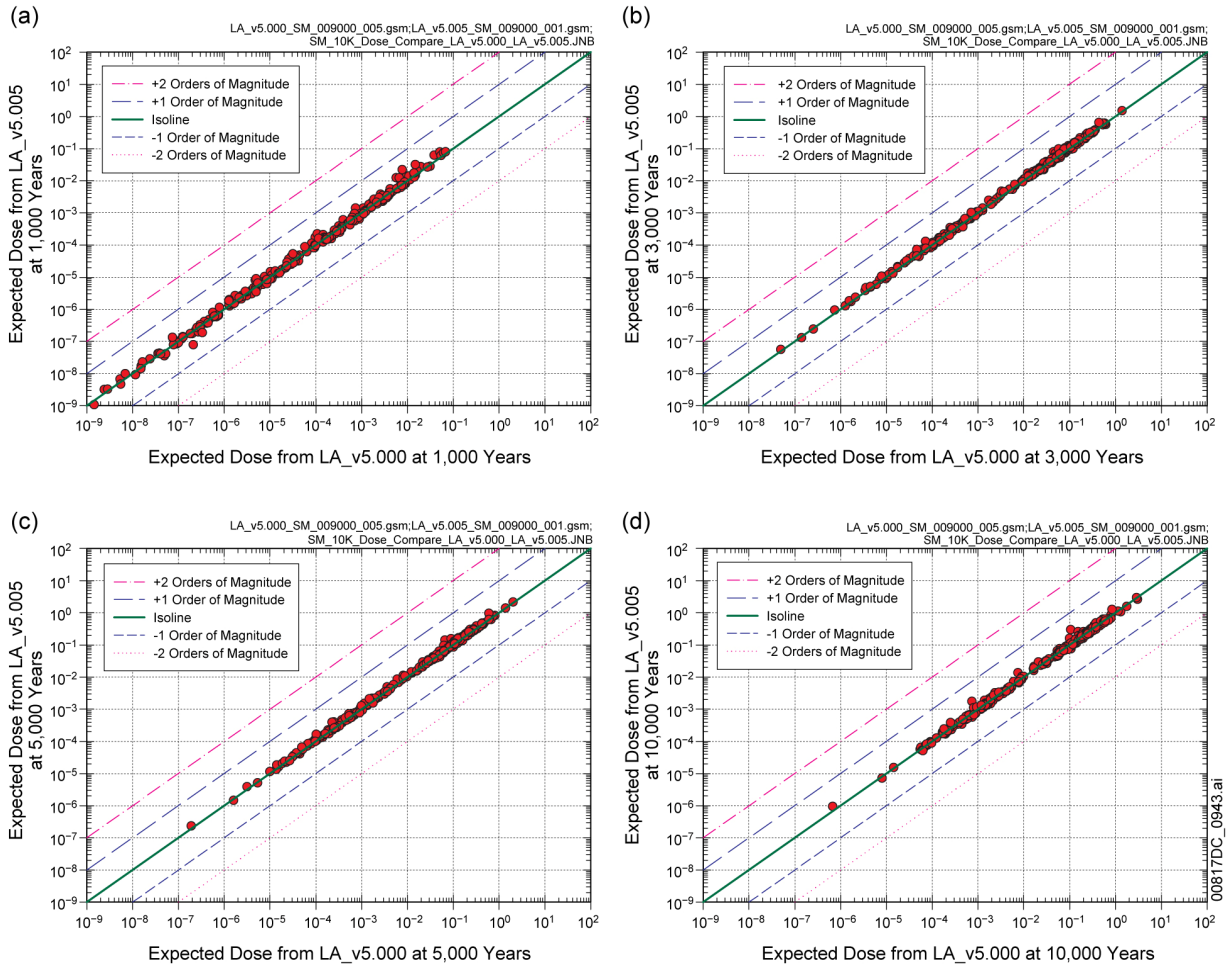

Source: Output DTNs: MO0710ADTSPAWO.000 [DIRS 183752]; and MO0709TSPAREGS.000 [DIRS 182976].

Figure 7.3.1-33[a]. Comparison of Expected Annual Dose for Individual Sample Elements in the Seismic Ground Motion Modeling Case between TSPA-LA Model v5.000 and TSPA-LA Model v5.005 at (a) 1,000; (b) 3,000; (c) 5,000; and (d) 10,000 Years

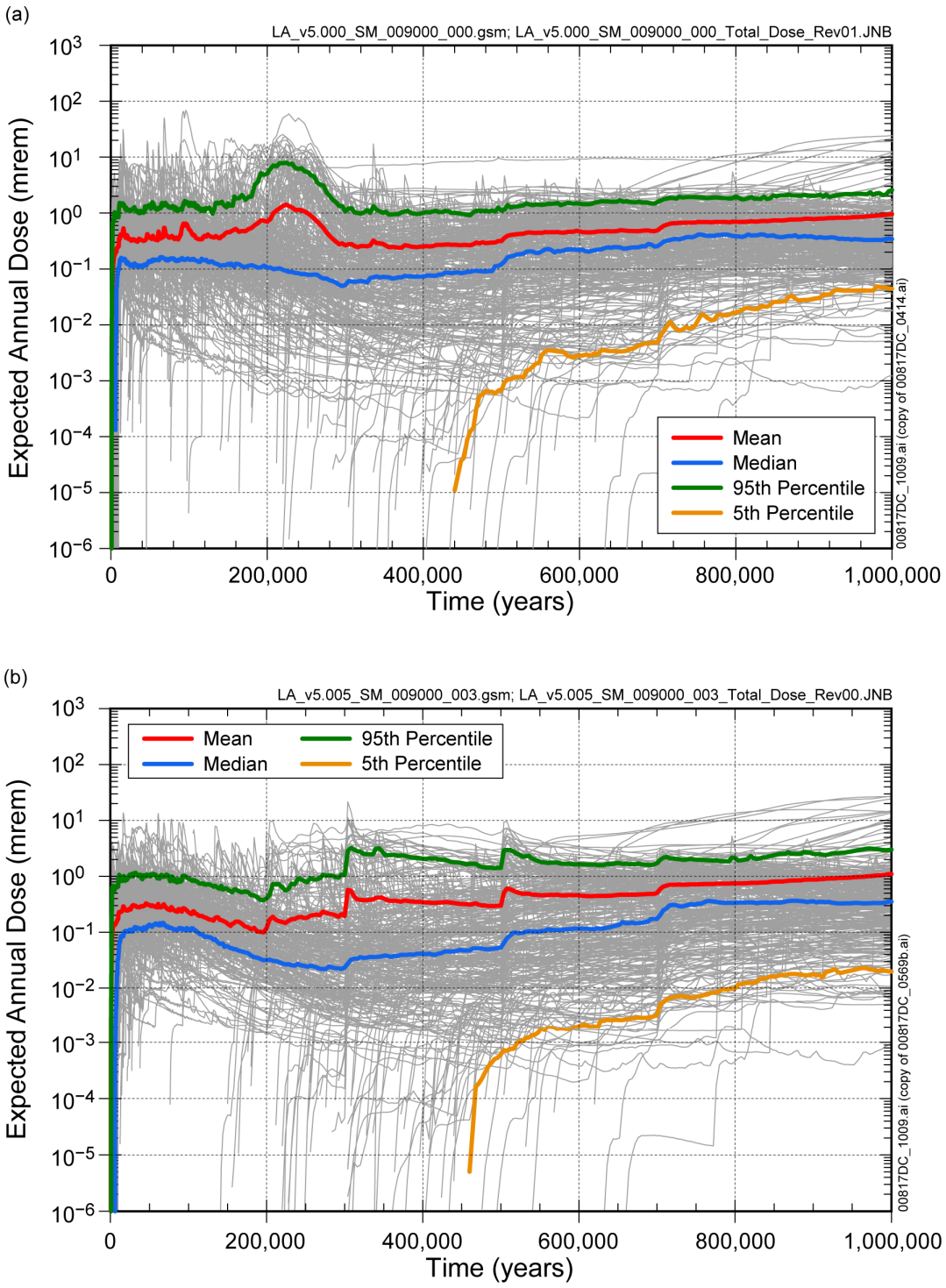

Source: Output DTNs: MO0709TSPAREGS.000 [DIRS 182976]; and MO0710ADTSPAWO.000 [DIRS 183752].

Figure 7.3.1-34[a]. Expected Annual Dose for 1,000,000 Years for the Seismic Ground Motion Modeling Case from (a) TSPA-LA Model v5.000 and (b) TSPA-LA Model v5.005

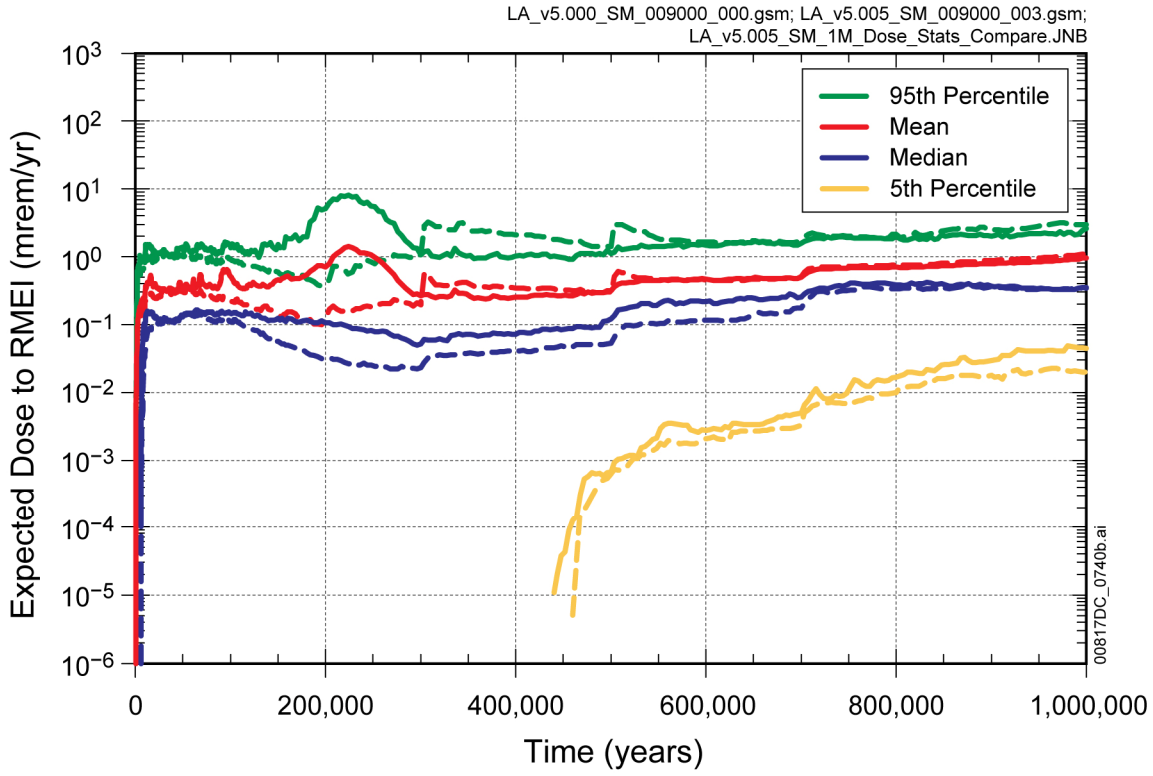

Source: Output DTNs: MO0710ADTSPAWO.000 [DIRS 183752]; and MO0709TSPAREGS.000 [DIRS 182976].

NOTE: Solid lines indicate TSPA-LA Model v5.000 and dashed lines indicate TSPA-LA Model v5.005.

Figure 7.3.1-35[a]. Comparison of Statistics for Expected Annual Dose over 1,000,000 Years in the Seismic Ground Motion Modeling Case between TSPA-LA Model v5.000 and TSPA-LA Model v5.005

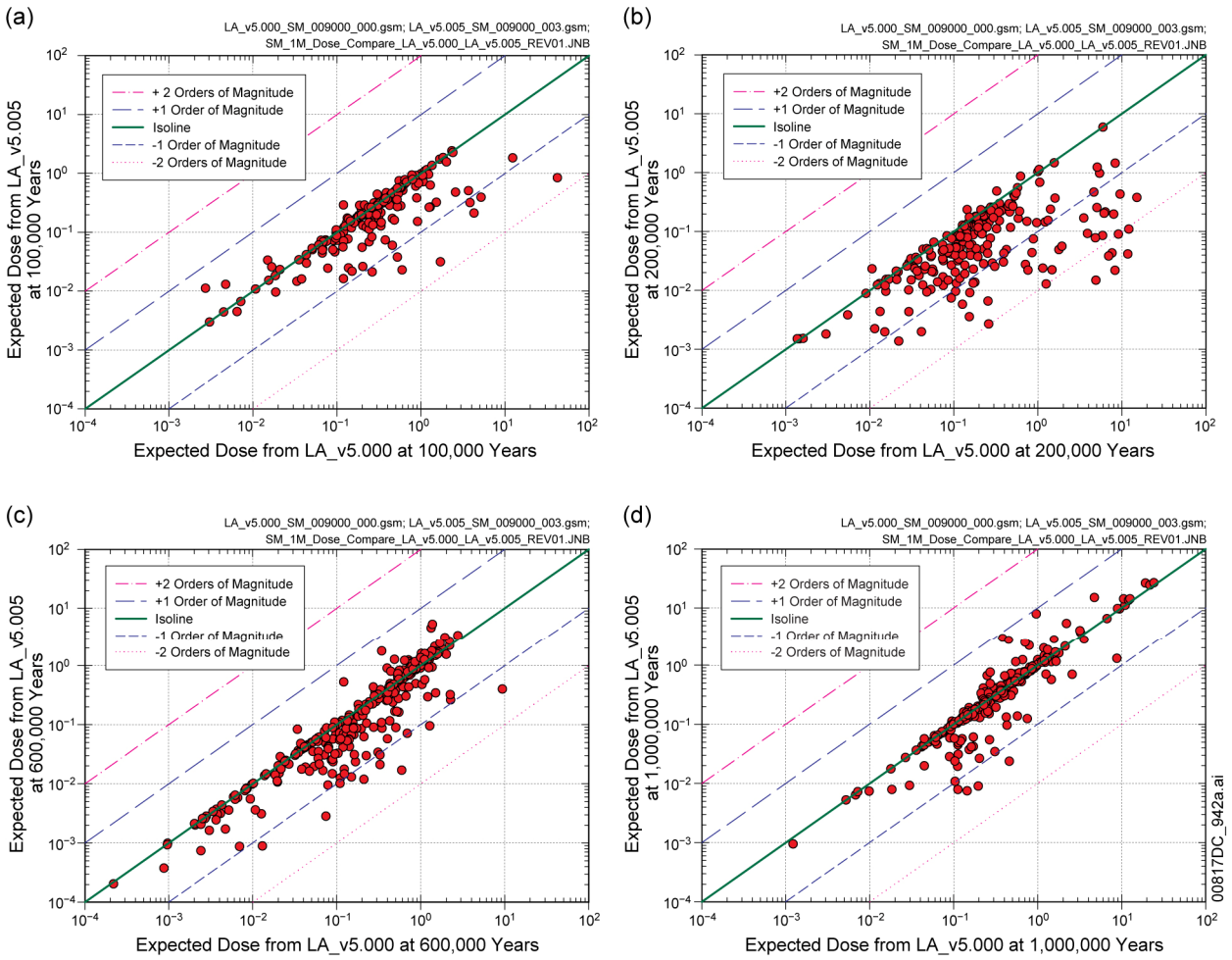

Source: Output DTNs: MO0710ADTSPAWO.000 [DIRS 183752]; and MO0709TSPAREGS.000 [DIRS 182976].

Figure 7.3.1-36[a]. Comparison of Expected Annual Dose for Individual Sample Elements in the Seismic Ground Motion Modeling Case between TSPA-LA Model v5.000 and TSPA-LA Model v5.005 at (a) 100,000; (b) 200,000; (c) 600,000; and (d) 1,000,000 Years

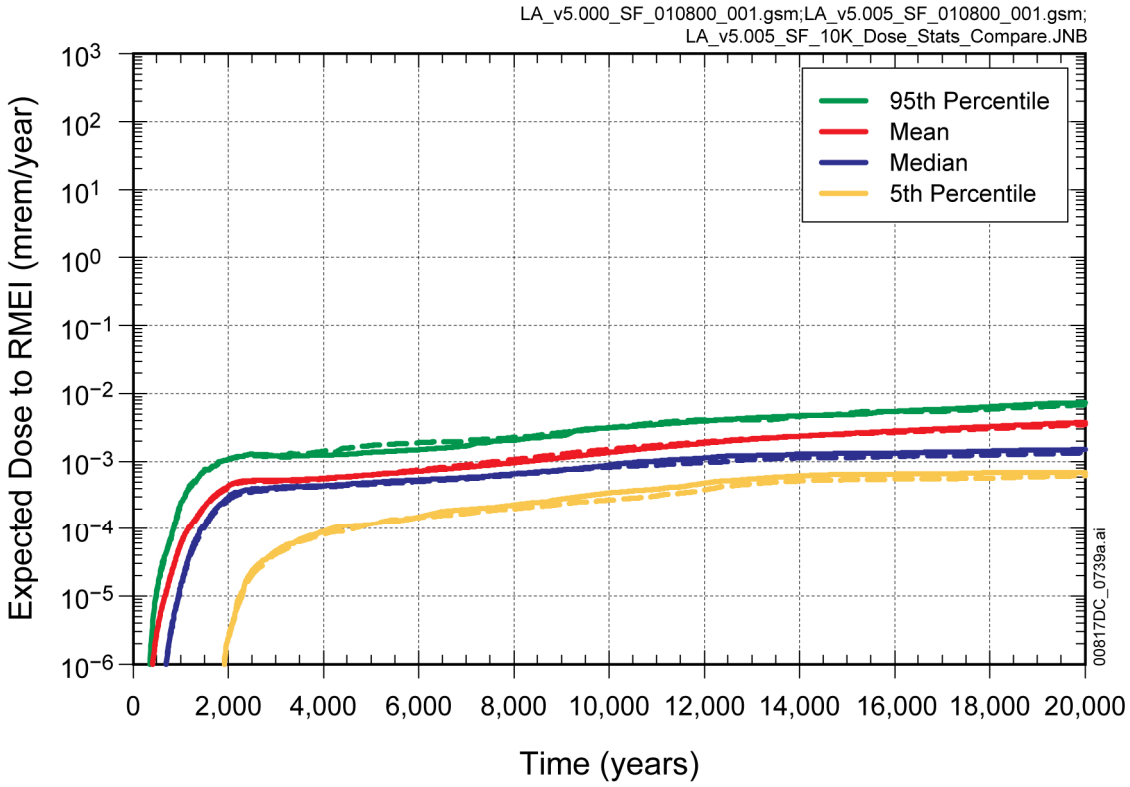

Source: Output DTNs: MO0710ADTSPAWO.000 [DIRS 183752]; and MO0709TSPAREGS.000 [DIRS 182976].

NOTE: Solid lines indicate TSPA-LA Model v5.000 and dashed lines indicate TSPA-LA Model v5.005.

Figure 7.3.1-37[a]. Comparison of Statistics for Expected Annual Dose over 20,000 Years in the Seismic Fault Displacement Modeling Case between TSPA-LA Model v5.000 and TSPA-LA Model v5.005

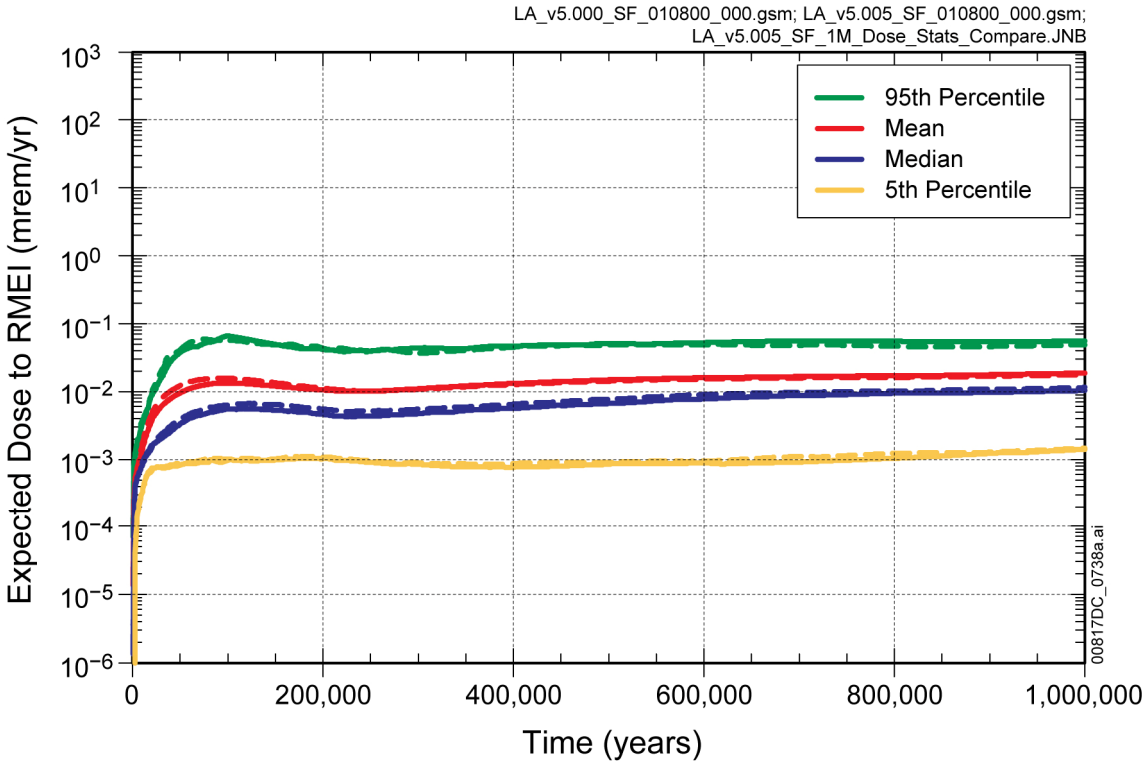

Source: Output DTNs: MO0710ADTSPAWO.000 [DIRS 183752]; and MO0709TSPAREGS.000 [DIRS 182976].

NOTE: Solid lines indicate TSPA-LA Model v5.000 and dashed lines indicate TSPA-LA Model v5.005.

Figure 7.3.1-38[a]. Comparison of Statistics for Expected Annual Dose over 1,000,000 Years in the Seismic Fault Displacement Modeling Case between TSPA-LA Model v5.000 and TSPA-LA Model v5.005

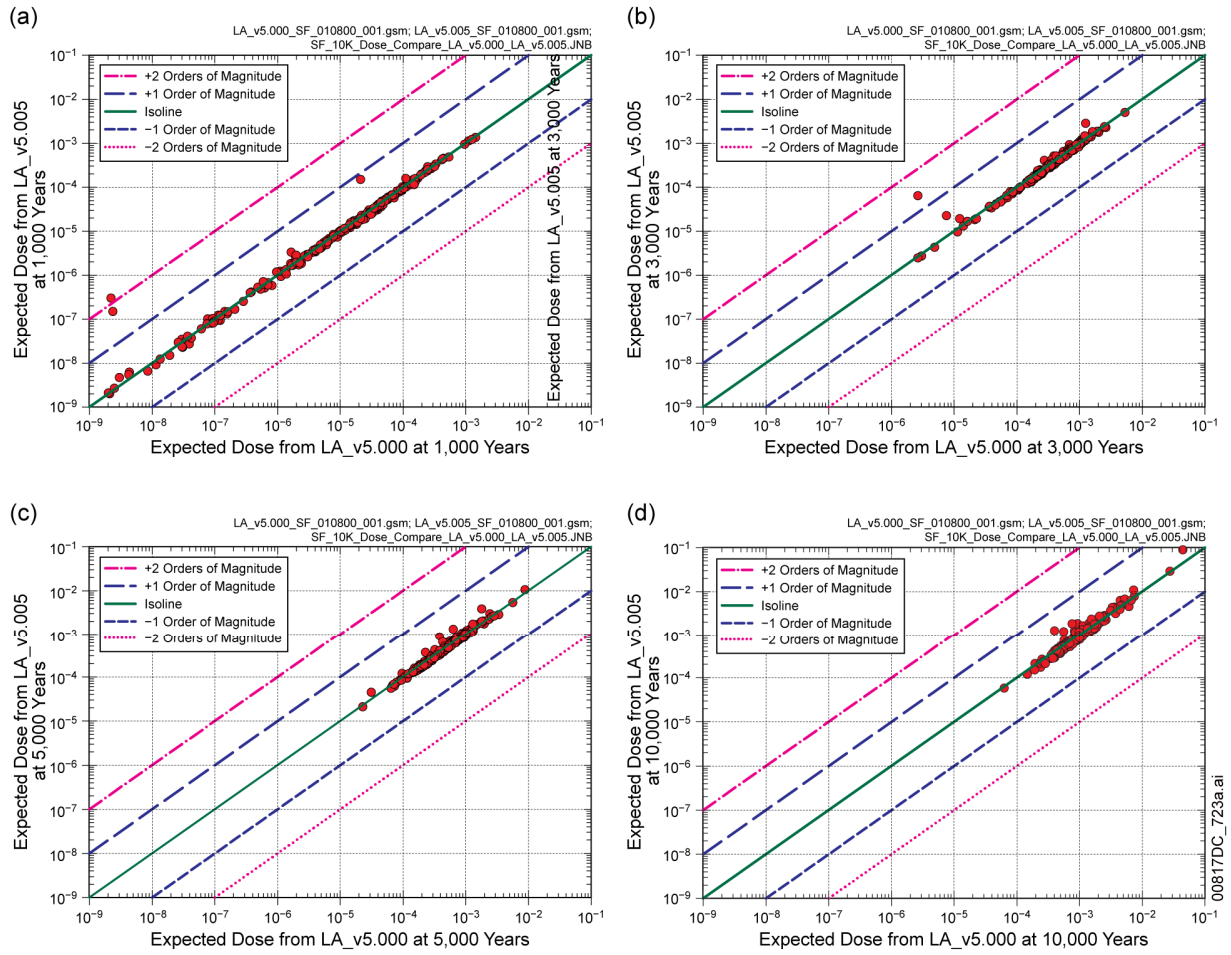

Source: Output DTNs: MO0710ADTSPAWO.000 [DIRS 183752]; and MO0709TSPAREGS.000 [DIRS 182976].

Figure 7.3.1-39[a]. Comparison of Expected Annual Dose for Individual Sample Elements in the Seismic Fault Displacement Modeling Case between TSPA-LA Model v5.000 and TSPA-LA Model v5.005 at (a) 1,000; (b) 3,000; (c) 5,000; and (d) 10,000 Years

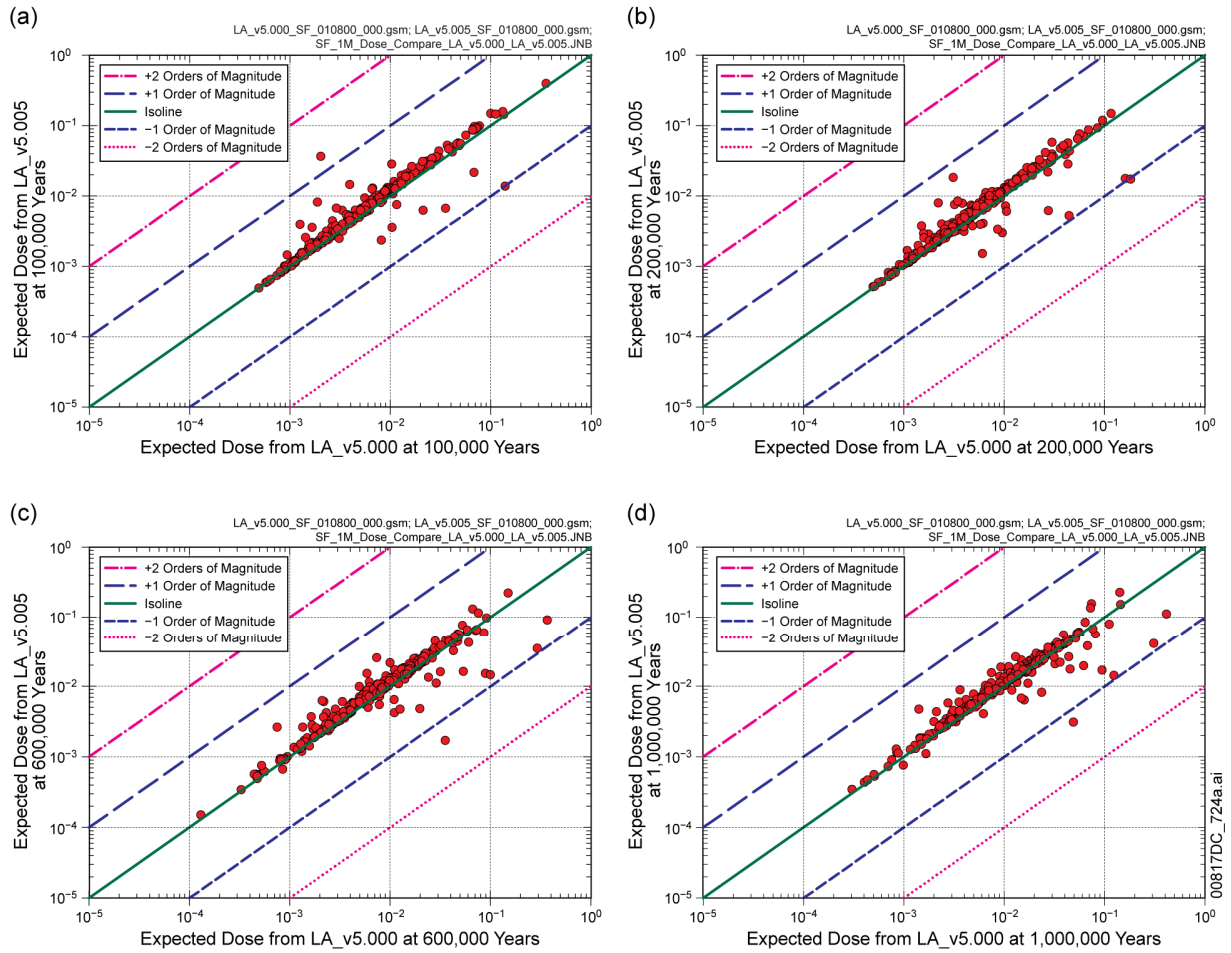

Source: Output DTNs: MO0710ADTSPAWO.000 [DIRS 183752]; and MO0709TSPAREGS.000 [DIRS 182976].

Figure 7.3.1-40[a]. Comparison of Expected Annual Dose for Individual Sample Elements in the Seismic Fault Displacement Modeling Case between TSPA-LA Model v5.000 and TSPA-LA Model v5.005 at (a) 100,000; (b) 200,000; (c) 600,000; and (d) 1,000,000 Years

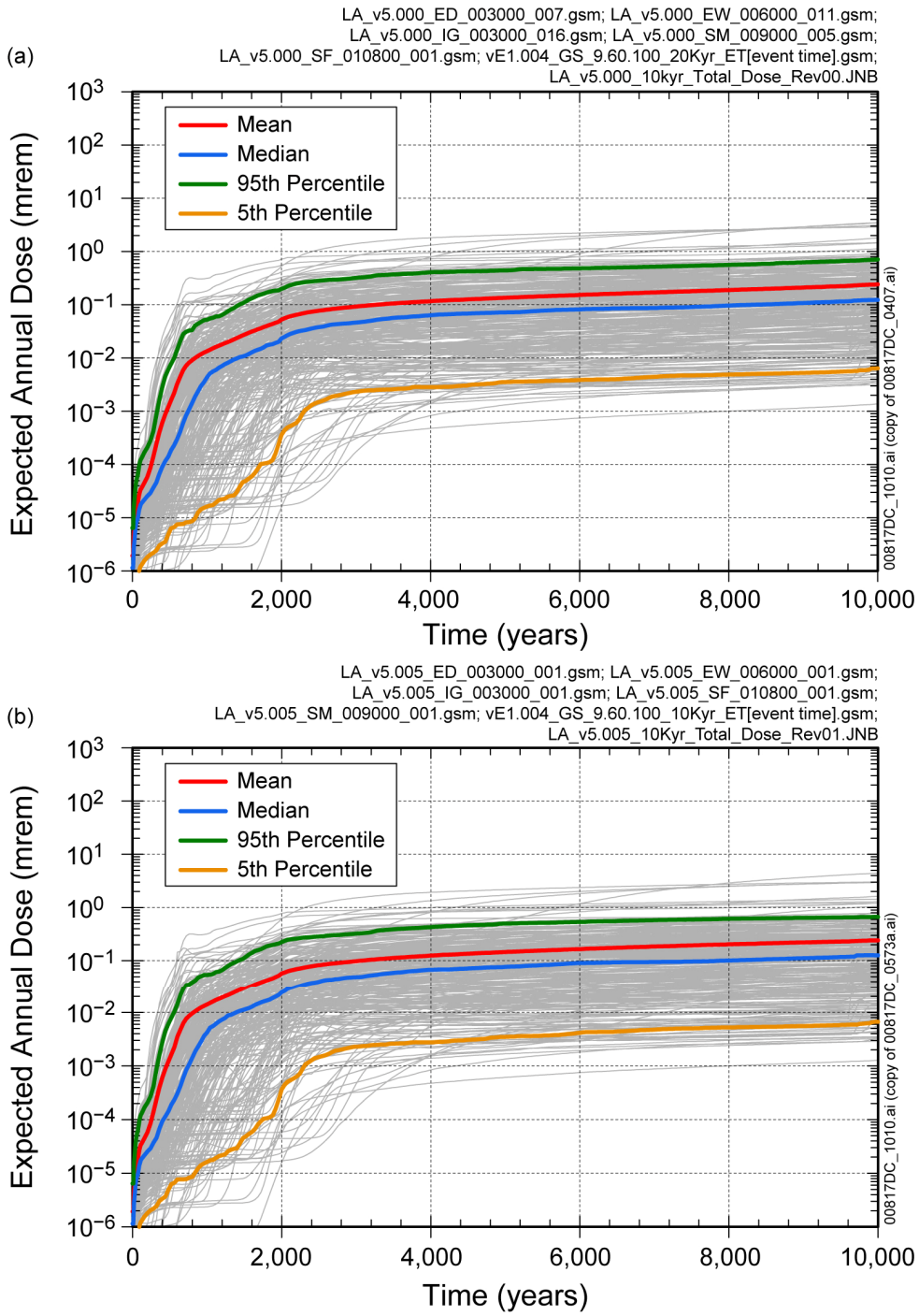

Source: Output DTNs: MO0709TSPAREGS.000 [DIRS 182976]; and MO0710ADTSPAWO.000 [DIRS 183752].

Figure 7.3.1-41[a]. Total Expected Annual Dose for 10,000 Years from (a) TSPA-LA Model v5.000 and (b) TSPA-LA Model v5.005

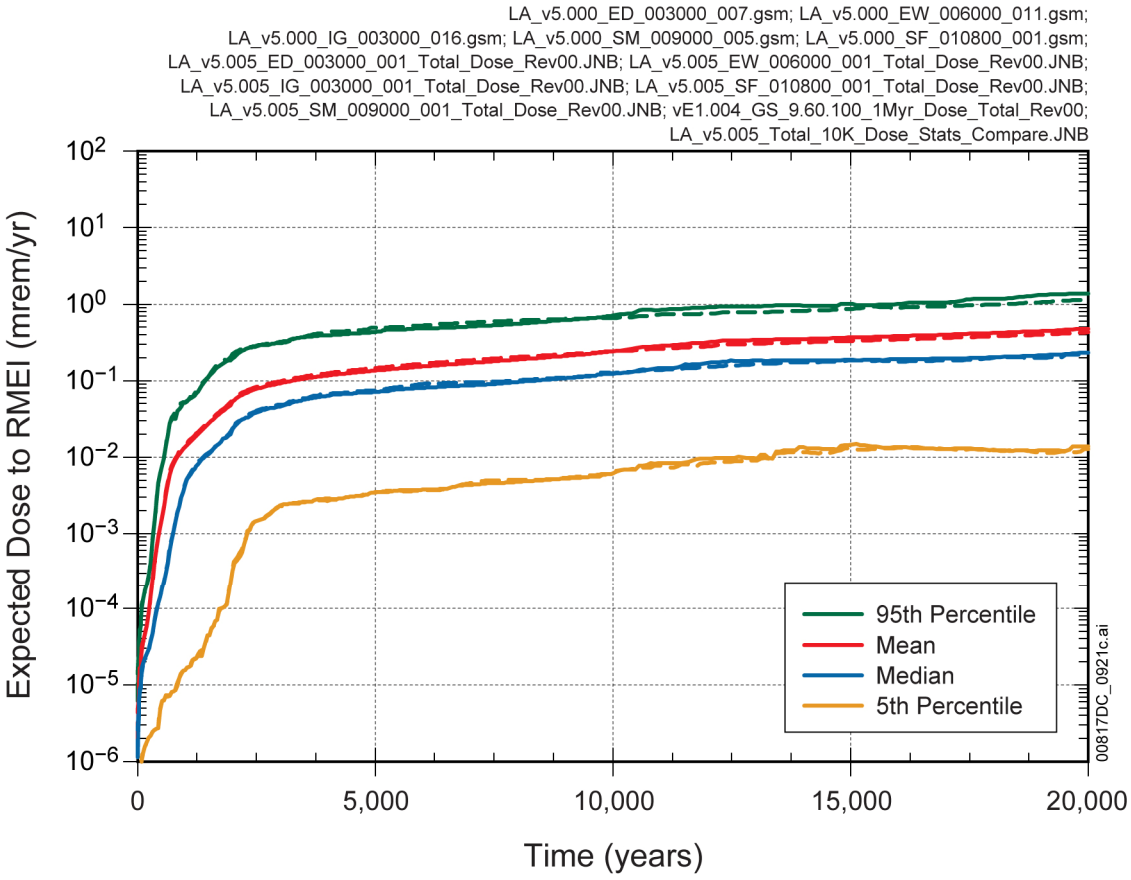

Source: Output DTNs: MO0710ADTSPAWO.000 [DIRS 183752]; and MO0709TSPAREGS.000 [DIRS 182976].

NOTE: Solid lines indicate TSPA-LA Model v5.000 and dashed lines indicate TSPA-LA Model v5.005.

Figure 7.3.1-42[a]. Comparison of Statistics for Total Expected Annual Dose over 20,000 Years between TSPA-LA Model v5.000 and TSPA-LA Model v5.005

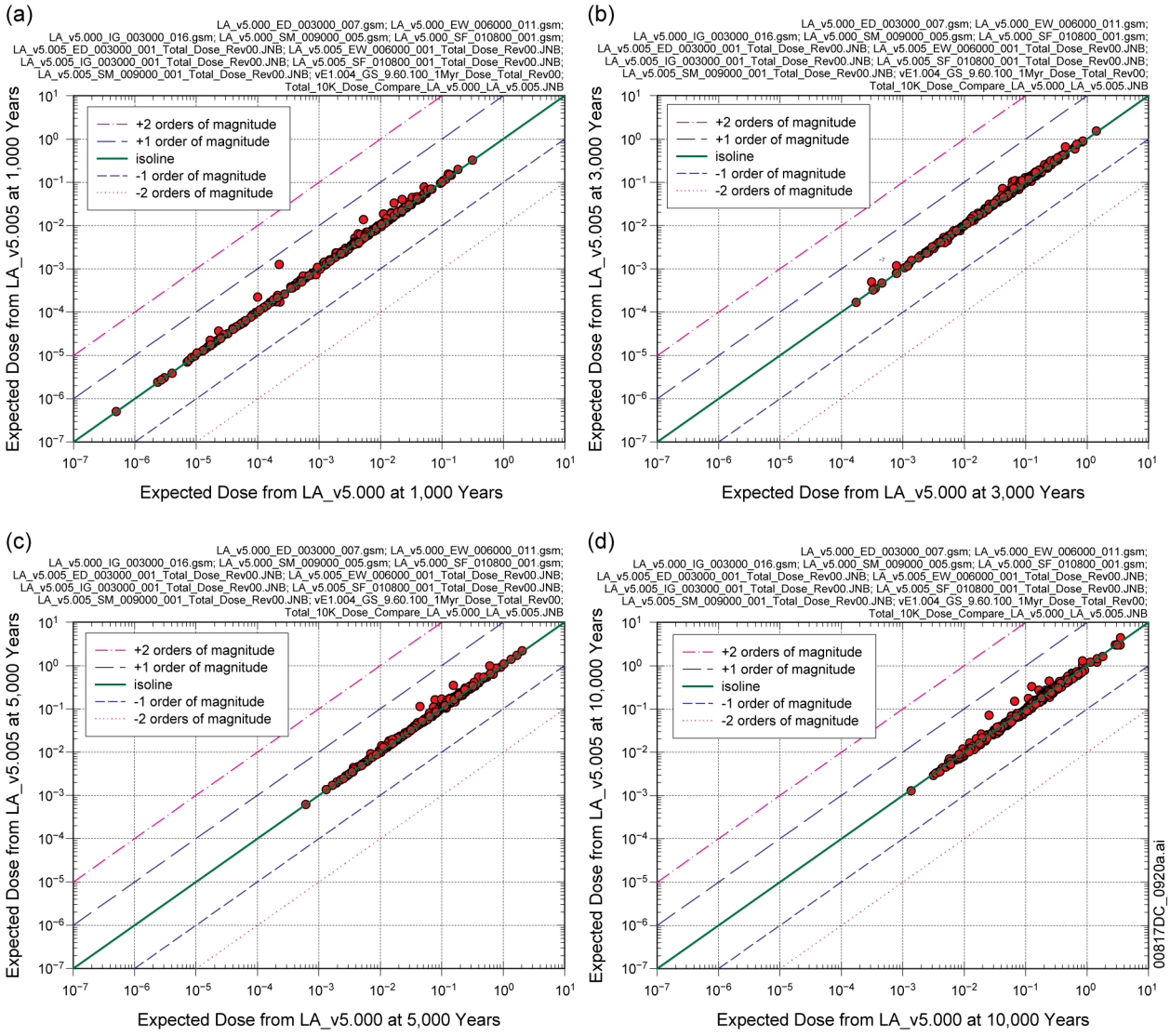

Source: Output DTNs: MO0710ADTSPAWO.000 [DIRS 183752]; and MO0709TSPAREGS.000 [DIRS 182976].

Figure 7.3.1-43[a]. Comparison of Total Expected Annual Dose for Individual Sample Elements between TSPA-LA Model v5.000 and TSPA-LA Model v5.005 at (a) 1,000; (b) 3,000; (c) 5,000; and (d) 10,000 Years

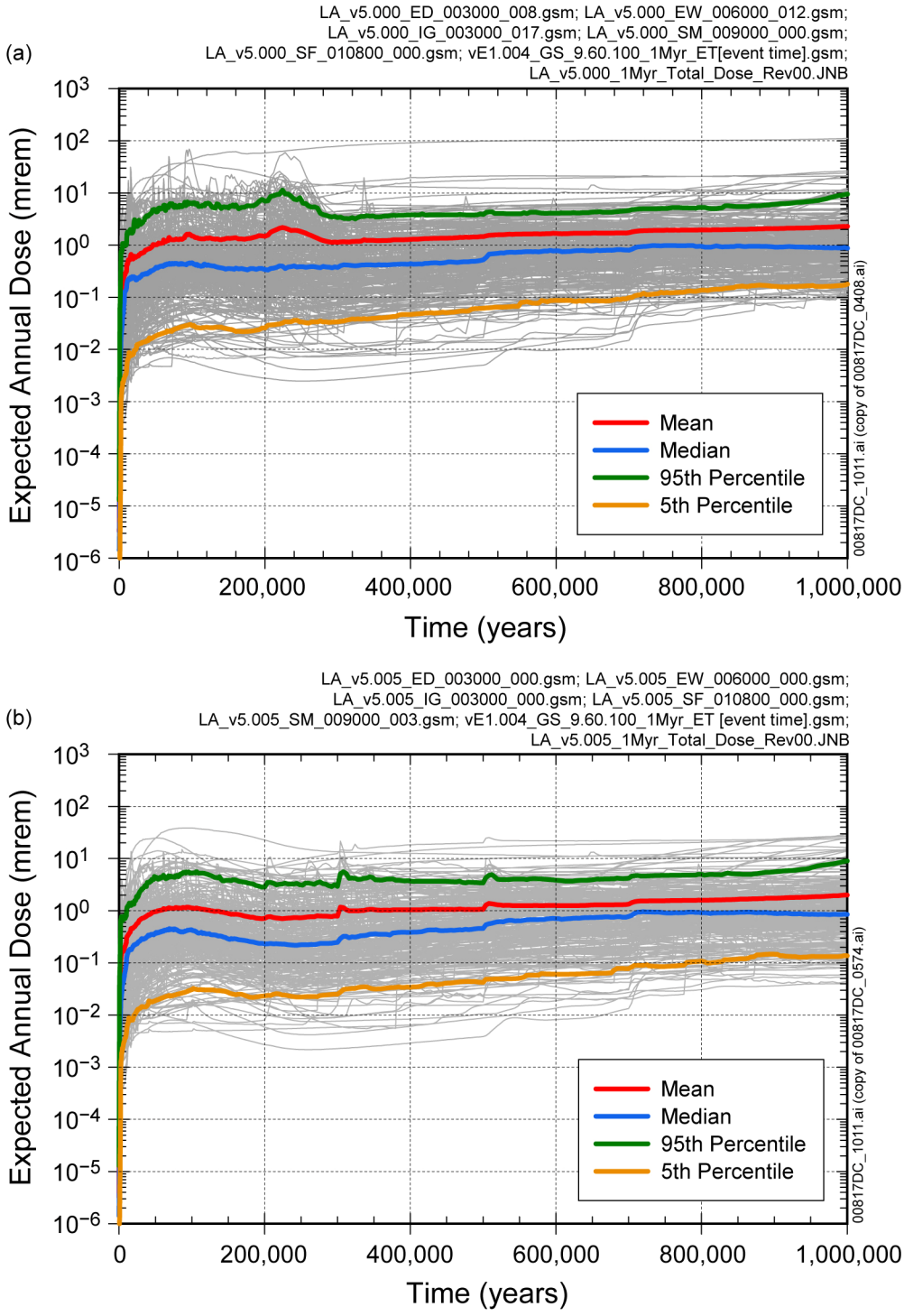

Source: Output DTNs: MO0709TSPAREGS.000 [DIRS 182976]; and MO0710ADTSPAWO.000 [DIRS 183752].

Figure 7.3.1-44[a]. Total Expected Annual Dose for 1,000,000 Years from (a) TSPA-LA Model v5.000 and (b) TSPA-LA Model v5.005

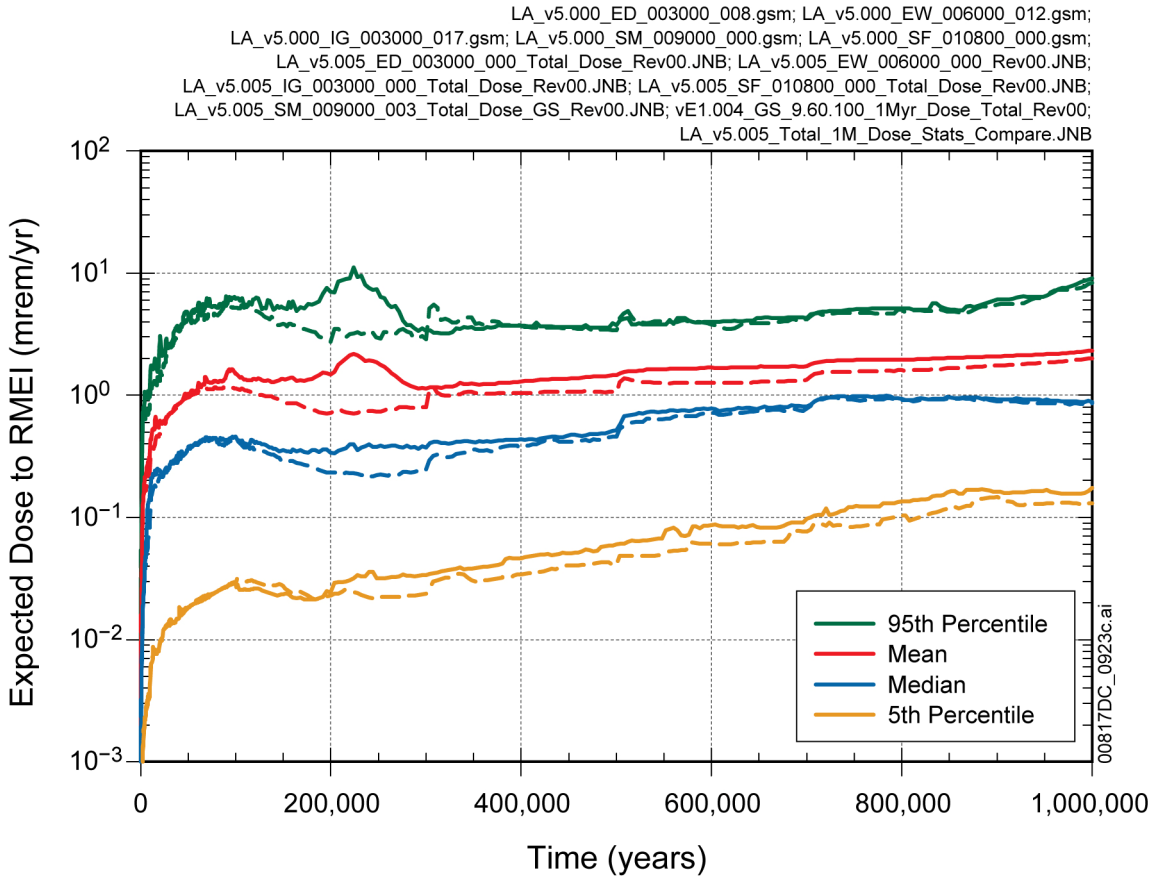

Source: Output DTNs: MO0710ADTSPAWO.000 [DIRS 183752]; and MO0709TSPAREGS.000 [DIRS 182976].

NOTE: Solid lines indicate TSPA-LA Model v5.000 and dashed lines indicate TSPA-LA Model v5.005.

Figure 7.3.1-45[a]. Comparison of Statistics for Total Expected Annual Dose over 1,000,000 Years between TSPA-LA Model v5.000 and TSPA-LA Model v5.005

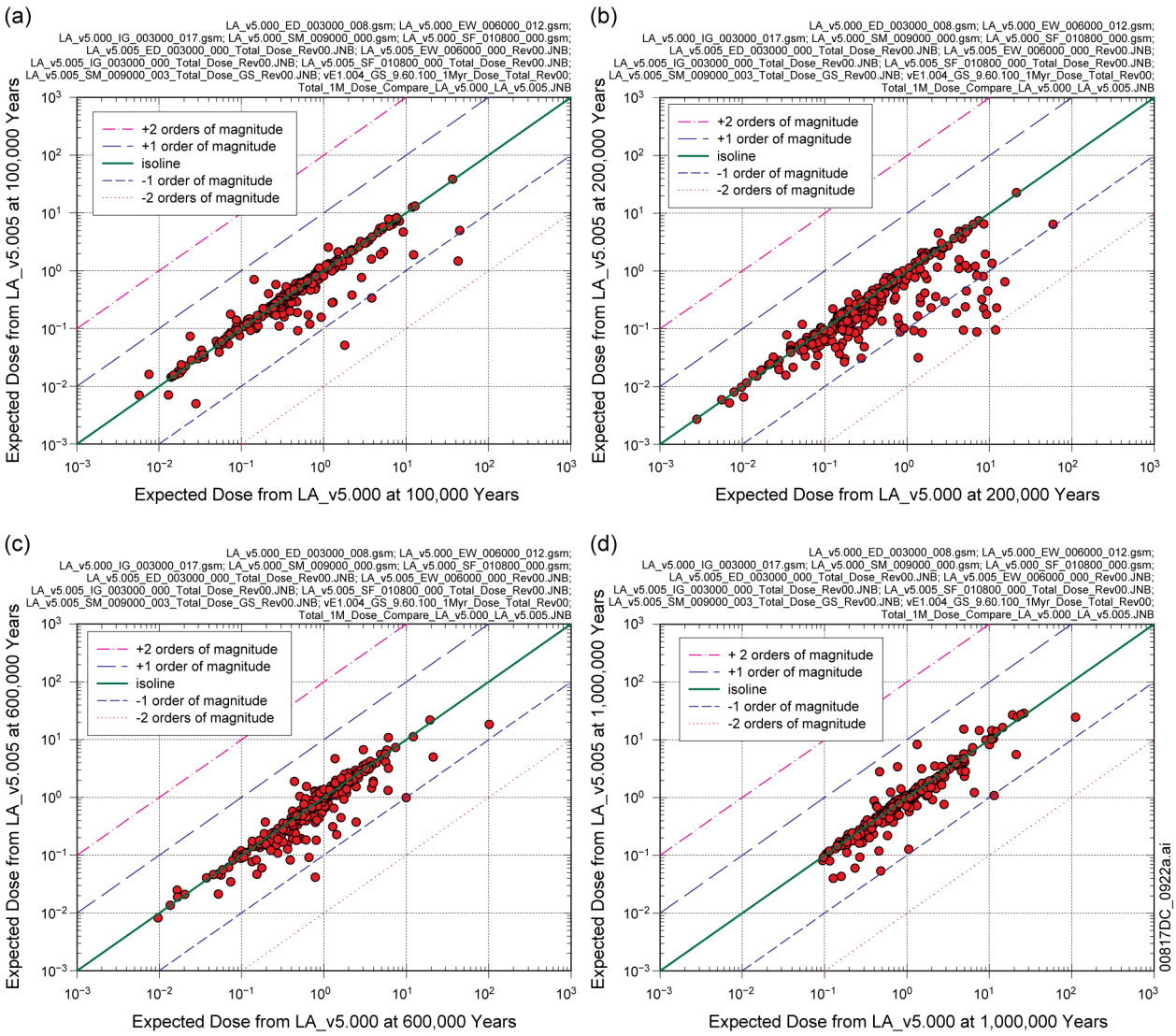

Source: Output DTNs: MO0710ADTSPAWO.000 [DIRS 183752]; and MO0709TSPAREGS.000 [DIRS 182976].

Figure 7.3.1-46[a]. Comparison of Total Expected Annual Dose for Individual Sample Elements between TSPA-LA Model v5.000 and TSPA-LA Model v5.005 at (a) 100,000; (b) 200,000; (c) 600,000; and (d) 1,000,000 Years

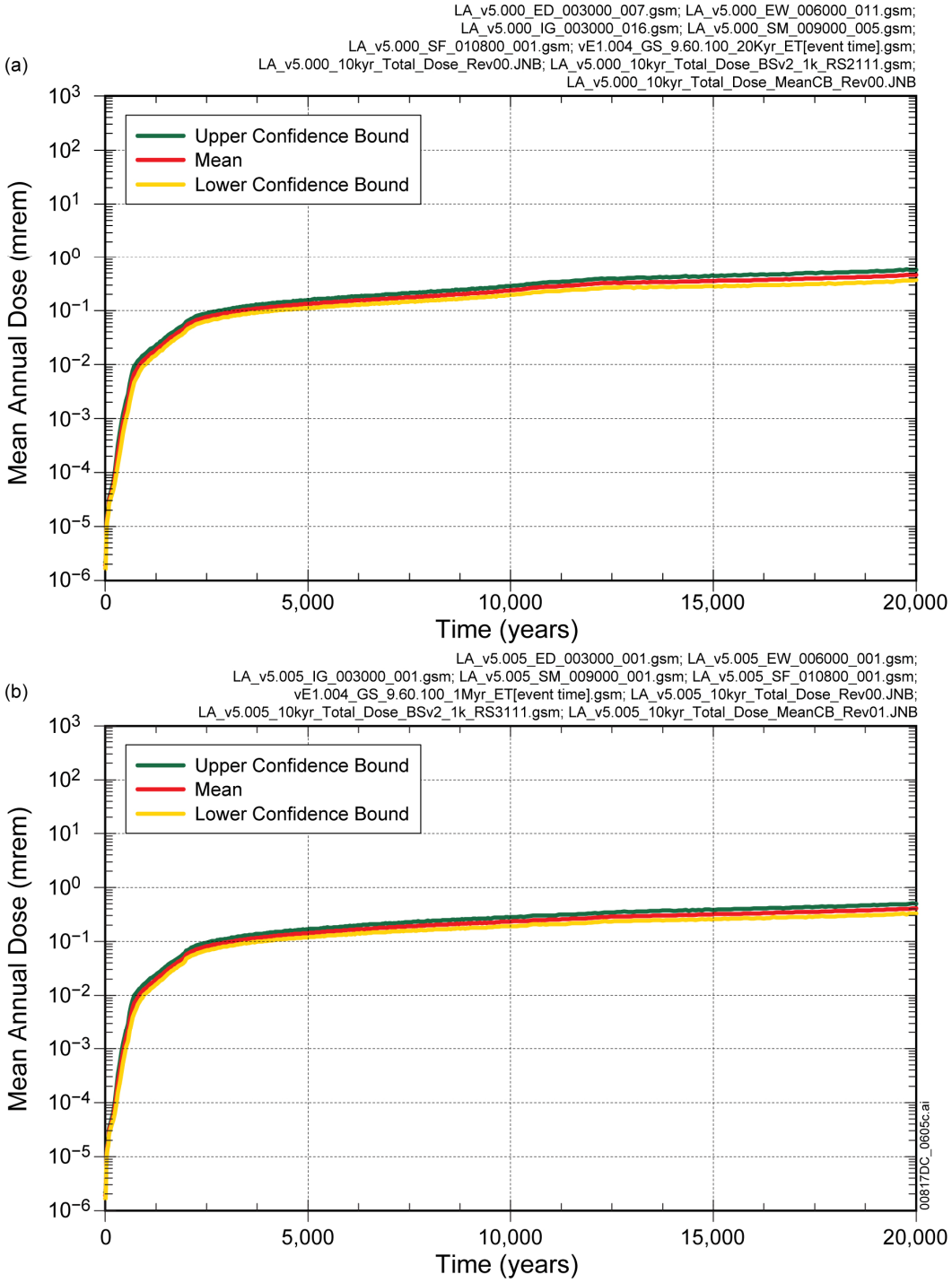

Source: Output DTN: MO0801TSPAADSA.000 [DIRS 185078].

Figure 7.3.1-47[a]. Confidence Interval for Total Mean Annual Dose for 20,000 Years for (a) TSPA-LA Model v5.000 and (b) TSPA-LA Model v5.005 Computed with the Bootstrap Technique

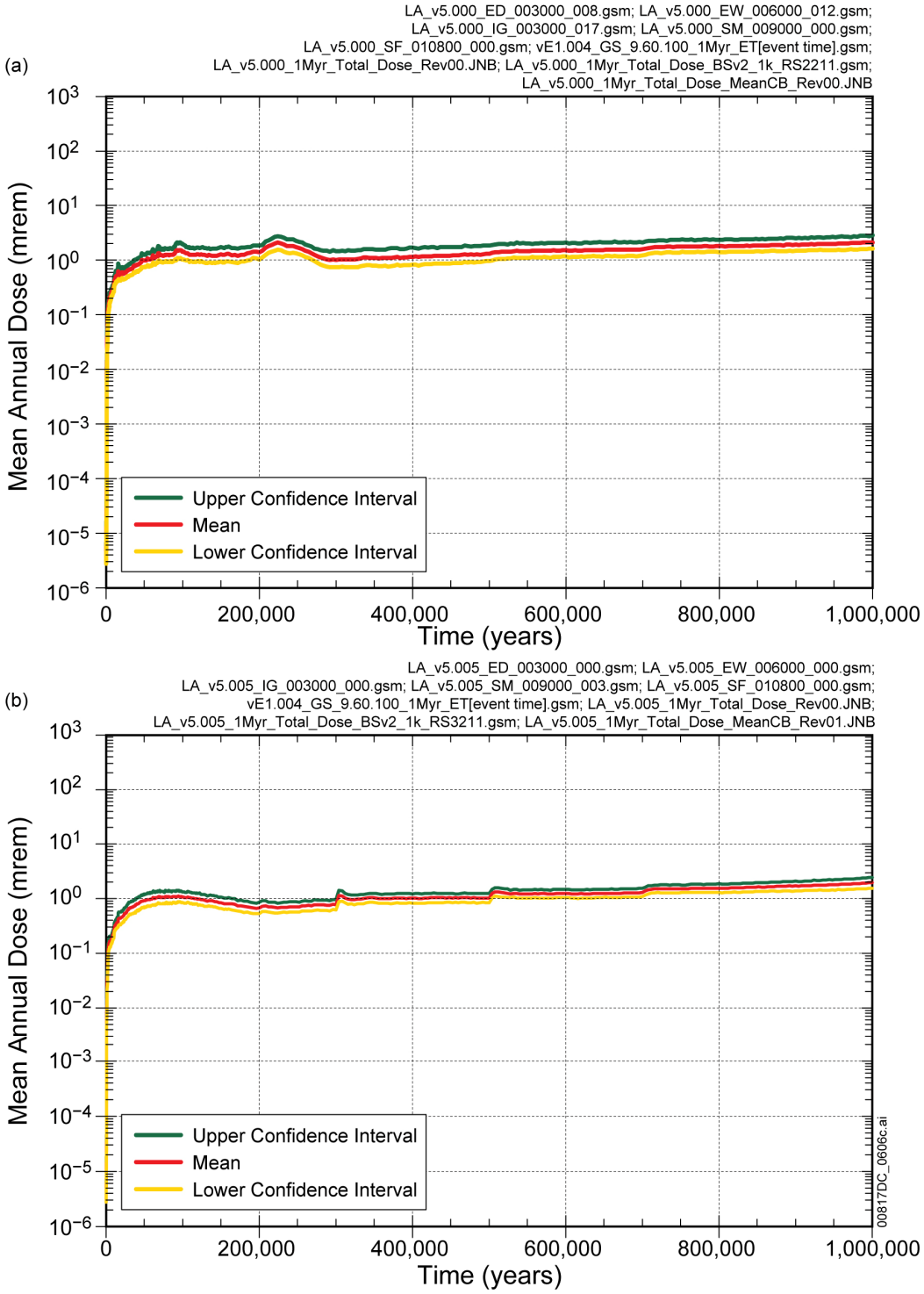

Source: Output DTN: MO0801TSPAADSA.000 [DIRS 185078].

Figure 7.3.1-48[a]. Confidence Interval for Total Mean Annual Dose for 1,000,000 Years for (a) TSPA-LA Model v5.000 and (b) TSPA-LA Model v5.005 Computed with the Bootstrap Technique

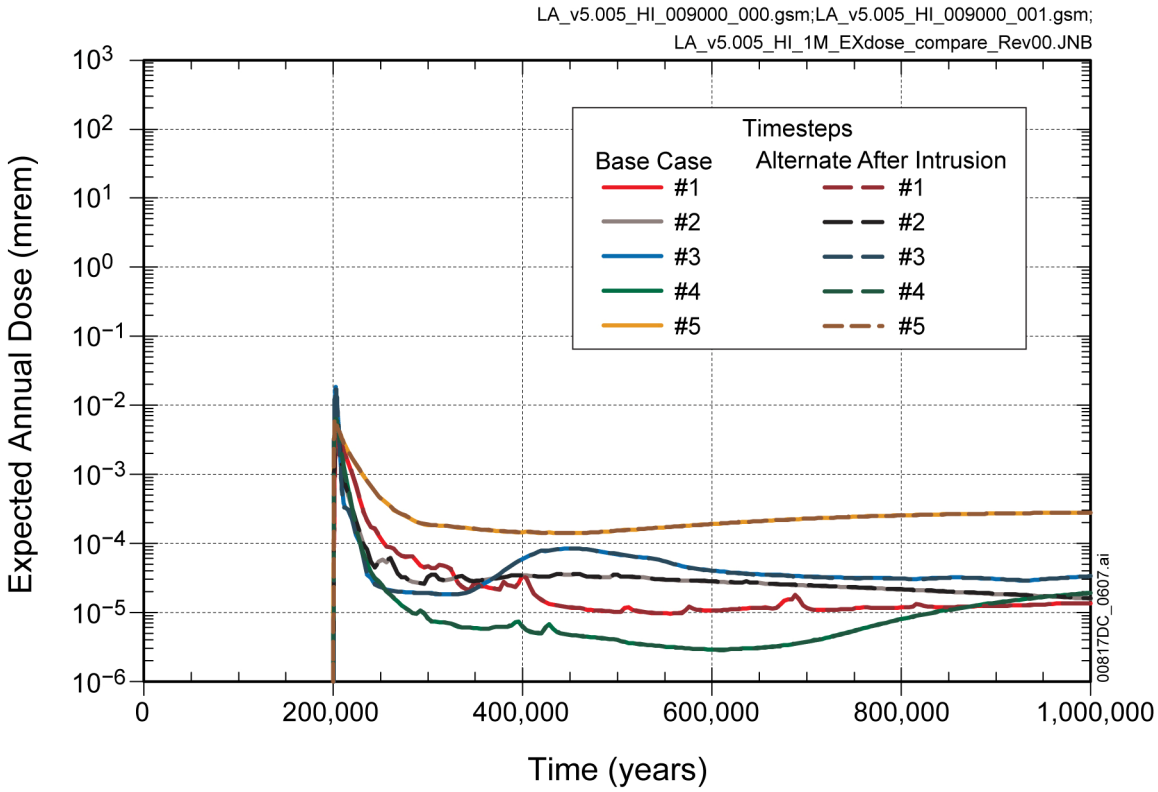

Source: Output DTNs: MO0710ADTSPAWO.000, File: v5.005_HI_009000_000 [DIRS 183752], for Base Case; and MO0801TSPAADSA.000, File: v5.005_HI_009000_001 [DIRS 185078], for Alternates.

Figure 7.3.3-10[a]. Expected Annual Dose from a Human Intrusion at 200,000 Years for Two Timestep Schemes

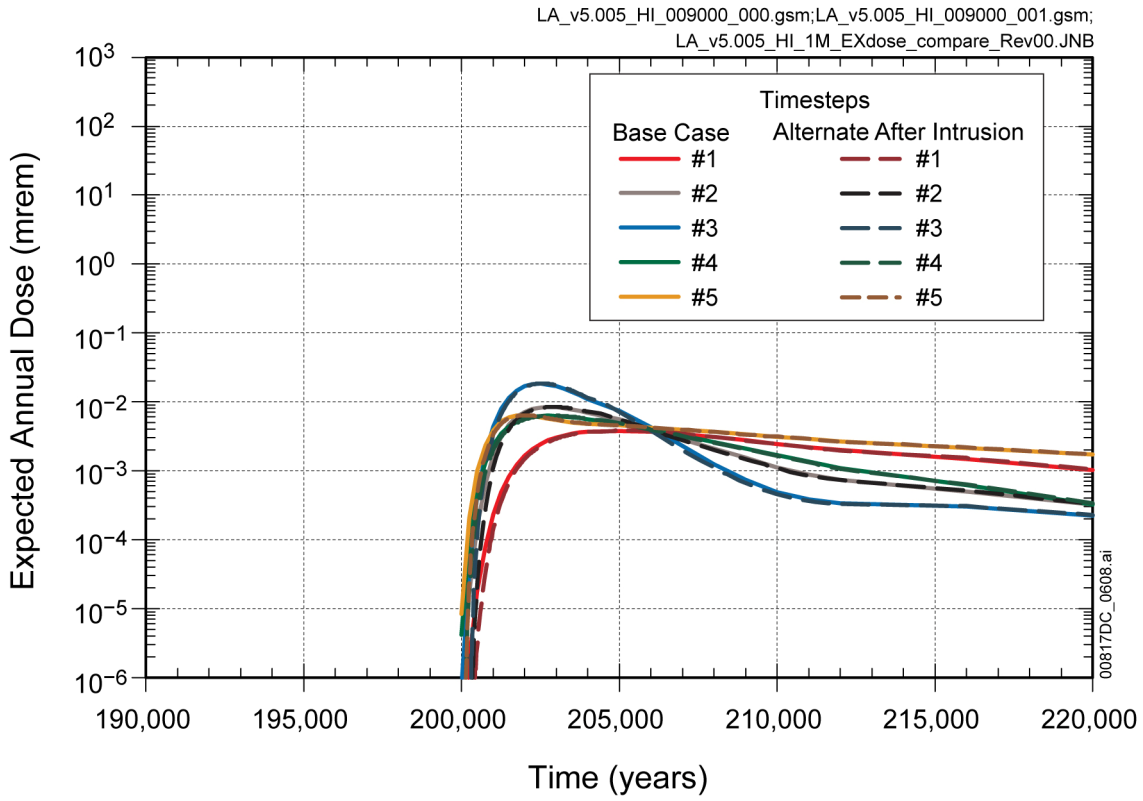

Source: Output DTNs: MO0710ADTSPAWO.000, File: v5.005_HI_009000_000 [DIRS 183752], for Base Case; and MO0801TSPAADSA.000, File: v5.005_HI_009000_001 [DIRS 185078], for Alternates.

Figure 7.3.3-11[a]. Detail of Expected Annual Dose from a Human Intrusion at 200,000 Years for Two Timestep Schemes

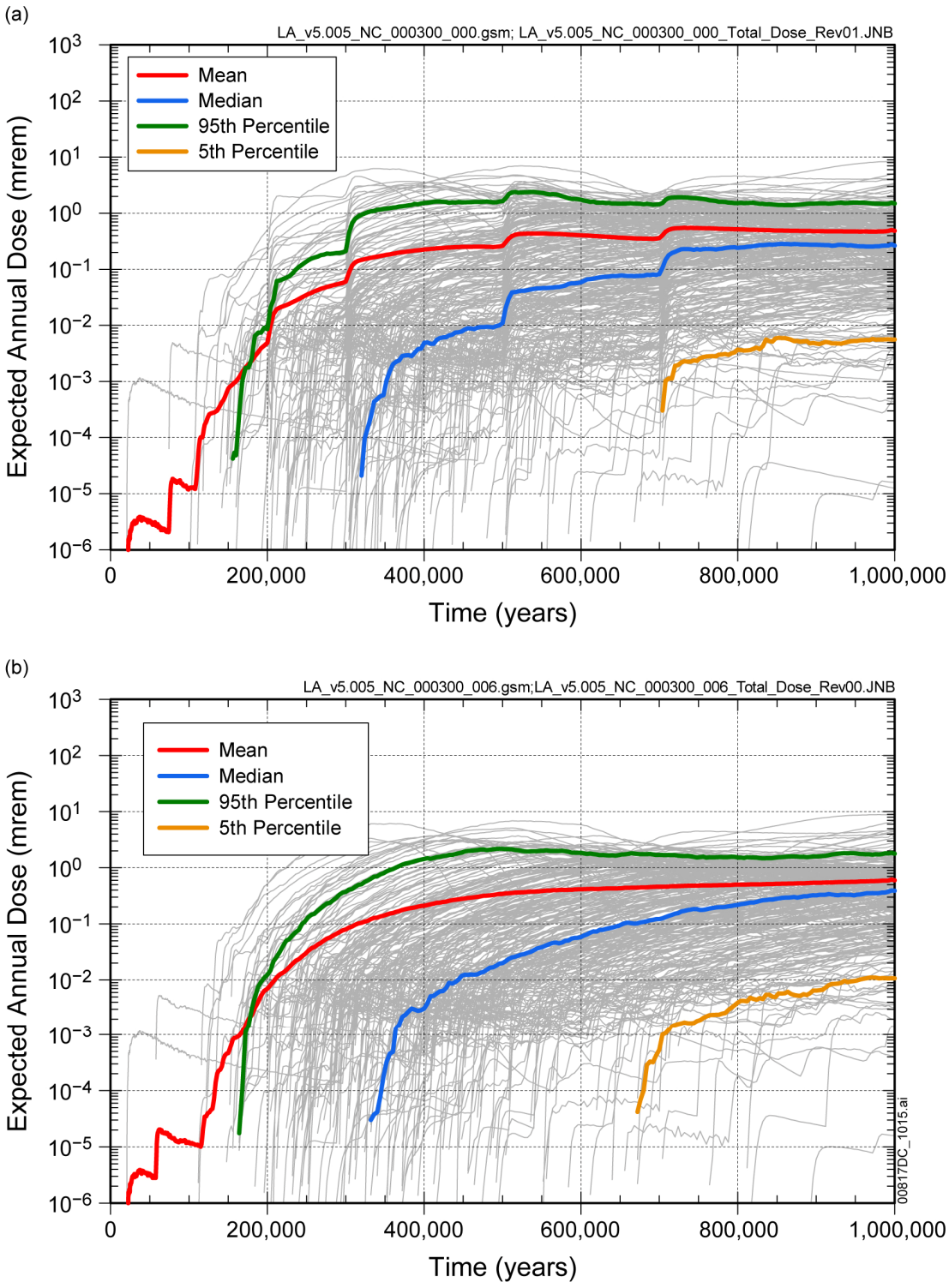

Source: Output DTNs: MO0710ADTSPAWO.000 [DIRS 183752]; and MO0801TSPAWPDS.000 [DIRS 185077].

Figure 7.3.3-12[a]. Expected Annual Dose for 1,000,000 Years for the Nominal Modeling Case from (a) TSPA-LA Model v5.005 and (b) Alternative Timestep Scheme

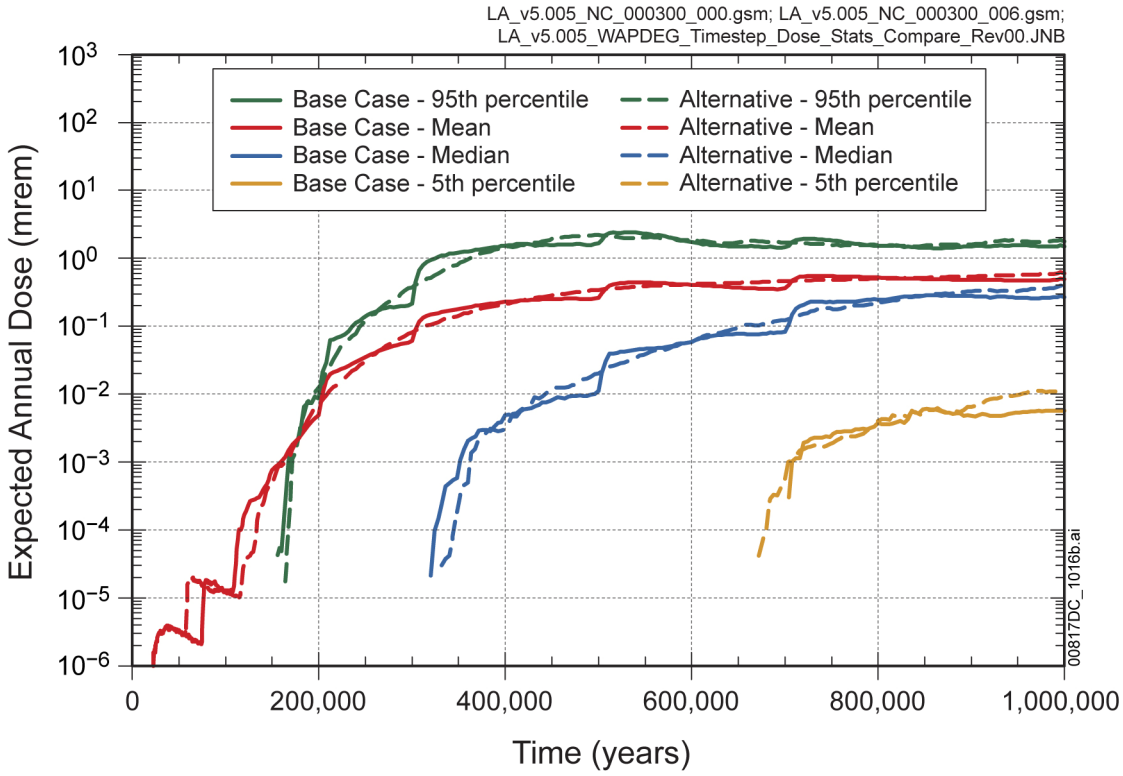

Source: Output DTNs: MO0801TSPAWPDS.000 [DIRS 185077].

Figure 7.3.3-13[a]. Expected Annual Dose Statistics for 1,000,000 Years for the Nominal Modeling Case Using Two Timestep Schemes

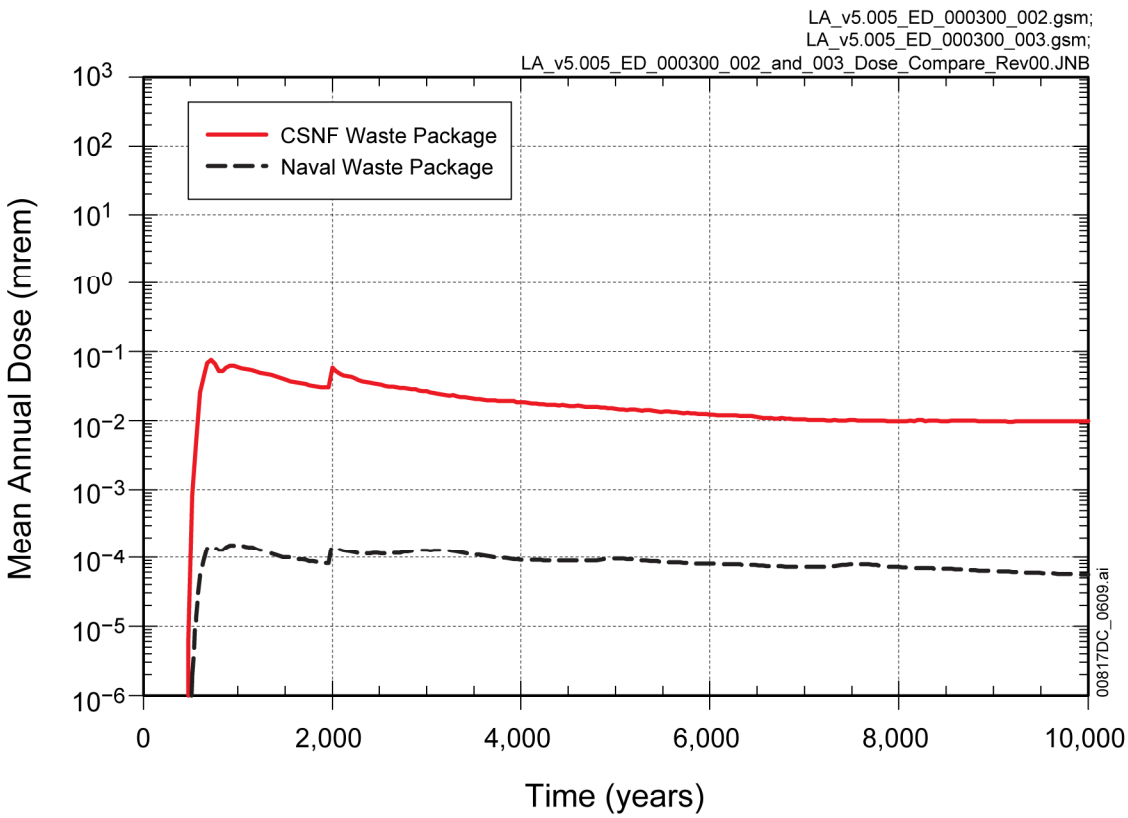

Source: Output DTN: MO0801TSPANSNF.000 [DIRS 184619].

Figure 7.5-4[a]. Comparison of Mean Annual Dose for a Single CSNF WP and a Single Waste Package with a Naval Source Term for the Drip Shield Early Failure Modeling Case

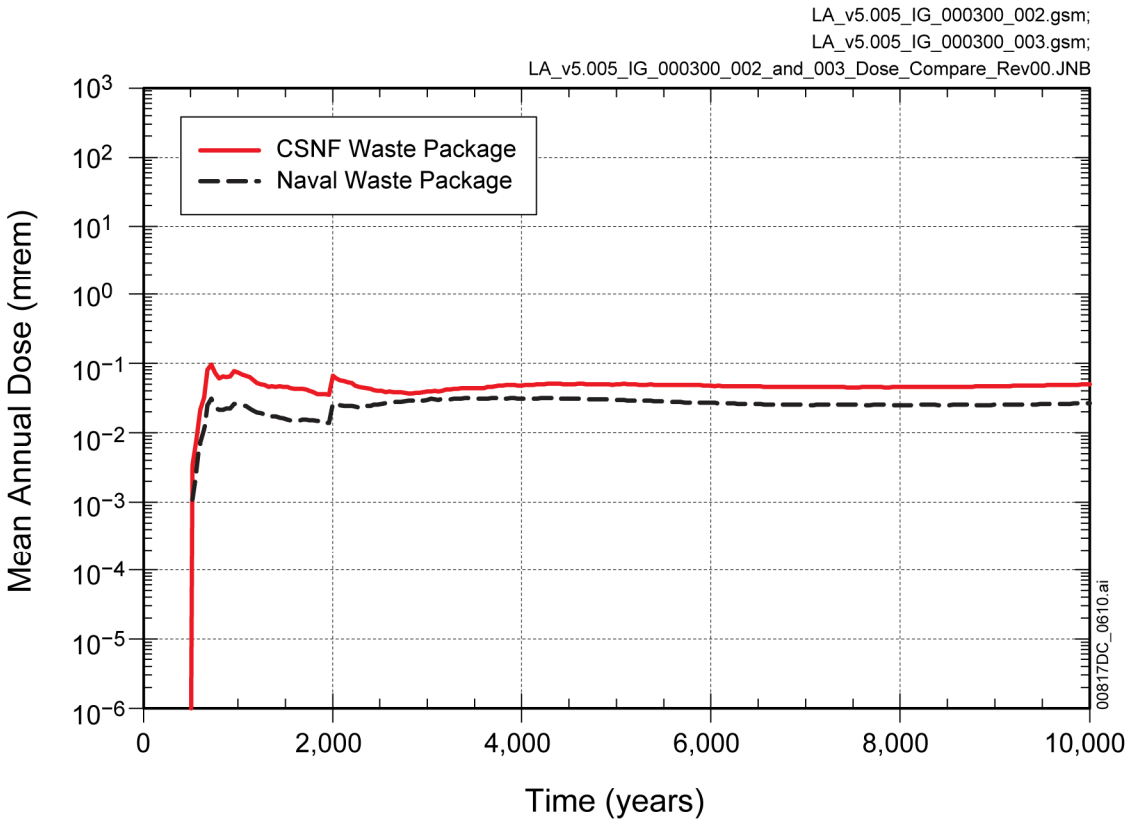

Source: Output DTN: MO0801TSPANSNF.000 [DIRS 184619].

Figure 7.5-5[a]. Comparison of Mean Annual Dose for a Single CSNF WP and Single WP with a Naval Source Term for the Igneous Intrusion Modeling Case